Designing and Developing Stable Body Flight in Drones

A thesis

Submitted in fulfilment

Of the requirements for the degree of

Master of Engineering

At

The University of Waikato

By

Sean Haisley

2021

Abstract

Drones are an ever-expanding field finding use and application in more and more area, such as construction, logging and transport. As a drone flies, it tilts its body in the direction of flight, however in some cases this tilting of the body is an undesired side effect of the drone's movement and results in drones not being applied efficiently in such a field. Therefore, the question arises, "Can a drone be developed to allow for stable-bodied flight in order to provide a non-tilting platform for carrying payloads in the future?" The goal of this thesis is to find a solution to that question. By looking at drones that currently provide similar solutions, this thesis provides possible concept solutions and determines the best design for implementing this stable-bodied flight and then covers the components that would be required and the manufacturing process of such a drone. The analysis of the design show that drone designs with gimbal, whether it be the body or the propellers that are contained by the gimbals, allow for infinite degrees of freedom, which is useful in maintaining stable flight. Testing and design development, show that a drone where the propellers are gimbal rotated allows for the highest level of control, whereas turning the drone body into a gimbal, creates a simpler and aerodynamic design. Both designs are developed further, leading to the conclusion that the gimbal rotor drone is a more complex design, requiring machine learning to determine the optimal angles of attack and thrust for each of the propellers, in order to maintain stable flight. Due to this and the aerodynamic advantage of the gimbal body design, this drone is selected as a final design.

Keywords

Aerodynamics; Accelerometer; Air speed; Angle of attack; Components; Concepts; Control; Closed-loop feedback circuit; Degrees of freedom; Design; Drag; Drone; Duct; Fibreglass; Filter; Frame; Gimbal; Global Positioning System; Gyroscope; Inertial Measuring Unit; Landing; Lift; Machine Learning; Magnetometer; Manufacture; Pitch; Polymer; Propeller; Prototype; Roll; Relative Wind; Rotary Wing; Stable-bodied flight; Streamline; System; Take-off; Thrust; Turbulence; Weight; Yaw

Table of Contents

List of Figures

List of Tables

List of Abbreviations

A = Cross-sectional Area
ABS = Acrylonitrile butadiene styrene
AFCS = Automatic Flight Control System
AHRS = Attitude Heading Reference System
AOA = Angle of Attack
BCI = Brain Computer Interface
BEC = Battery Elimination Circuit
CAD = Computer Aided Design
c_L = Coefficient of Lift
cm = Centimetres
CNC = Computer Numerical Control
CSI = Camera Serial Interface
DC = Direct Current
DSI = Display Serial Interface
ECI Frame = Earth-Centred Inertial Frame
EKF = Extended Kalman Filter
ESC = Electronic Speed Control
DC = Direct Current
DOF = Degrees of Freedom
F = Fahrenheit
g = Grams
GB = Gigabyte
g/cm^3 = Grams per Centimetre Cubed
GNC = Guidance, Navigation & Control
GPS = Global Positioning System
GUI = Graphical User Interface
HALE = High Altitude Long Endurance
HAT = Hardware Attached on Top
HIPS = High Impact Polystyrene
HDMI = High-Definition Multimedia Interface
HTOL = Horizontal Take-Off & Landing
I = Inertia
IMU = Inertial Measuring Unit
INS = Inertial Navigation System
I/O = Input / Output
K = Kelvin
KB = Kilobytes
Kg = Kilograms
Km = Kilometres
Km/h = Kilometres per Hour
L = Lift
LAN = Local Area Network
Li ion = Lithium Ion
Li-Po = Lithium-Polymer
LSB = Laminar Separation Bubble
mAh = Milliamp Hours

m = Metres
M = Mass
mA = Milliamps
MALE = Medium Altitude Long Endurance
MAV/µUAV = Micro Air Vehicle
MDF = Medium-Density Fibreboard
MPa = Megapascals
m/s = Metres per Second
N = Newtons
Ni-Cd = Nickel-Cadmium
Ni-Mh = Nickel-Metal Hydride
NZD = New Zealand Dollars
ρ = Density
Pa = Pascals
PLA = Polylactic Acid
PSI = Pound per Square Inch
PVC = Polyvinyl Chloride
PWM = Pulse Width Modulation
RAM = Random-Access Memory
R = Radius
RC = Radio Control
RF = Radio Frequency
S = Wing Area
SD = Secure Digital
SSH = Secure Shell
UAS = Unmanned Aerial System
UAV = Unmanned Aerial Vehicle
USB = Universal Serial Bus
v = Velocity
V = Voltage
VNC = Virtual Network Computing
VTOL = Vertical Take-Off & Landing
W = Watts
Wh/kg = Watt-Hour per Kilogram
Wh/L = Watt-Hour per Litre

Acknowledgements

First and foremost, I owe a deep sense of gratitude to my supervisor Harish Devaraj, without whom, this Master's Thesis would not be completed.

I am extremely thankful to my friend and fellow student Tim Sun, who was there to assist me with manufacturing the drone parts, in prepping the moulds and laying the fibreglass layers while I was away working at my other jobs. With his constant desire to learn, I was able to bounce ideas off him and learn from these exchanges to develop a final design.

I would like to give a warmest thanks to my friends and family who showed love and support, allowing me to skip on dishes or making sure to give me the best opportunity for clear thought while I performed my masters.

Finally, I would like to show my appreciation to Brett Nichol and the rest of the staff in the Engineering block, as they were always willing to provide a helping hand when it came to hashing out design ideas, methods of manufacture and the best way to approach a design when developing a final product.

Chapter 1: Introduction

"Can a drone be developed to allow for stable bodied flight in all directions in order to provide a stable platform to carry payloads for future use?"

This chapter will provide the background (section 1.1) into the research project, followed by the context (section 1.2) and purpose (section 1.3) of developing such a product. The significance and scope will then be defined in section 1.4, where the definitions of terms will also be described. Finally, the rest of the thesis will be outlined in section 1.5.

The aim of this master's thesis is to outline the process by which a solution to stable body flight was developed. The stable body flight will allow future drones to remove the need for pitching and rolling to change direction of flight.

1.1 BACKGROUND

Drones are a new and developing product that have swiftly taken over the market in many different fields, from surveying and military purposes to transport and even recreational use. The most common drone in use is the quadcopter, which uses four propellers to produce lift and can provide very steady, level flight.

With an ever-expanding field, drones are being applied in more and more differing settings and situations, of which one of the greatest potentials for development lies in the field of transportation. Currently, drones are being used for package delivery, such as with Amazon's Prime Air (Amazon, 2021) or even medical delivery, such as Zip line (Zipline, 2021) in Rwanda. Global companies, like Uber and Hyundai are even looking into drone transportation for people (McNab, 2020).

The potential of drones appears to be limitless, and with quadcopters and their ability to hover leading the way, these appear to be the best drone for further development. At the moment, however, they are still in their initial stages and therefore much development must be undertaken to make drones the leading solution to most problems.

One aspect of quadcopters that can still be developed is stable bodied flight, ensuring a constant flat platform as the drone is flying. Most quadcopters currently have fixed motors, with the motors and propellers facing straight upwards. Therefore, in order to fly in different directions, the drone must introduce pitch or roll to the body, hence tilting the quadcopter and

as a result leading to the loss of that stable, flat platform, as well as creating a larger surface area when flying through the air, causing more air resistance. The means by which most drones counteract this tipping effect on carried objects, is by the introduction of a gimbal arm, such as seen with videography drones, that have gimbal mounted cameras attached to the quadcopter. However, at this point there are no drones on the market, where the body can remain stable throughout its various manoeuvres.

1.2 CONTEXT

This project was started with the question "Can a drone be developed to allow for stable-bodied flight in order to provide a non-tilting platform for carrying payloads in the future?"

This drone would be a solution to the problem stated previously (section 1.1), allowing the payload to not experience the effects of rolling and pitching that are created by the drone flying around. This means that the drone can then be used in any situations where it is critical or preferred that the payload does not experience too much shifting and changing of direction.

1.3 PURPOSES

With the aim of the project being to develop stable-bodied flight in drones, these drones would predominantly find use in the field of transportation (Engineers Australia, 2021). Depending on the movements that standard drones are required to make, passengers could experience large amounts of rolling and pitching during take-off, landing and general manoeuvring around (Albert A. Espinoza, 2020). By introducing stable-bodied flight, the drone would effectively have what could be compared to suspension in cars.

Another practical use for such a drone would be in the cases of logging (Rayonier, 2021) or construction (Kardasz, Doskocz, Hejduk, Wiejkut, & Zarzycki, 2016), any case in which objects are suspended by lines underneath the drone and require precise movements or placement (GPS World Staff, 2018). A typical drone would introduce a tipping effect, which would translate through the lines to the object that is being carried by the drone, therefore leading to swinging, as a result translating back up to the drone, causing the drone to then be unstable. Another case would be in thickness testing where any tilting off the drone body would result in accurate thickness readings (Intertek, 2021).

In addition to this, the ability of the drone to fly without tilting the body, results in less of the drone body being exposed to the effects of oncoming air resistance, as it flies in that direction. With the loss in air resistance, the drone that does not expose a large surface area in

the direction of flight will be capable of flying relatively faster than a drone that tilts in the direction of flight.

As can be seen from these examples and many more yet undiscovered cases, there are multiple situations in which stable-bodied flight in drones is useful.

1.4 SIGNIFICANCE, SCOPE AND DEFINITIONS

This thesis will delve into various designs that can provide the desired result and determine what components are required to create said product. It will then look at the process involved in getting these components working together to achieve said goal.

This product is important, as it will develop an initial stepping-stone from which further developments can be made towards the topic of stable bodied flight. By having an initial design, it can be scaled up, scaled down, or retrofitted with further design ideas to further improve the design, in order to be used in different applications. Currently, there are no major examples of drones that are aimed at providing such a solution, therefore, having a first design would open up many opportunities for new and improved models.

To be able to develop such a drone, basic knowledge on how to create a drone would be required, and from there, any further ideas and concepts would have to be adapted to fit with the characteristics of the drone, that allow it to function properly, such as blade rotation direction, or their control methods. This knowledge would include general flight, lift and aerodynamics, and could range to machine learning and navigation for accurate drone control. As a result, to provide this solution, an in-depth understanding of the topics involved with these aspects will need to be attained.

In drone flight, the main characteristic that allows the drone to fly is lift, which is the upwards thrust that is provided by the propellers and motor. To vary the direction of flight, the motors on drones change their speeds, which therefore changes the lift thrust output of each motor, therefore changing the angle of attack (AOA) of the drone, hence tilting it in the direction of flight.

When referencing machine learning, this covers the topic of a computer's ability to adapt on its own. In this case, it is the ability of the computer to determine the appropriate AOA of the propellers, in order to maintain the stable flight of the drone itself.

1.5 THESIS OUTLINE

This thesis will cover the literature review (Chapter 2:) in which the history of drones will be explored (Section 2.1), following which the different classes of drones will be described (Section 2.2). After this, the thesis will delve into the basic concepts of how they work (Section 2.3). Following that, it will cover similar drones (Section 2.4) and how they relate to the project, then finally summarise the literature review and its implications for this project (Section 2.5).

In Chapter 3: the different design concepts will be explored, looking at their advantages and disadvantages in relation to the set goal, by which a selected design will be pursued for further development (Section 3.1). After selecting a design, the thesis will cover the different components (Section 3.2) that were involved with developing the design and building a working product.

Chapter 4: will take a deeper look at the development process, any problems encounters and what the workarounds of these issues were. Finally, Chapter 5: will give an overall rundown of the developmental process and the steps to selecting and developing a design; as well as any limitations of the design and how the process would have been undertaken if it were to be repeated.

Chapter 2: Literature Review

This chapter is a means of looking at what has gone before and determining the optimal situations in which the drone can be applied, therefore laying out a good plan of development for such a drone with stable-bodied flight. The first step is to look at the background of drones and identify the places in which they find their uses (Section 2.1). This will determine how developing a drone with stable-bodied flight can become useful and what its advantages are.

Section 2.2 will cover the different types of drone classes, giving a general overview of each one, in order to outline what type of drone this idea can be applied on and where the current limiting factors may be found.

To gain an understanding of how drones work and the different concepts involved with maintaining stable flight through aerodynamics, flight and control, Section 2.3 will take a deeper look at the basics of aerospace engineering and factors that need to be considered when developing or designing a drone.

Following this, the literature review will look at drones that work on a similar principle to the outlined task or attempt to tackle a similar issue (Section 2.4). It will cover the successes and failures and identify what can be improved or used to help develop a drone that allows for stable-bodied flight. Summarising all of this, Section 2.5 will point out what knowledge is useful in building the drone and what the implications of said knowledge has on the design process.

2.1 BACKGROUND AND APPLICATION

An Unmanned Aircraft System (UAS) is mainly comprised of the Unmanned Air Vehicle (UAV), the ground station (or remote station), the payload, system control and any launching/landing systems (Austin, 2010). Similar elements are found in UAS as can be found in manned aircraft, however with the difference being that the manned crew is replaced by on-board electronic or computer systems. The removal of people from the air vehicle means that the system can be scaled down by a large factor or replaced by other components that assist the function of the UAS. This allows UAS to use components and do things that a typically manned aircraft currently could not do, such as being fully battery powered. UAVs that are more intelligent are capable of flying themselves, and planning their own flight paths, which is very useful for cases such as videography (Hollister & Pavic, 2019).

Drones are not just found in videography, they can be found over a range of different fields for both civilian and military use. In civilian use, drones are commonly used for surveying, such as in agriculture, construction, conservation, etc. (Jackson, 2021) they can also be used for monitoring and security as has been seen used by police authorities, fisheries, surveillance, etc. Moreover, have even found use in search & rescue (Blue Skies Drones, 2021), along coastlines and in-land. Nevertheless, the popularized cases are for recreation, when it comes to aerial photography, hobbyists and more recently, drone racing.

The military is especially known for using UAVs in different roles, with the most famous uses being reconnaissance & surveillance and air strikes (Military.com, 2021). Generally, use of UAV in military roles is included in either of these fields, however even so the different situations in which these can be applied are numerous and as a result, drones have become common-place within the military.

2.2 DRONE CLASSES AND OVERVIEW

Aerial drones or UAVs have various different classifications depending on their purpose, method of flying, altitude at which it flies and size. This section will cover those different classes and describe their functions to indicate in which fields they find use. The first classification is based on the weight of the drone (Hassananlian & Abdelkefi, 2017). Super-Heavy Drones have a weight greater than 2000 kg, whereas Heavy Drones have a weight between 200 kg and 2000kg. A Medium drone weighs between 50 kg and 200 kg, while a Light/Mini Drone has a weighs from 5 kg to 50 kg. Anything below 5 kg is considered a micro air vehicle (MAV), which is the most common drone found in use for recreational use and is the type of drone that will find use in this project.

Instead of by weight, the UAVs can also be classified by their endurance and altitude, which is generally for military purposes. A High Altitude Long Endurance (HALE) drone flies at an altitude above 15000 m for 24+ hours (Airforce Technology, 2021). A Medium Altitude Long Endurance (MALE) drone flies at altitude between 5000-15000 m for 24+ hours (Airforce Technology, 2021). A Tactical UAV has a range between 100-300 km and a Close-Range UAV has a range of up to100 km. Below this are the MAV and µUAV, which have significantly shorter ranges. As previously mentioned MAVs / µUAVs are the only type of drone that will apply to this design.

The next classification covers the UAV's method of flight, which include VTOL, HTOL and hybrid models (*Figure 2.1*). VTOL (Vertical Take-Off Landing) include models such as

helicopter, heli-wing and quadcopter (Wingtra, 2021). These are usually capable of hovering and have a high level of manoeuvrability, however are limited in their cruise speed, due to the stalling of retreating blades. HTOL (Horizontal Take-Off Landing) are mainly fixed wing models, which usually have a higher cruise speed and tend to be capable of flying greater distances, but what they make up in speed and range, they lose in ability for hovering and manoeuvrability, often requiring a runway for take-off and landing. Hybrid models include tilt-wing, body and rotor, as well as ducted fans (Technology, 2021). These have the capability of taking off like an HTOL and flying like a VTOL drone, through methods such as tilting the propellers in the direction of flight. These air vehicles even have the ability to hover, however are more complex in their design.

a **b** **c**

Figure 2.1: (a) VTOL (Orms-Direct, 2021)*; (b) HTOL* (Fly Dragon, 2021)*; (c) Hybrid* (Geo-matching, 2021)

a **b** **c**

Figure 2.2: (a) tilt-rotor (Yonhap News, 2021)*; (b) tilt-wing* (Vertical Flight Society, 2021)*; (c) ducted fan* (Kim S. , 2021)

Tilt rotor drones (*Figure 2.2* (a)) tilt their rotors up for take-off and hovering, and then tilt them forward for forward flight (Ward, 2018). In contrast, tilt wing drones (*Figure 2.2* (b)) often have rotors fixed to the wing and tilt their wings in the direction of flight (Chana & Sullivan, 1992). In these cases, the tilt rotor was more efficient at hovering, whereas the tilt wing was more efficient at cruising flight. Ducted fan drones (*Figure 2.2* (c)) use the duct to direct the air flow around the propeller, also removing wing tip drag reduction, which often leads to more thrust provided by the propeller, however this comes with the cost of an increase in weight from the duct itself (Cai & Ang, 2011). Another problem encountered by ducted fan drones is flow separation from the duct as a result of a pressure gradient, leading to turbulence from eddies

and vortices (Deng, Wang, & Zhang, 2020). These are all factors that need to be taken into account when designing a drone that is capable of steady-bodied flight.

Drones that do not fit to any of these classes are considered unconventional drones. One version of this is a flapping wing drone, which are often inspired by birds or insects and use the flapping motion of the wings to provide thrust (Williams, 2020). With the inspiration from nature, they often have unique manoeuvrability advantages that can be compared to the insect or bird that they attempt to resemble. The unconventional drones are less likely to find use in developing steady-bodied flight; however, drones that are modelled after insects, such as dragonflies may be able to provide such characteristics.

2.2.1 Rotary Wing MAV

Rotary wing MAVs (*Figure 2.3*) are the most common version found for VTOL drones. Their small size and ability for high manoeuvrability makes them capable of flying in every direction, not just forward. As a result, they are perfect for surveying, as they can get to hard to reach places, such as under bridges, inside buildings and pipelines. Lift is generated by the constant rotation of the propellers, but the number of the propellers can range, with the most common arrangement being the quadcopter with four propellers. Propellers can also vary in their number of blades, affecting the amount of lifted provided by each propeller (Get FPV, 2021).

Figure 2.3: Rotary Wing MAVs (Flynt, 2017)

These rotary wing drones are limited in endurance due to the high power requirement of hovering. Challenges with this design include low thrust loading and a low rotor efficiency.

2.2.2 Convertible Rotor Aircraft

The tilt-rotor design combines the fixed and rotary wing drones. A major challenge experienced by tilt-rotor drones, is transitioning from rotary wing flight to fixed wing flight. They often experience a loss in stability in high-speed forward flight (Lu, Liu, Li, & Chen, 2019). The largest challenge lies in the control method in performing the transition between states. These drones are usually more difficult to scale down as additional components and complexity is introduced in allowing the wing or rotor to tilt.

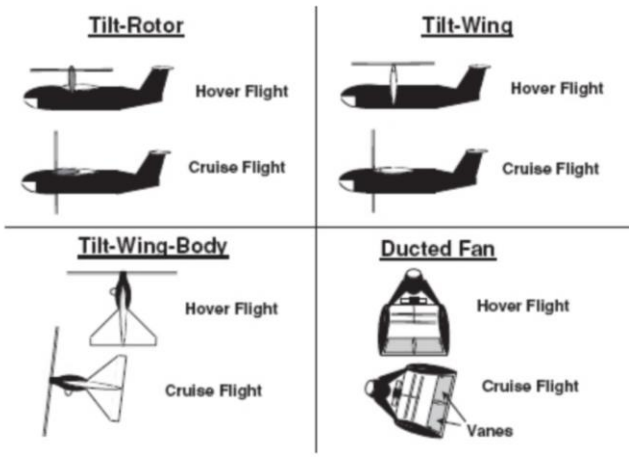

Figure 2.4: Convertible Rotor Aircraft (Hassananlian & Abdelkefi, 2017)

2.2.3 Drone Manufacturing

The process of manufacturing the drone has follow on effects to its performance and the manufacture comes with its own challenges. The materials required are also very important to determine how well the drone works and are determined by the weight, strength and stiffness requirements.

A typical fixed wing UAV consists of the wings, fuselage and tail. The wings can consist of a metal, such as aluminium in large UAVs, or for smaller MAVs, Kevlar, fiberglass, carbon fibre, wood, Styrofoam or plastics (PVC) are used (Lanning, 2020). More recently, composite materials are found more commonly in drone design, due to advances in the field of composite manufacturing allowing for more complex shapes and designs (Knight & Curliss, 2003). The properties of these are dependent on the manufacturing process. They tend to be very lightweight and strong, with a high accuracy and quality surface; however, this comes with the disadvantage of the high cost in developing and preparing the mould (Composites Lab, 2021).

The process for manufacturing composite materials include different steps, like 3D CAD modelling, CNC milling, wet lay-up, prepreg laminating, high temperature curing, and off

mould fettling/dressing. The different methods of manufacturing composite materials include matched die moulding, vacuum bagging, filament winding and resin transfer moulding, with vacuum bagging being the cheaper method (Aerospace Engineering, 2012).

Table 2.1: Drone Material Comparisons (Hassananlian & Abdelkefi, 2017)

Material	Density (g/cm^3)	Tensile strength @73°F (psi)	Stiffness MPa	Methods of manufacturing	Price
Aluminium	2.7	30,000	70,000	Forging	Expensive
Wood	0.8	550	10,000	Adhesive bonding	Cheap
Styrofoam	0.18	100	5000	Hotwire cut by CNC	Cheap
Plastics (PVC)	1.15	7000	3000	Vacuum forming	Very cheap
Carbon fibre	1.78	10,0000	50,000	Epoxy resin	Very expensive

The above table shows different materials that are commonly used in the construction of UAVs. It outlines the different densities, tensile strengths, stiffness's, methods of manufacturing and comparative prices. Balsa wood is commonly used in the construction of the drone's fuselage and tails, due to being lightweight, easily manufactured and quite cheap, however it is soft and low strength compared to the other materials (Baichtal, 2015).

The wings of fixed wing drones are often made of foam or composite materials. Due to the low strength of foam, it is mainly used in the cases of MAVs and µUAVs. The easiest and most efficient way of shaping foam is to use a hot wire cutter (Engineered Foam Products, 2021). Other common materials include the composite materials of carbon fibre and fibreglass. When combined with resins, carbon fibre has a higher strength index, a lower weight-to-strength ratio and a higher rigidity compared to fibreglass, whereas fibreglass is a cheaper and more durable option (Rock West, 2017). The complexity of manufacturing with both can be high.

Optimally, the drone design would be developed using carbon fibre or a thermoplastic, such as PVC, as these would provide the greatest strength to weight ratios, however the design would also have to take into account the complexity of the manufacturing method and the material costs.

2.2.4 Propulsion Systems and Actuators

The propulsion of each of the drones and generation of motion vary greatly depending on the shape and flight mode of each of the drones. In fixed wing UAVs propulsion is usually

provided in similar fashions as to conventional aircrafts, such as rotor or jet engines, and therefore these systems do not require the development of new and unique propulsion systems. The two factors that affect propulsion the most are power and energy density (OpenEI, 2021). The power density is dependent on the amount of power output per volume, while the energy density is dependent on the conversion efficiency from energy provided by the power source to the engine. As a rule of thumb, in most drones, the propulsion system constitutes approximately 40-60% of the take-off weight and its performance determines how well the vehicle performs.

One form of propulsion found in fixed, tilt and rotary wings is fuel engines, such as gas turbine, jet or injected engines. Of these engines, the gas turbine engines are superior because of their high power to weight ratio, longer functioning time and their reliability is higher.

In MAVs it is more common to find one of four propulsion systems, which include batteries, fuel cells, micro-diesel and micro gas turbine, with the micro gas turbine engines being the smallest and lightest of the fuel-powered drones (Adamski, 2017). The easiest propulsion for MAVs is using electric motors as they have high reliability, efficiency and controllability (Morris, 2015). The two major types of electric motors that could be used for propulsion are brushed and brushless motors. Brushless motors can be produced to be smaller and more lightweight compared to the brushed motors and tend to have a higher efficiency and speed. These are commonly found on rotary wing drones. In these cases, the propeller is key to the amount of lift that the motor can provide. A major advantage of using electric motors for MAVs is the ability to control the motor speed, to allow for variable flight, with minimal vibration (Renesas, 2021).

The drone design in this project will most likely use brushless motors, due to the mentioned properties of being smaller, more lightweight and faster. To pair with this, the best energy source would be batteries, as this is a quick and easy means by which to provide energy.

2.2.5 Power Supply

Fossil Fuels such as gasoline and methane are common fuel sources for engine-powered drones, however nowadays it is more common to find drones that run off battery power, such as Li-PO batteries, for their high specific power (inutes of flight time for MAVs.

Table 2.2), or in the case of µUAVs, lithium batteries, due to being very lightweight (Triggs, 2021). Fossil fuels can provide more energy compared to batteries, but have a lower

efficiency, and are more volatile in smaller UAVs (GreigRS, 2021). Typically, either power source provides a maximum of 30 minutes of flight time for MAVs.

Table 2.2: Battery Comparison Chart (Hassananlian & Abdelkefi, 2017)

Characteristic	Ni-Cd	Ni-Mh	Li-Po	Li-S
Specific Energy (Wh/kg)	40	80	180	350
Energy Density (Wh/l)	100	300	300	350
Specific Power (W/kg)	300	900	2800	600

MAVs and µUAVs are finding more and more use in various fields; however, the limiting factor remains their flight time. One means by which to improve their efficiency of flight is by reducing their drag, by means of their shape, wing span, etc. (Krossblade Aerospace, 2021) This in turn reduces power consumption, improving flight efficiency. Current methods are also looking into the use of solar powered drones, laser powered drones or even piezoelectric energy sources to increase a drone's flight endurance.

Depending on the size and weight of the drone design, it will most likely run using Li-Po batteries, however this will still give it a limited flight time (AliExpress, 2021). As mentioned above, improving the aerodynamics and reducing the drag of the drone can lead to a higher flight efficiency, therefore showing the importance of such a design.

2.2.6 Guidance, Navigation and Control (GNC)

Typically, you can control a drone by three methods. These include radio control, video base and autopilot. Radio-control (RC) requires the use of a transmitter in the form of Remote Control and a receiver on the drone (Carpenter, 2021). This case generally requires 4-6 channels for controlling flight level, with additional channels in the case of cameras or other on-board devices and works on a frequency of 2.4 GHz. The average range for this controller is approximately 30 km (Buzz Flyer, 2021).

Another common method of controlling drones is through autopilot navigation systems, where the drone transmits data like velocity and altitude to a ground station, and instructions can be sent back to the drone from the ground station. This system has an average range with an altitude of 12 km and radius of 50 km (Jia, Guo, & Wang, 2018).

More recent forms of controlling drones include using brain-computer interface (BCI), such as presented by the University of Minnesota (University of Minnesota, 2013) or even hand gesture controlled drones.

For the cases of autopilot, self-flying drones and many other examples, the drones need to be capable of positioning themselves in reference to the Earth and their surroundings. This is usually done using a Global Positioning System (GPS) and an Inertial Navigation System (INS). Both systems are used to get the position, velocity and altitude; however, the GPS achieves this by finding itself in reference to the Earth, by making contact with at least four satellites. This positioning method is prone to external interference and has a slow update rate (Patrik, et al., 2019).

Therefore, to assist the GPS, an INS is used, which finds its position and orientation relative to itself. An INS typically includes a gyroscope and accelerometer, occasionally including a magnetometer, which finds its orientation in reference to the Earth's magnetic field. The INS is very prone to noise and drift, therefore to combat this a Kalman Filter is applied to the measurements to fuse them and provide more accurate results (Kim & Bang, 2018). An Extended Kalman Filter (EKF) can be used to fuse the measurements of the GPS with those of the INS to provide even more accurate positioning.

To optimally design the drone, the most important factor that will be involved is the INS system. The INS system is critical for determining the orientation of the drone and determining whether it is stable or not, whereas the other systems are, such as the GPS and radio control or self-flying systems are important for actually controlling the drone (Acharya, 2014).

2.3 PRECISION FLIGHT AND CONTROL (HOW THEY WORK)

Lift is created within an aircraft by creating a lower pressure above a winged surface and a higher pressure below the winged surface. This is achieved by accelerating air downwards, causing an upwards force greater than the force of gravity. A fixed wing aircraft achieves this through forward flight, whereas helicopters and quadcopters use a rotating blade to create this desired effect.

The amount of lift created is a result of the mass flow of air in the downwards direction and can be modelled by $L=1/2\rho Av^2C_L$, where ρ is air density, A is the cross-sectional area of the affected airflow, v is the airspeed and C_L is the coefficient of lift (Ather, 2020).

2.3.1 Fixed-Wing Drag

The reaction force to an aircraft's forward motion is drag, hence the thrust provided by the propulsion system must be greater than this for an aircraft to reach and maintain airspeed. There are three major types of drag encountered by UAVs flying at subsonic speeds.

An important factor that determines the effects of a fluid, or in this case air, on the drag is its Reynolds Number, relative to the fluid density, flow speed and dynamic viscosity of the fluid (Rapp, 2017). The Reynolds Number is a dimensionless value that helps predict the flow pattern of the air around the different bodies, as they are moving. The lower the Reynolds Number, the more likely the structure will experience laminar or uninterrupted flow, the greater the Reynolds Number, the greater the effects of turbulence or laminar transition. Generally, the larger the profile of an air frame, the larger the Laminar Separation Bubble (LSB) (O'Meara & Mueller, 1987) and therefore, the greater the turbulence, however this also depends on the shape of the frame (Austin, 2010).

2.3.1.1 Parasitic Drag

The first of these is the parasitic drag caused by skin friction, interference drag, and form drag (NASA, 2021). Skin friction (*Figure 2.5* (a)) is because of the air closer to a surface moving more slowly, than the air far away. Interference drag (*Figure 2.5* (b)) is the result of mixing airflow streamlines between two different components, such as wings and fuselage. Form drag (*Figure 2.5* (c)) is created by the size and shape of the object and results from flow separation (FAASafety, 2021).

Parasitic drag will increase with an increase in air density and airspeed. This type of drag is considered parasitic, as it does not assist in the aircrafts ability to fly, due to it being created by components that do not assist in lift and just acts to slow down the movement of the aircraft (FAA, 2017). An estimation of the sum of the parasitic drag can be found by adding together the drag forces of the separate components of the aircraft, such as fuselage, tail, etc., or it can be tested in a wind tunnel to help calculate the drag coefficient. To minimise parasitic drag, the best solution is to design an aerodynamically optimal frame, with a smooth surface finish.

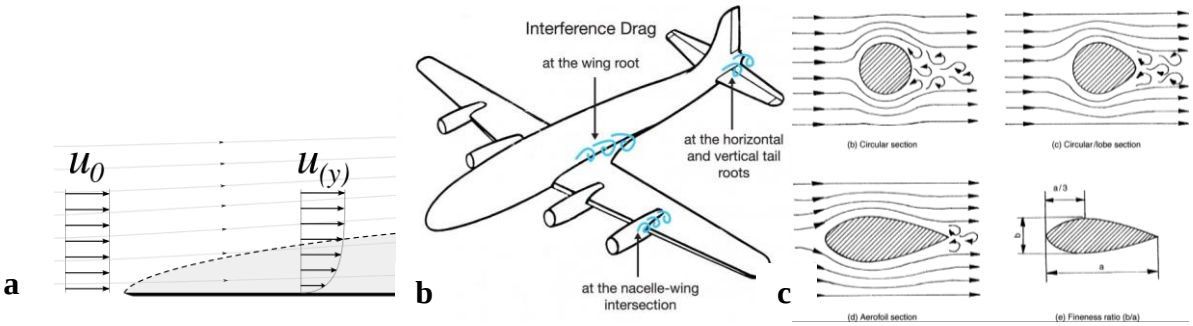

Figure 2.5: (a) skin friction (AerospaceEngineeringBlog, 2016)*; (b) interference drag* (Groupidea, 2015)*; (c) form drag* (Windsor, 2014)

2.3.1.2 Profile Drag

Profile drag is because of the form drag and skin friction on the wings cutting through the air, is what creates the different airspeeds above and below the wing, therefore generating lift (*Figure 2.6*). By increasing the speed of the airflow above the wing, it creates a region of lower pressure, while the air below the wing moves at a slower airspeed, causing a higher-pressure region (Cebeci & Smith, 1968). This induces an upwards force in the wings, therefore causing lift.

An increase in the AOA of a wing will not greatly affect the profile drag, but it will increase the lift generated. However, if the angle of incidence to the relative wind is too great (~17°), then the airflow at the top of the wing becomes detached, no longer creating that low pressure region from high air speed. Therefore, lift is no longer generated (Skybrary, 2019). At higher speeds, the air speed is higher, producing more lift; therefore, the wing does not need to compensate for lift with a higher AOA.

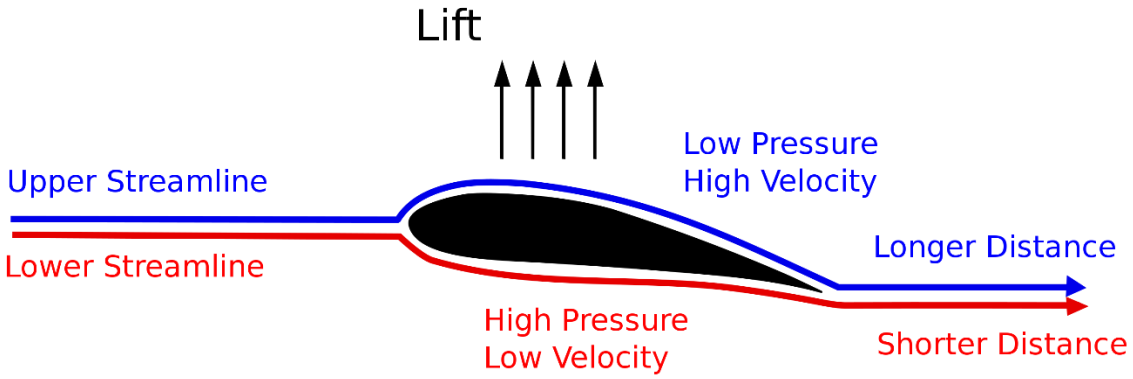

Figure 2.6: Wing Lift Generation (Wikipedia, 2021)

2.3.1.3 Induced Drag

Induced Drag is a form of drag that results from the lift generated by profile drag on the finite length of an aircraft's wings spilling over the edge and causing an upwards deflection of the wingtip (Hoerner, 1965). The different air speeds and pressures above and below the wing cause vortices to form at the wing tips and therefore lead to swirling flow that is strongest at the wing tips and decreases towards the root of the wing. At the wing tips, this induced flow causes an increased AOA, which therefore increases lift through an increase in downwards force. This force is known as induced drag (SKYbrary, 2021).

Long, thin wings lead to low induced drag, whereas short wings with a long chord lead to high-induced drag. The greater the AOA, the greater the induced drag, therefore inversely when an aircraft is flying at a higher speed and the angle of incidence is closer to the relative wind, the induced drag decreases.

2.3.1.4 Total Drag

The sum of the drags will give you the total aircraft drag. Due to the induced drag decreasing with an increase of airspeed and the parasitic drag increasing with an increase in airspeed, an intermediate airspeed can be determined where induced drag will equal the parasitic drag, causing the minimum total drag (*Figure 2.7*). Additionally, total drag x airspeed = power used by aircraft, which allows for a second airspeed with minimum power consumption. A third airspeed will provide the most efficient fuel to distance ratio, usually being faster than the other two factors. These will all change depending on the altitude and temperature and largely contribute to the aircraft design.

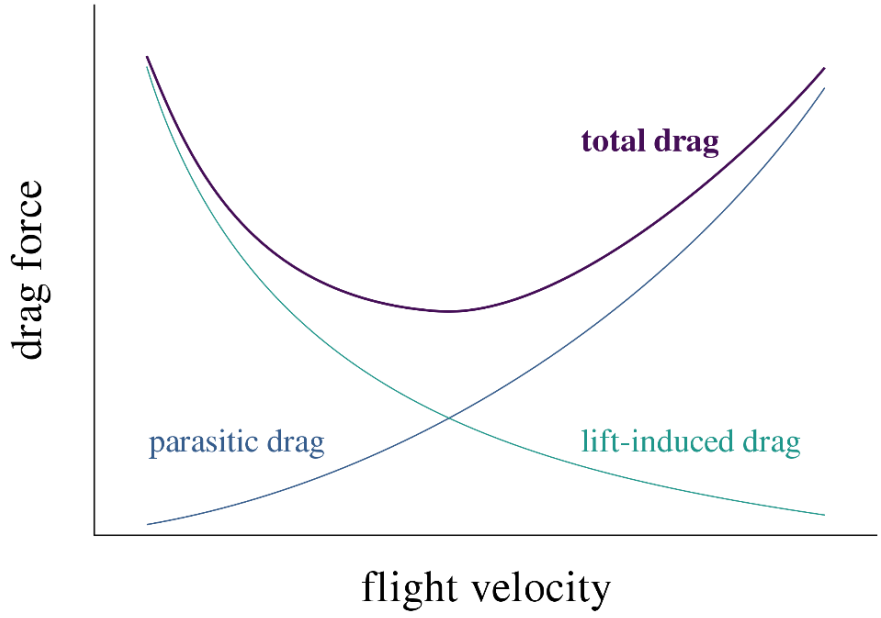

Figure 2.7: Parasitic Drag – Induced Drag Relationship

The basic rule-of-thumb for flying is producing enough lift to overcome aircraft weight at any given airspeed and for thrust to be greater or equal to the total aircraft drag. Flight cannot be sustained in fixed-wing aircraft if either of these criteria are not met. The thrust should be capable of providing speeds much higher than the minimum airspeed in order for turbulence or any manoeuvring to not increase drag or reduce lift, causing the aircraft to stall. The practical minimum flight speed v_{min}, is a margin above the absolute minimum speed.

2.3.2 Fixed-Wing Lift

The lift equation can be modelled by (Glenn Research Center, 2021):

$$L = C_L \times \frac{\rho \times v^2}{2} \times A$$

As previously mentioned, lift in wings is modelled by the above equation, where C_L is the coefficient of deflection of the airstream in reference to the wing area, S. The wing shape, size, Reynolds number and wing incidence determine it. It increases with incidence, finding a max value ($C_{L.max}$), before sharply reducing (Hoerner, 1965).

Absolute minimum flight speed with no margin can be obtained using the equation (Austin, 2010):

$$V = \left(\frac{2L}{\rho \cdot S \cdot C_{L \cdot max}}\right)^{1/2}$$

However, a more realistic value can be obtained by allowing a margin in the speed or lift coefficient, where C_{Lo} (operating C_L) should be less than $C_{L.max}$ for that airfoil section (Houghton, Carpenter, Collicott, & Valentine, 2013). A C_{Lo} of 0.2 less than the $C_{L.max}$ is generally a good estimate for the minimum speed for level flight in smooth air, however, realistically; a smaller C_L value would just result in better flight characteristics. A $C_{L.max}$ of ~1.2 is a typical value that can be found on moderately cambered wings that do not have a flap. Flaps are not commonly found on UAV, as they often add complication and weight. Generally, the longer the wing the greater, the wing efficiency

2.3.2.1 Wing Loading

The wing loading is the mass of the aircraft, divided by the area of its wing. Vehicles with larger surface area to mass ratios, are more prone to being effected by gusts of air, as they generate an aerodynamic force, however they also produce more lift (Science Learning Hub, 2021). In contrast, the greater the mass, the greater the inertia, hence the smaller the acceleration from imposed forces. Therefore, a more densely packed aircraft is less affected by turbulence. This can be seen by comparing turbulence factors of a flying wing to that of a rocket. In this case, UAVs have the advantage over manned aircraft in that they can be more densely packed than if a human was required.

The problem encountered by fixed wings is that their surface area is dependent on the speed required for take-off and landing, therefore there may be the need for compromise between turbulence and low-speed performance. Alternatively, some jets have the ability to change their wings surface area (Page, 1965).

Typically, the lower the value of wing loading, the greater the initial response to air gusts, hence an aircraft with a larger surface area to mass ratio will have a greater vertical acceleration in response to a vertical gust of wind. However, on the opposite spectrum aircraft with a high wing loading produce high induced drag at low speeds.

In the case of most UAVs, their wing loading is extremely low, making them extremely vulnerable to turbulence, such as gusts of wind, that they cannot be flown in these conditions.

2.3.3 Rotary-Wing Drag

Rotary-wing aircraft effectively work the same way as fixed wing aircraft, except the wing is replaced by a blade that acts in a rotational fashion. The movement and shape of the blade creates a lower pressure above the blade and a higher pressure below, it therefore

generating lift (Rotaru & Todorov, 2017). In addition, the rotor disc area in which the blades are rotating creates an additional pressure gradient above and below it to provide extra lift.

2.3.3.1 Induced Drag

While at hover, a rotary wing vehicle pulls down air from above which is distributed around the rotor disc area. However, once the helicopter starts to move forward, part of the rotor disc area moves into undisturbed air, which causes a higher angle of attack compared to the part of the rotor working in the descending air, which in turn causes the part of the rotor disc area in the undisturbed air to produce more lift. As the rotary wing vehicle reaches higher speeds, more of the rotor disc area is in the undisturbed air, up to ~70 km/hr, where the rotor disc area is no longer affected by the descending air of its own rotary movement. At this point, the induced power and drag of a rotary wing aircraft can be modelled in a similar fashion to that of a fixed wing.

Effectively, there are three flying states for rotary wing aircraft, which are hovering, where all of the rotor disc area rotates in descending air, hence not affected by the lift differential. Low speed flight, where the rotor disc area rotates in partial undisturbed air, hence is affected by the lift differential. Moreover, high-speed flight, where all of the rotor disc area rotates in undisturbed air, hence it is not affected by the lift differential (Copters, 2021).

2.3.3.2 Parasitic Drag

Similar drag affects rotary wing aircraft as is found on fixed-wing aircraft, however as a result of the more complex flight path of the rotor, profile drag or profile power are affected by different factors, whereas parasitic drag consists of the fuselage, undercarriage, cooling drag, etc., which can be calculated in a similar fashion to that of the fixed-wing. (Newman, 1994)

2.3.3.3 Profile Drag/Power

Profile power for rotor blades in hover is usually computer calculated, with the use of blade element theory. By splitting the blade into separate elements and calculating the local element velocity in reference to its distance from the central rotating hub, the elemental drag can be determined and from there, the power.

Due to the effects of the induced drag and an increase in lift when flying forwards, the profile power changes in forward flight. In forward flight, the blade elements no longer follow a circular path, instead being modelled by a spiral path, which changes its symmetry when accelerating. This forward flight results in a higher profile power when compared to hover, due to the increase in lift, as well as the blade elements experience translation, as well as rotation.

However, at speeds approaching the rotation speed of the rotor, the retreating side of the rotor approaches stalling speed, hence providing less lift whereas the advancing side of the rotor moves relatively faster providing more lift, therefore, single rotary air vehicles experience a sideward rolling force, due to a separate lift differential (Rotorworks Inc, 2019).

2.3.3.4 Air Turbulence Reduction

It is desirable to reduce the effects of air turbulence, as turbulence can affect on-board sensors and navigational sensors. To achieve this, it is best to design for high aerodynamic stability and large aerodynamic surface area, with a high surface area to mass aspect ratio.

When designing an airframe, it is best to get the frame to near neutral aerodynamic stability, to ensure minimal air turbulence disturbance. However, with this it will require systems that ensure the aircraft continues in the desired heading and does not wander off course from external factors, such as wind or payload movement. These systems would need to be included in an automatic flight control system (AFCS), which controls and maintains the aircraft flight path (Flight Mechanic, 2021).

2.3.3.5 Rotary Wing Loading

Helicopters tend to have very high wingtip speeds ~200 m/s with very high wing loading >4000 N/m^2, therefore have a low response from vertical gusts of wind (Fradenburgh, 1991). However, they are still very prone to horizontal gusts, due to having a single rotor. Forward flight produces vibrational forces; however, these are predictable frequencies and can be isolated with well-tuned airframe-to-rotor suspension.

2.3.4 VTOL (Vertical Take-Off Landing) Configurations

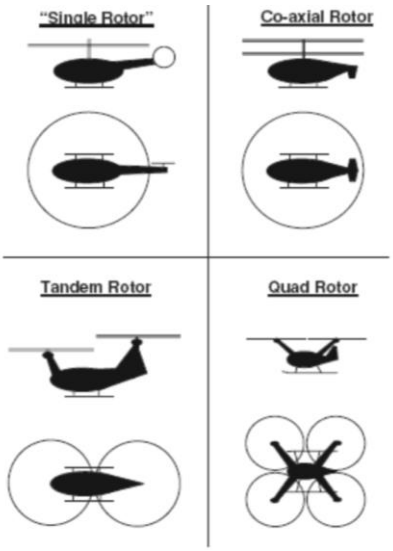

Figure 2.8: Different VTOL configurations (Austin, 2010)

2.3.4.1 Single Rotor (Penny-farthing)

According to Newton's third law, "every action has an equal and opposite reaction", the rotation of the rotor, creates a rotational force on the aircraft body. A second tail rotor is used, to counteract this, which exerts a horizontal force in order to eliminate the rotational force created by the main rotor. This however increases the power demands of the main rotor and the asymmetry of the design introduces complexity to the control design. Single rotor aircraft tend to be more efficient, due to the longer the blade length, the higher the efficiency (Position Partners, 2020).

2.3.4.2 Co-axial Rotor

This configuration is not very common in manned aircraft as it has a much-increased height, which creates difficulties in maintenance and storage; however, this problem is not present for UAVs. This configuration eliminates the need for a tail rotor, as it is more symmetrically stable than a single rotor aircraft, without adding complexity to the automatic flight control system (AFCS) as the power units and transmission are similar (English, 2020). Additionally, its symmetry allows it to respond the least to air turbulence compared to other helicopter configurations. Decreasing the rotor tip speed lowers noise generated; however, this decreases the blade loading and makes it more vulnerable to vertical gusts. Coaxial rotors outperformed the equivalent single rotors with the same total number of blades, blade loading and tip speed in hover flight, due to a lower power loss as some of the single rotor aircrafts power is diverted to the tail rotor. In addition, the effects of 'swirl' energy in the rotor

downwash are reduced, hence even less power is wasted. The rotor gap, the distance between the two rotors, is defined as a percentage of the rotor diameter. As the power loading of a typical coaxial rotor aircraft with inter-rotor spacing of 11.25% increases, so too the does the hover efficiency (thrust obtained from same amount of power). Heavier aircraft, with higher power loading have greater effects of induced swirl (Kim & Brown, 2010).

2.3.4.3 Tandem Rotor

The rotor mass to lift ratio greatly increases, the longer the blades of the propeller are, therefore, a more efficient solution is to increase the number of smaller rotors for aircraft above a specific gross weight, as seen in the chinook, creating a more power efficient and symmetric configuration compared to the single rotor (Yoma, 2017). This gross weight is increasing with the development of better materials. However, until VTOL reach such a gross weight, there is no point developing tandem UAV.

2.3.4.4 Quadcopter

The Quadcopter works on a similar principle to the tandem rotor in that increasing the number of small propellers, increases the power efficiency rather than using just one large propeller, however at a loss of thrust efficiency, due to shorter blades. To fly in different directions, the drone varies the speeds of its motors, causing a greater amount of lift on the different sides, therefore allowing the quadcopter to tilt in the direction of flight.

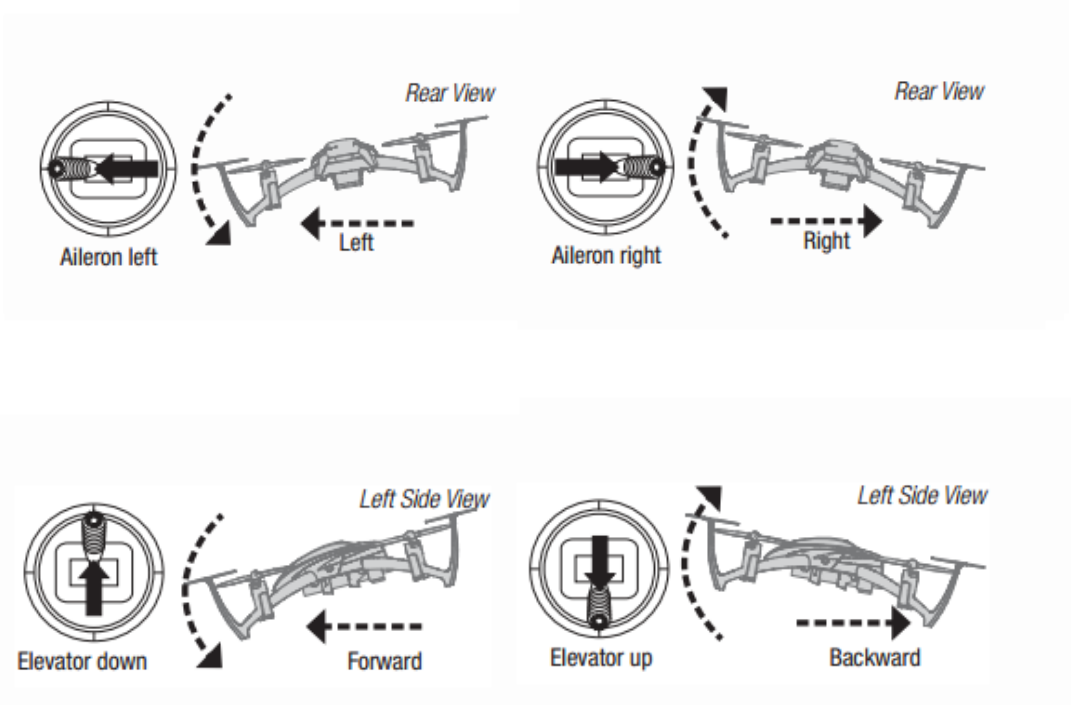

Figure 2.9: Quadcopter Flight Techniques (UAV Coach, 31)

2.3.4.5 Hybrids

Rotary wing helicopters are limited in cruise speed to 370 km/hr, due to the stalling of the retreating blades, however for more range a faster aircraft is required. Yet the ability for VTOL is a valued asset, therefore came the desire to combine the hovering ability of a rotary aircraft, with the cruising flight of an HTOL.

Current methods of achieving this design include tilt rotors, such as osprey (Airforce Technology, 2021), where a rotor is attached to the ends of the wings, which is capable of tilting forward through 90°, acting as a propeller in cruise flight. The tilt rotor aircraft keeps the wing horizontal and tilts the rotor relative to the wing, using pylons whereas a tilt wing aircraft has the wing and the rotor as one assembly and tilts these relative to the fuselage (Young, 2018).

Either tilt rotor can have an engine for tilting the rotor based within the rotor pylons, as a result tilting with the rotors, or it can be fixed to the fuselage, and use gears and shafts that pass through the wing hinge bearings to tilt the rotor. Alternatively, in the fixed wing aircraft the engine is most commonly fixed with in the wing and tilt with it, or similar to the tilt rotor can be placed within the fuselage (Chopra & al., 2011).

The tilt rotor proved to be more efficient in hovering, whereas the tilt wing proved to be more efficient in cruise flight. However, due to the excessive weight for producing this ability, they miss payload carry capacity.

2.4 SIMILAR DRONES

Currently there are not a lot of drone designs that are capable of stable-bodied flight, especially ones that are capable of doing so in multiple different directions. Those that are capable of doing so, employ some form of hybrid method, which include tilt motor or tilt wing. Of these, very few are capable of keeping stable bodied flight in more than one direction of flight, generally being forwards and backwards.

2.4.1 Standard Quadcopters and Multi-copter

Although not capable of flying in any direction without affecting its roll or pitch, the typical multi-copters are well equipped for stable hover flight, and this has only been improved in recent years, with increased IMU sensitivity and better microcontroller systems. A recent example showed a quadcopter capable of balancing a wine glass without spilling the contents of the glass, going to show the leaps that have been achieved in flight stability for standard

quadcopters. Additionally, multi-copters with up to eight propellers have proven to be extremely reliable in hover, with the greater than number of propellers, the more stable the drone (Zhu, Nie, Zhang, Wei, & Zhang, 2020).

The stability factor of these drones have found there use in aerial videography and photography, as well as surveying.

Figure 2.10: Octocopter (Microtell Informatics, 2021)

2.4.2 Dual-axis Tilt Rotor

The most common of these designs is the dual-axis tilt motor, which has become well spread amongst racing drones. In this setup, the propeller can be pitched forwards on a rotating pylon, in order to change the angle of attack. In this case, the body is capable of remaining stable as it flies forwards or backwards, however this sort of drone cannot change direction easily without rolling in the direction of the motion (Junaid, Sanchez, Bosch, Vitzilaios, & Zweiri, 2018). To fly in the desired direction without rolling, the drone would first have to turn to face in the direction of flight by using its yaw factor, which is a relatively slow method of changing direction.

Figure 2.11: Tilt-Rotor Quadcopter (Lanner, 2017)

2.4.3 Omnidirectional Tilt Rotor

Similar to the dual-axis tilt rotor the omnidirectional tilt rotor tilts the propeller by rotating a pylon, hence changing the AOA of the motor, however with the difference being that has more propellers. The only versions of this currently present are the Voliro drone and the New Atlas drone, both originally developed at ETH in Switzerland. These models have six and twelve coaxial rotors respectively, mounted on six arms that can each rotate 360°, providing 12 degrees of freedom. This set up allows the New Atlas to fly and hover in different orientations, which as a result, also makes it capable of flying in any direction keeping the body completely stable, as four of the propellers would allow it to maintain altitude, while the remaining two allow it to move in the desired direction.

This design would be a viable solution to ensuring completely stable-bodied flight in drones, however it only allows for two of the propellers to provide thrust in any given direction at a time, which is not create the maximum speed capabilities, that would be provided by more propellers providing thrust in a given direction. Therefore, to optimize this design, a design should be created that allows for infinite degrees of freedom and, hence not be limited to the 12 degrees of freedom (DOF) of these drones. Additionally, the use of six arms limits the shape to which this drone can be designed, therefore limiting the aerodynamic capabilities of such a drone frame, and hence to further improve the design, a design should be developed with a reduced number of arms.

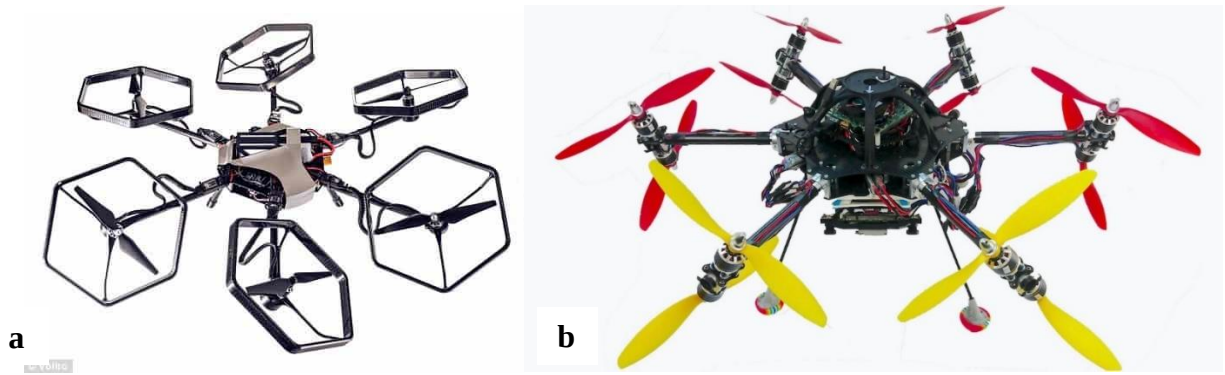

Figure 2.12: Omnidirectional Tilt-Rotor Drones (a)Voliro Drone (EP Films, 2019) *(b)New Atlas Drone* (Blain, 2020)

2.4.4 Four-Arm Omnidirectional Tilt Rotor Drone

Similar to the Voliro and the New Atlas drones developed at ETH, this drone works using the principle of changing the AOA of the motors by rotating the pylon on which the propeller is attached. This design would also be capable of maintaining stable bodied-flight and due to only having four arms, instead of the six present on the previously mentioned drones, it would be a more aerodynamic design, having less parasitic drag. However, this comes with a reduction in total output power compared to the six/twelve propellers of the drones designed at ETH, as well as a decrease in degrees of freedom with this design only having only 8 degrees of freedom, resulting in less overall stability to the drone.

At this stage, there appear to be no drones of this design that have yet been developed.

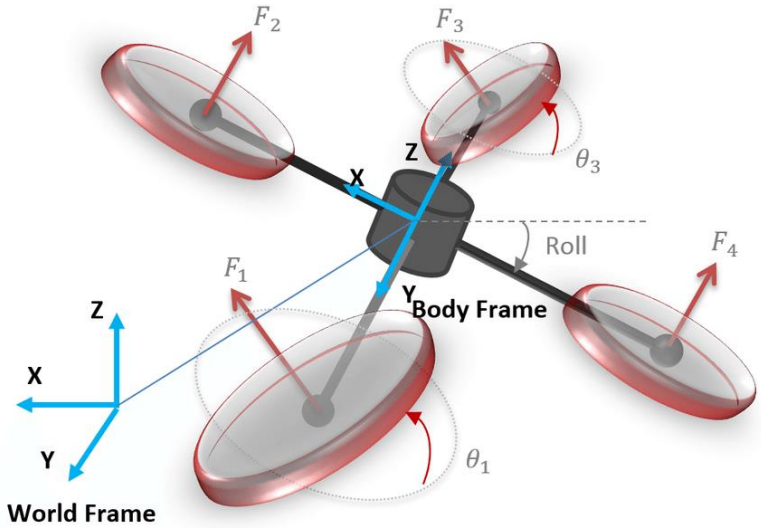

Figure 2.13: Four-Arm omnidirectional Tilt Rotor Drone (Nemati, Soni, Sarim, & Kumar, 2016)

2.5 SUMMARY AND IMPLICATIONS

From the information provided from the literature review, it can be seen that drones are an exceptionally useful field with a lot of room for growth and hence an ever-expanding topic that can lead to many more developments in technology. Various different aircraft designs allow for stable flight within drones; however, the goal is to develop a UAV that is capable of stable bodied flight while hovering as well as in directional flight. This has been proven most practical by means of combining VTOL, with certain flight characteristics of HTOL aircraft in the form of tilt-rotor aircraft.

Most drones fly by tilting in the direction of flight, either through pitching or rolling in that direction, with very few drones, allowing for stable-bodied flight by eliminating the effects of pitching and rolling. Current designs that are capable of stable-bodied flight are omnidirectional tilt rotor drones, such as the New Atlas and Voliro drones, which are capable of flying in any direction and in any orientation, which currently have 12 degrees of freedom.

The aim of this project will therefore be to see if these designs can be further developed to create a drone with infinite degrees of freedom, while at the same time being more aerodynamic. Elements that will need to be considered for this design include its take-off weight, its output power, its wing loading ability and its aerodynamic design.

Chapter 3: Research & Design

This chapter will cover the different proposed concept designs (Section 3.1.1), then go into further detail on the design selected for further development (Section 3.1.2), which best achieves the objective of stable-bodied flight, outlined in section 1.3 of Chapter 1. Section 3.2 will cover the various components that are needed to get a functioning quadcopter solution, selection of the components used, as well as the code and requirements for running them.

3.1 DESIGN CONCEPTS

In designing the drone frame size, weight and shape had to be taken into account. The drone had to be large enough to carry all the required components for drone control, as well as controlling the components affecting stabilisation, while at the same time allowing for the size of the propellers. All of these components add to drone's weight; the lift provided by the motors had to be sufficient for flight. Optimally, the shape would be as streamlined as possible.

An indication of the aerodynamics of the airframe is the loss of airspeed of the relative wind as the drone flies in that direction, due to the effects of drag. Therefore, when discussing the aerodynamics of a frame, the loss in airspeed will be referenced. The streamlines of each of the drones were analysed in forward flight, as this would be the natural direction of flight. The number of the streamlines shown are dependent on the amount of surface area and the variation of reference points; therefore, the designs with more complex surface areas have more streamlines.

3.1.1 Initial Concepts

3.1.1.1 Concept 1: Uni-directional Tilt Rotor

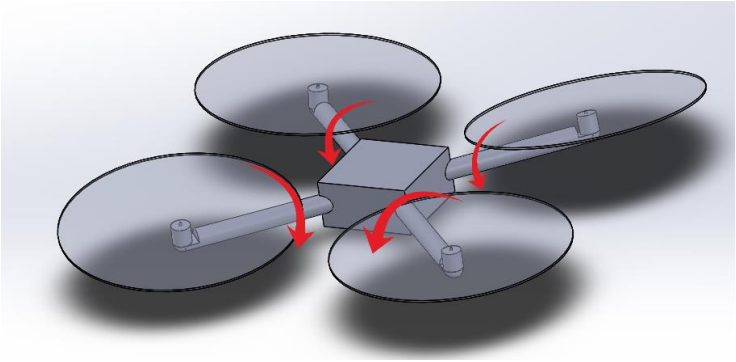

The uni-directional tilt rotor setup, similar to one of the previously proposed designs (Nemati, Soni, Sarim, & Kumar, 2016), works by changing the angle of attack of the rotor

through rotating the rotor arms from within the body of the drone. This would be a simple design to build, requiring just four additional motors on top of the four thrust motors for rotating the arms. To efficiently apply this design, the drone body would need to be evenly balanced, so as not to cause it to fly unstably, creating drag. For forward flight with this model, two methods of flying can be used.

The first method of flying would allow two of the propellers to be facing upwards to provide lift for the drone, while the other two side motors face in the direction of flight. This flight pattern means that the forward thrust would only be because of the two side propellers. Hence, you would not have all of the propellers angled in the direction of flight, however depending on the lift force of the upwards facing propellers. It means that two forward facing propellers could have an AOA that is almost directly in line with the direction of flight. This flight pattern would be very easy to enact, as two of the propellers are just facing upwards, while the other two just need to be rotated forward in order to fly in the desired direction.

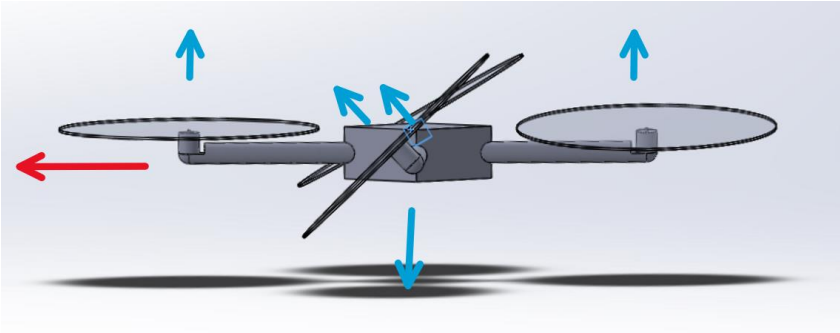

This design's first method of flying does not create a large amount of turbulence, with a maximum loss of airspeed of approximately 17 m/s on the trailing end of the drone (*Figure 3.1*). The profile drag, is affected mainly by the cross section of the angled body, with a slight influence from the arms that are perpendicular to the relative wind, where the loss in airspeed behind the arms and motors is approx. 4 m/s. Using Pythagorean theorem the maximum drag force could be calculated to ~0.0028 N and due to their being a positive force in the y-axis of 0.016 N, this design provides a small amount of lift (see *Table 3.1*).

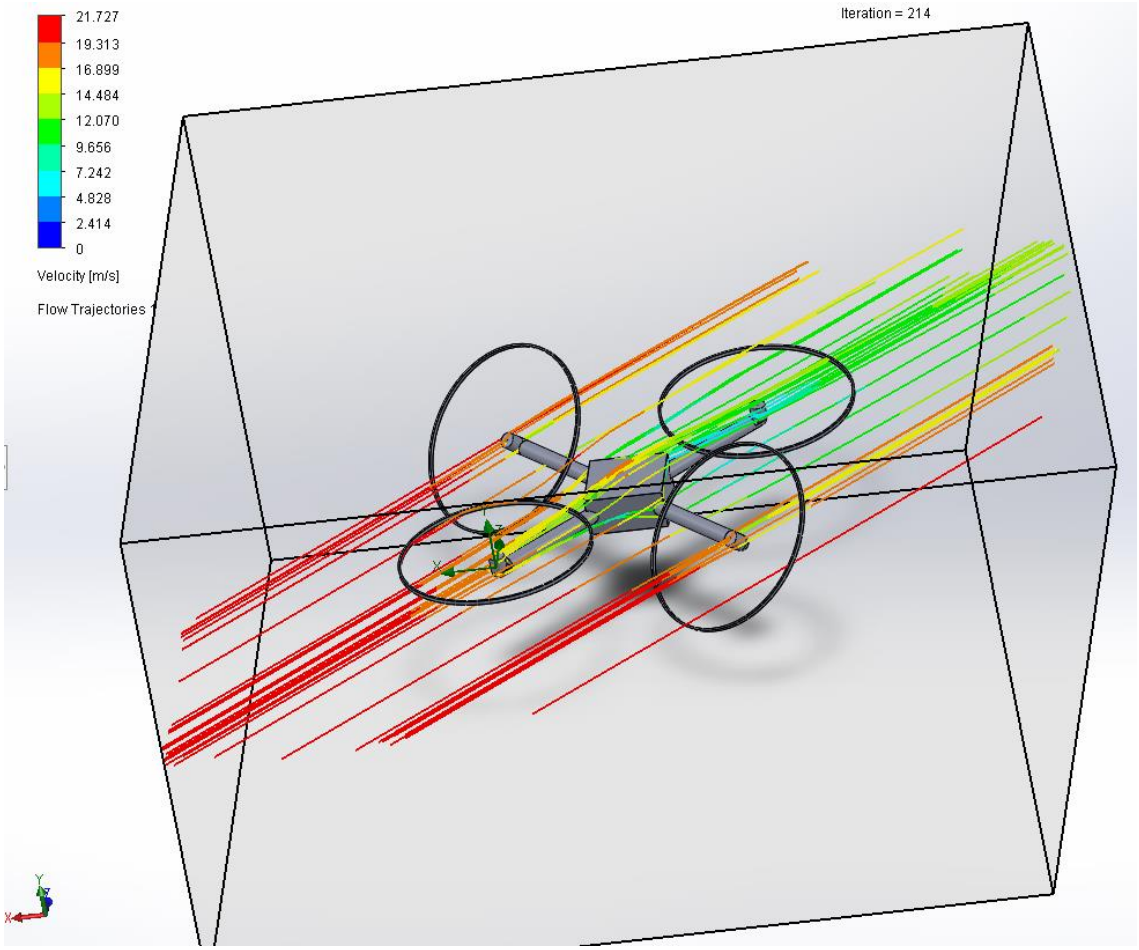

Figure 3.1: Aerodynamics of first method of flying for uni-directional tilt rotor

Table 3.1: Aerodynamic Data of First Flight Method of Uni-directional Tilt Rotor Drone

Goal Name	Unit	Value	Averaged Value	Minimum Value	Maximum Value
GG Maximum Total Pressure 1	[Pa]	101737.1465	101737.1271	101737.0073	101737.2581
GG Maximum Total Temperature 1	[K]	293.3952035	293.3951555	293.3951189	293.3952229
GG Maximum Velocity 1	[m/s]	22.39925789	22.39520676	22.39034577	22.39992261
GG Maximum Velocity (X) 1	[m/s]	0.474209463	0.619449457	0.238169254	2.056586429
GG Maximum Velocity (Y) 1	[m/s]	10.27271217	10.26608536	10.26014501	10.27656376
GG Maximum Velocity (Z) 1	[m/s]	17.52406614	17.5761892	17.50900516	17.6361865
GG Force (Y) 1	[N]	0.016438154	0.016253378	0.015851052	0.01667727
GG Friction Force (X) 1	[N]	-0.00208461	-0.002091888	-0.002112447	-0.002074814
GG Friction Force (Z) 1	[N]	0.002086515	0.002080389	0.002069275	0.002091037

Iterations [ ]: 214

Analysis interval: 27

The second method of flying with this drone has each of the propellers changing their angle of attack in order to fly in the desired direction. With this design, none of the propellers would be facing directly in the direction of desired flight; however, all of the propellers would be contributing to flying in the desired direction. Determining the correct angles for the drone

to produce sufficient lift, while at the same time flying forward can add complexity to the design, especially when taking into account the effect of two propellers working counter to each other as seen towards the back end of the drone.

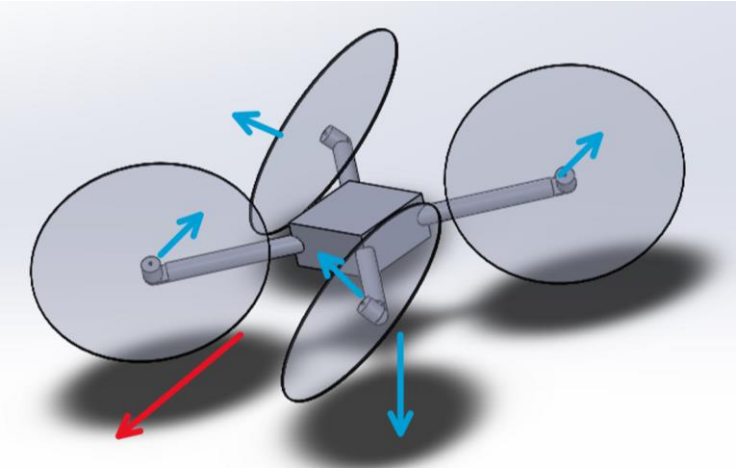

The design's second method of flying also does not create a large amount of turbulence, with a typical loss in airspeed of approximately 17 m/s, similar to that of the other method of flying. However, in contrast to the previous method, this method of flying has a large surface area, directly perpendicular to the relative wind and has a flat trailing end (*Figure 3.2*). Therefore, the profile drag of this method of flying is higher, with the highest drop in air speed of approx. 19 m/s being directly behind the trailing edge of the drone (see *Table 3.2*). The loss of air speed because of the arms and motors is slightly higher at approx. 6 m/s compared to the previous method of flying, due to the second rear arms being situated in the already disrupted air stream from the front arms. The maximum drag force is ~0.0037 N, being slightly higher than the previous method of flying, while there is a negative force in the y-axis of 0.02 N, hence a downwards force when flying in this fashion.

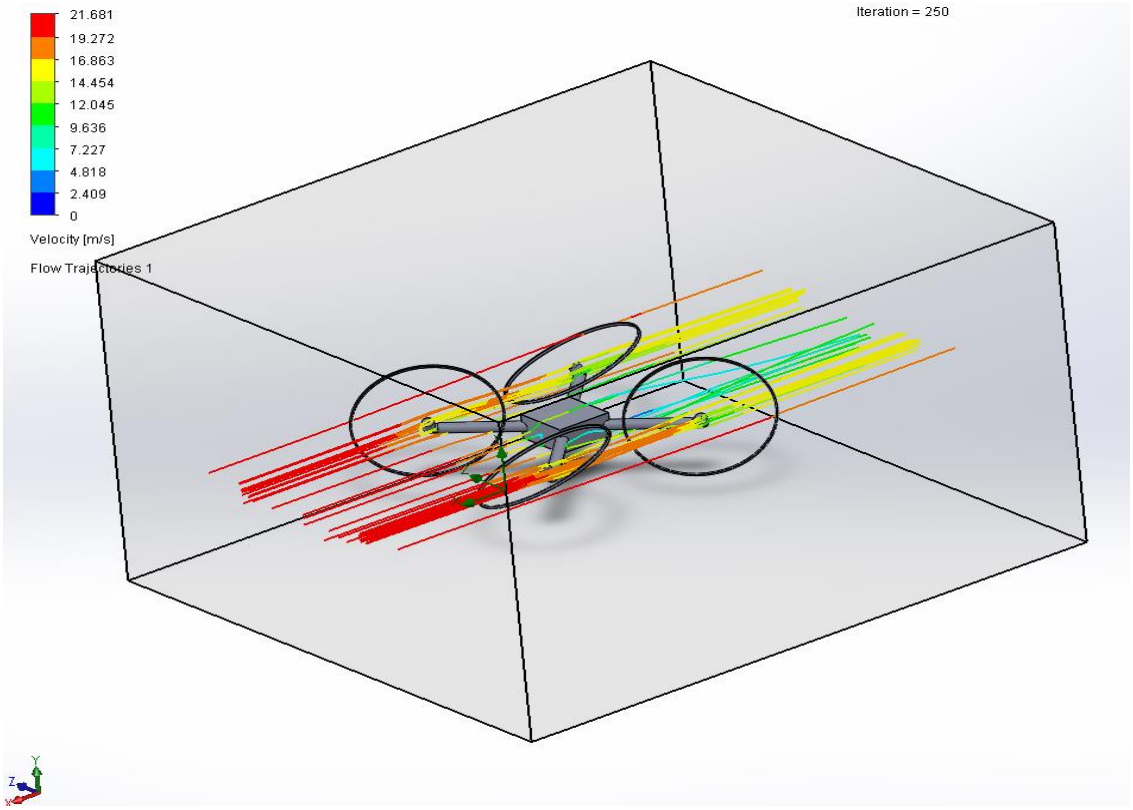

Figure 3.2: Aerodynamics of Second Method of flying uni-directional tilt rotor

Table 3.2: Aerodynamic Data of Second Flight Method of Uni-directional Tilt Rotor Drone

Goal Name	Unit	Value	Averaged Value	Minimum Value	Maximum Value
GG Maximum Total Pressure 1	[Pa]	101881.9514	101873.3808	101865.6189	101881.9514
GG Maximum Total Temperature 1	[K]	293.3990131	293.3990524	293.3989353	293.3992545
GG Maximum Velocity 1	[m/s]	23.55469359	23.409998	23.21912433	23.55469359
GG Maximum Velocity (X) 1	[m/s]	1.525869103	1.612816772	1.166767545	3.41815182
GG Maximum Velocity (Y) 1	[m/s]	17.23102984	17.80060526	16.62648118	18.91391485
GG Maximum Velocity (Z) 1	[m/s]	7.849449414	8.020596173	7.765848742	8.333991659
GG Force (Y) 1	[N]	-0.02076998	-0.021298137	-0.021970047	-0.020690444
GG Friction Force (X) 1	[N]	-0.00369065	-0.003711996	-0.00377931	-0.003656179

Iterations [ ]: 209
Analysis interval: 27

These two methods of flying can be combined in order to allow the drone to fly in all directions, with ease. The current design always leaves one face of the drone creating a much greater surface area for air resistance, depending on which sides have a flat leading and trailing edge perpendicular to the relative wind. However, this can be minimized by changing the shape of the design into a circular shape, as it would mean that no one surface has a less aerodynamic shape.

3.1.1.2 Concept 2: Tip-tilt Rotor

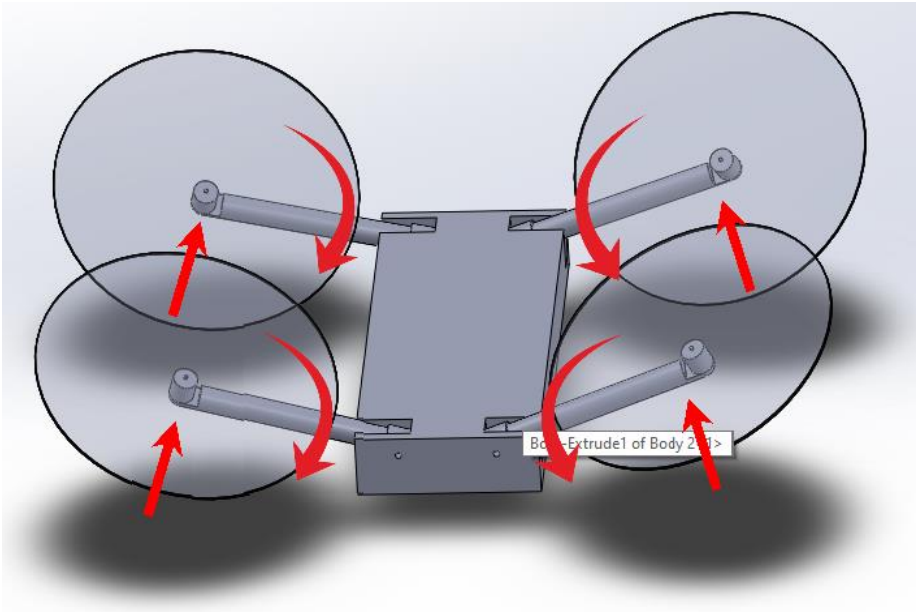

This design is inspired by the helicopters from James Cameron's 2009 Avatar movie. In this design, the propellers are situated on either side of the drone and are capable of rotating forwards and backwards, as well as tipping up and down in order to change its angle of attack. This design is more optimal for forward flight and would allow for easy rotation around the centre of the drone. The ability of the arms to move up and down are in order to allow each arm to adjust its position independently in order to adjust to external factors such as wind or to allow it to fly in various different directions.

This drone design would allow the drone to easily direct all of its propellers in a forward direction, so that it can fly in said direction, which would result in the drone being a faster design then that in concept 1. To fly in a sideward direction, the angle of the arms would be changed, so that the net force would be in the desired direction, while still maintaining the appropriate lift force, to counter the force of gravity. This design would not be as fast at flying in any direction as concept 1.

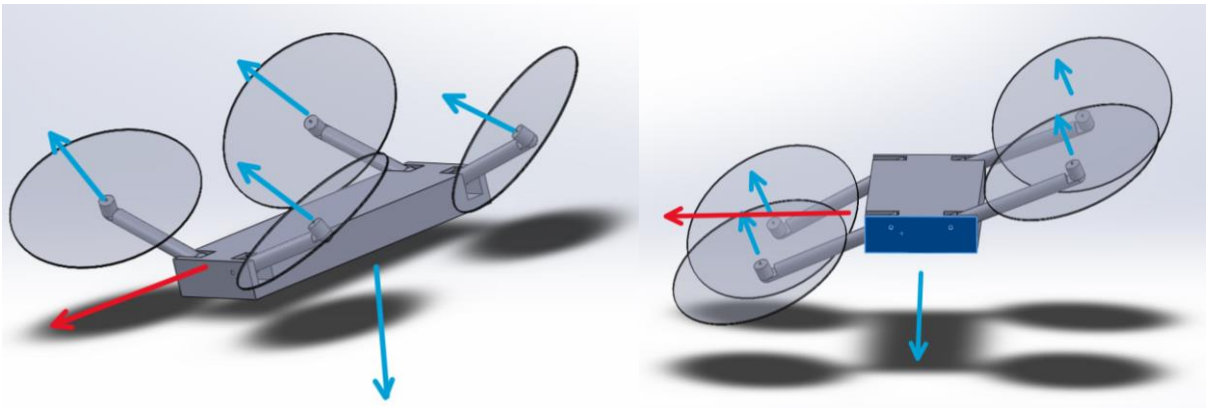

Concept 2 also does not create a large amount of turbulence behind the drone, with the loss in airspeed being similar to that of the previous design at about 17 m/s, however in this design, the head disturbance caused by the form drag, causes the effects of turbulence to be seen just after the nose of the drone, with airspeeds reaching negative values, due to the effects of swirling. Similar to the second flight method of concept 1, there is a greater loss in airspeed experienced after the rear arms at ~6 m/s, due to the air disruption of the first arm affecting the head airflow of the second arm. The maximum friction force experienced by this design is ~0.0042 N, which is higher than the friction force experienced by the previous design (See *Table 3.3*). Additionally, this design has a negative force in the y-axis of ~0.00044 N, showing that there is a downwards force on this design in forward flight due to its shape.

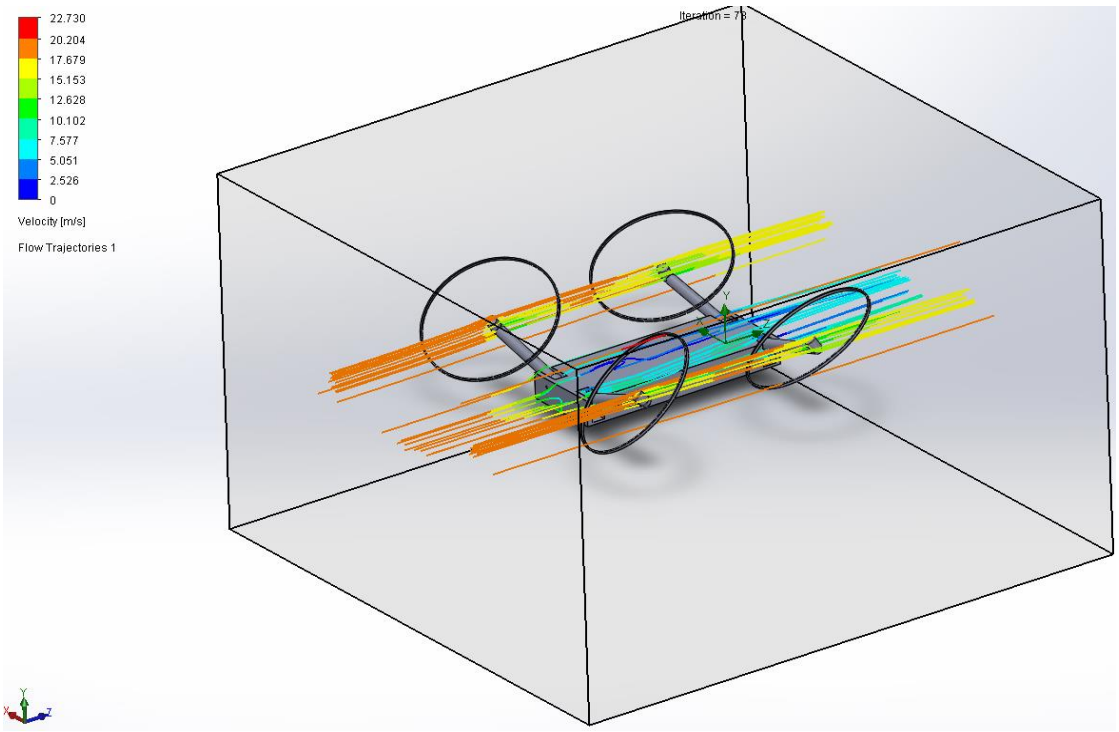

Figure 3.3: Aerodynamics of tip-tilt rotor drone

Table 3.3: Aerodynamic Data for Tip-Tilt Rotor Design

Goal Name	Unit	Value	Averaged Value	Minimum Value	Maximum Value
GG Maximum Total Pressure 1	[Pa]	101865.817	101892.0512	101865.2938	101913.2504
GG Maximum Total Temperature 1	[K]	293.401832	293.4019748	293.3997	293.4042449
GG Maximum Velocity 1	[m/s]	23.94530847	23.75237947	23.47061126	24.0208649
GG Maximum Velocity (X) 1	[m/s]	12.50345615	12.003811	11.24118675	12.78035809
GG Maximum Velocity (Y) 1	[m/s]	15.01465446	15.12341538	14.64344166	15.81021894
GG Maximum Velocity (Z) 1	[m/s]	23.43985771	23.28999061	23.05055458	23.52324839
GG Force (Y) 1	[N]	-0.00082382	-0.001961384	-0.003324494	-0.000435382
GG Friction Force (Z) 1	[N]	0.004171341	0.004005433	0.0038387	0.004171341

Iterations [ ]: 78

Analysis interval: 24

This drone could also be redesigned to have a rotor coming from each face of the drone, rather than just the two side faces, as seen in the above image. Redesigning the drone in this manner would mean that it would be better capable of flight in any direction and possibly be more stable, with a more balanced shape; however, it would come at a loss in ability for forward flight. To increase the aerodynamics of the body itself, tapered edges would reduce the effects of profile drag on the design.

The complexity in this design arises in ensuring that the drone body remains flat, while the angle of attack of each of the propellers is changed. In addition, allowing each arm to tilt up and down, while at the same time being able to rotate these arms would introduce additional complexity and weight, as the arms would need to be moved using individual motors.

3.1.1.3 Concept 3: Multi-Directional Gimbal-Tilt Rotor

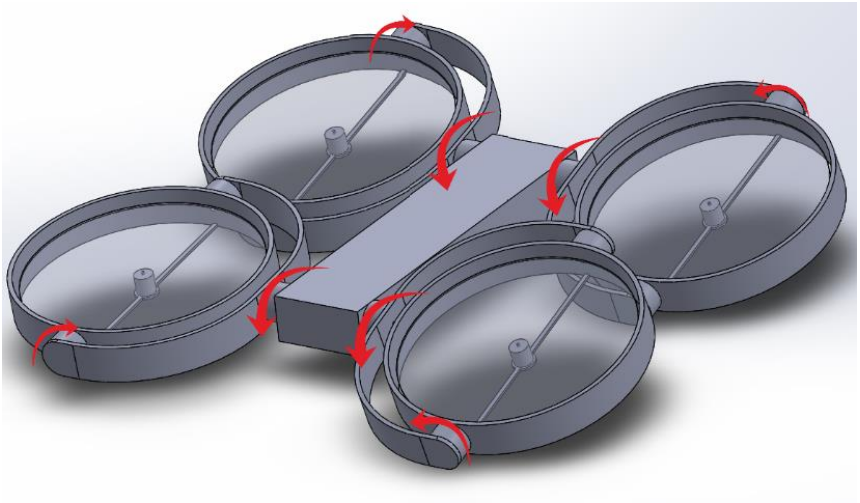

Concept 3 acts on using individual gimbal systems for each of the propellers, in order to allow the rotors to have infinite degrees of freedom and allow the drone to fly in any given

direction. This design has gimbals on both of the side faces of the drone, which would be actuated using motors that allow for positional control, therefore maintaining the given angle. The positional control of the rotors could be achieved by either directly mounting the motors to the different rotating joints of the drone, which result in a large number of motors being required in order to provide the correct positioning of the rotors, especially, when maintaining a well-balanced design. The other option for providing actuation of the gimbals would be to use cables in a pulley system, which would allow the motors to remain on board the body of the drone, removing the need for directly mounting the motors to the separate gimbal joints.

For forward flight, the drone would have to tilt the gimbal arms forward, allowing all of the motors to be facing in such a direction. To fly sideward, the motors connecting the gimbal arm to the ducts would rotate to allow the duct to face to the side and therefore allow for flight in that direction.

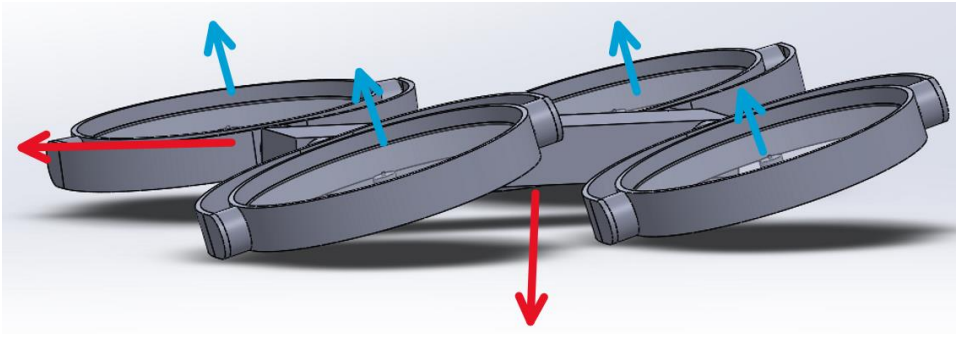

In contrast to the previous two designs, this model creates quite a bit more turbulence; however, in this case, a lot of the turbulence is because of the gimbal arms and ducts, rather than just the body. The greatest loss of airspeed still remains being behind the body at approx. 17 m/s as well, however, behind the gimbal arms, the loss in air speed reaches a maximum of approx. 12 m/s, with the trailing arms also being affected by the air flow following the leading arms (*Figure 3.4*). The drag force experienced by this design reaches a maximum of ~0.0167 N, which is significantly higher than the drag forces created by the previous two designs (See *Table 3.4*). In forward flight, this design has a positive force of 0.22 N in the y-axis, indicating that this design has an ever so slight lift advantage.

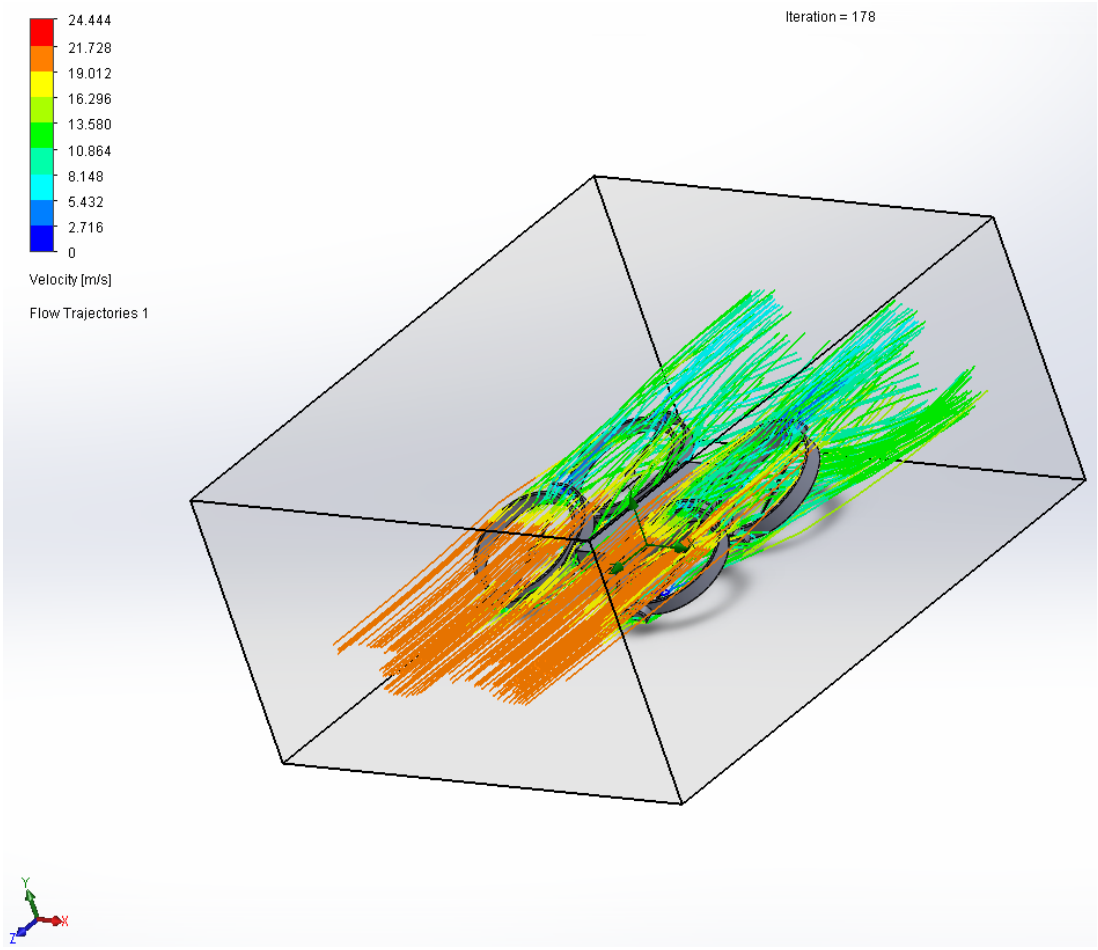

Figure 3.4: Aerodynamics of multi-directional gimbal-tilt rotor

Table 3.4: Aerodynamic Data for Multi-Directional Gimbal-Tilt Rotor

Goal Name	Unit	Value	Averaged Value	Minimum Value	Maximum Value
GG Maximum Total Pressure 1	[Pa]	102177.8488	102185.4974	102175.3119	102193.2278
GG Maximum Total Temperature 1	[K]	293.4860852	293.4196884	293.4017368	293.4860852
GG Maximum Velocity 1	[m/s]	25.49627387	25.49961642	25.42590913	25.52883405
GG Maximum Velocity (X) 1	[m/s]	14.80862709	14.82106886	14.77929636	14.89005881
GG Maximum Velocity (Y) 1	[m/s]	18.18510925	16.8826052	15.3853325	18.44149127
GG Maximum Velocity (Z) 1	[m/s]	5.25112904	4.967497554	4.339966982	5.339288106
GG Force (Y) 1	[N]	0.221441706	0.220854568	0.219935782	0.22190769
GG Friction Force (Z) 1	[N]	-0.01682287	-0.016787778	-0.016837278	-0.016736443

Iterations [ ]: 178
Analysis interval: 32

What this design lacks in aerodynamics, it more than makes up for in directional control of the rotors. By having each motor attached to its own gimbal system, it is capable of directing each of the rotors individually for it to constantly adjust their angles of attack to ensure stability. Complexity is introduced to this design, when taking into account all the various motors that need to be actuated in order to control the angles of the gimbals. This could be solved using

machine learning in which the drone controls the angles and of the rotors itself, deciding the optimal angles for maintain absolute stability within the body of the drone.

This drone, could either be designed with all of the propellers on the side faces, as seen above and similar to concept 2, or have a propeller on each face, similar to concept 1. Either design would come with its own advantages and disadvantages, as previously discussed with concept 2, where 2 propellers on either side would allow for better forward flight and 1 propeller on each face would allow for better dynamic flight. Flight in any direction would be very simple as the main motors attaching the gimbal system to the drone would rotate forward to fly in that direction, whereas the gimbals connected to the duct would just have to rotate sideward for the drone to fly in that direction.

3.1.1.4 Concept 4: Gimbal-Tilt Body

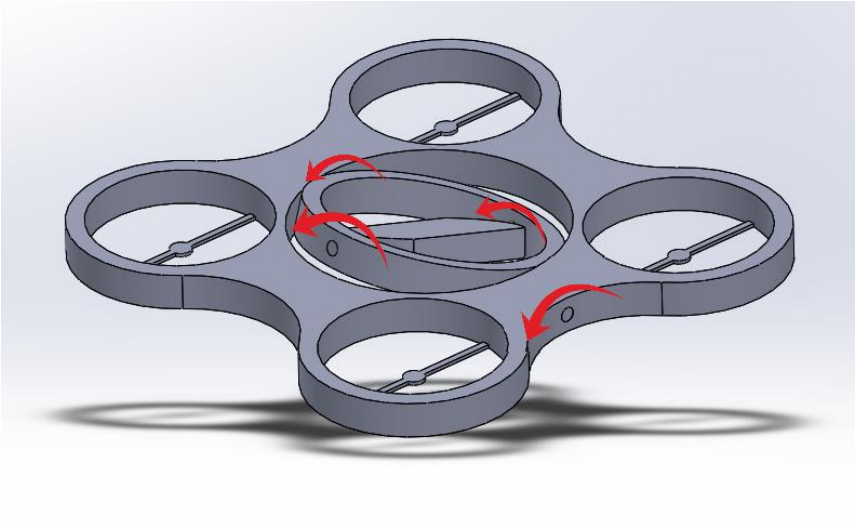

Concept 4 uses a simple gimbal concept in which the centre of the drone remains stable, while the rest of the drone moves around the central gimbal. This design is the simplest of all of the designs, as it does not require any extra on-board motors for it to change the AOA of the propellers, instead it would fly in a similar fashion to any other drone, simply by changing the rotation speed of each of the propellers in order to provide more or less lift. To ensure that the centre of the drone remains completely stable, the drone would require as little as possible friction between the different sections of the drone, to ensure that no swinging gets introduced to the payload. Additionally, this drone has a limited carry capacity, as it would only be able to carry a payload that is capable of fitting within the centre of the gimbal.

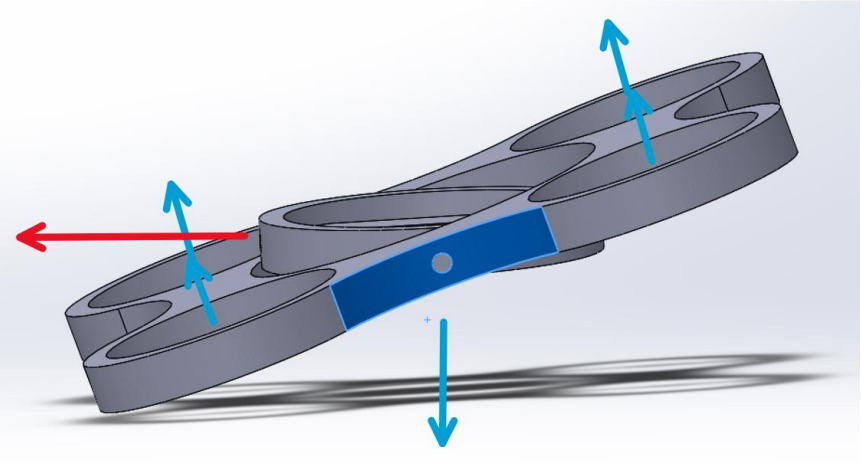

This design is the least aerodynamic of all of the designs, with high turbulence forming at the centre of the gimbal, with negative airspeeds, due to swirling, as well as behind the trailing edge of the drone, where there also small effects of swirling. The form drag of this design causes a large separation of flow behind the design leading to a great amount of instability behind the drone. The drag force on this design is ~0.014 N, which is only slightly lower than that experienced by the concept 3 design, however while flying forward, it has a negative force of ~0.014 N in the y-axis, meaning that there is a little bit of a downwards force from the design.

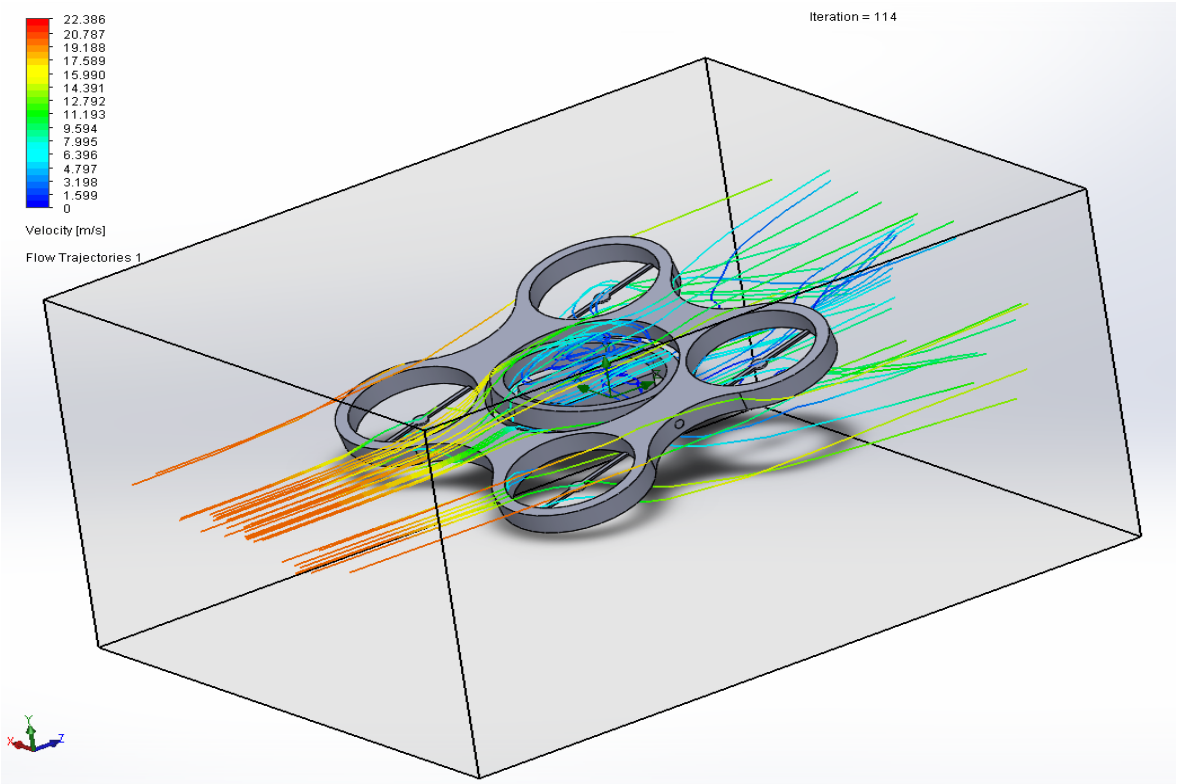

Figure 3.5: Aerodynamics of gimbal-tilt body

Table 3.5: Aerodynamic Data of Gimbal-Tilt Body Drone

Goal Name	Unit	Value	Averaged Value	Minimum Value	Maximum Value
GG Maximum Total Pressure 1	[Pa]	102745.8684	102742.7993	102721.3591	102754.7308
GG Maximum Total Temperature 1	[K]	293.4011637	293.4007842	293.3995526	293.4020427
GG Maximum Velocity 1	[m/s]	23.56642964	23.53331456	23.30327071	23.70818995
GG Maximum Velocity (X) 1	[m/s]	19.72027618	19.42267943	19.01209668	19.72027618
GG Maximum Velocity (Y) 1	[m/s]	15.46589573	16.59579399	15.38202506	18.16341034
GG Maximum Velocity (Z) 1	[m/s]	22.15243725	22.34752083	22.1462782	22.47490988
GG Force (Y) 1	[N]	-0.14854917	-0.145434637	-0.149731279	-0.142103226
GG Friction Force (Z) 1	[N]	0.014006121	0.013747637	0.013511357	0.014006121

Iterations [ ]: 114

Analysis interval: 22

As previously mentioned, this drone design works in the same fashion as a typical drone, by increasing the output thrust of the individual lift motors, in order to change their AOA and therefore tilting in the direction of desired flight. The current design has a large amount of surface area that would create a significant amount of air resistance and turbulence, however by reducing the surface area of the outer gimbal, so too could the overall air resistance be reduced. While not being the most aerodynamic design compared to the other concepts, what it lacks in aerodynamic capability, it would make up for in simplicity, lower weight and dynamic ability.

3.1.1.5 Final Drag Comparison

Of the four designs, the multi-directional gimbal-tilt rotor drone produces the most drag with 0.0167 N, because of its ducts, which interfere with its ability to remain streamlined. Following this, the gimbal-tilt body drone creates the next highest drag force of 0.014 N, because of its large body surface area. The friction forces from the other two concepts are significantly less, due to much less surface area, however the drag from the tip-tilt rotor drone is slightly higher at 0.00417 N, compared to that of the uni-directional tilt-rotor drone at 0.0028 N in the first flight method and 0.00366 N in the second flight method.

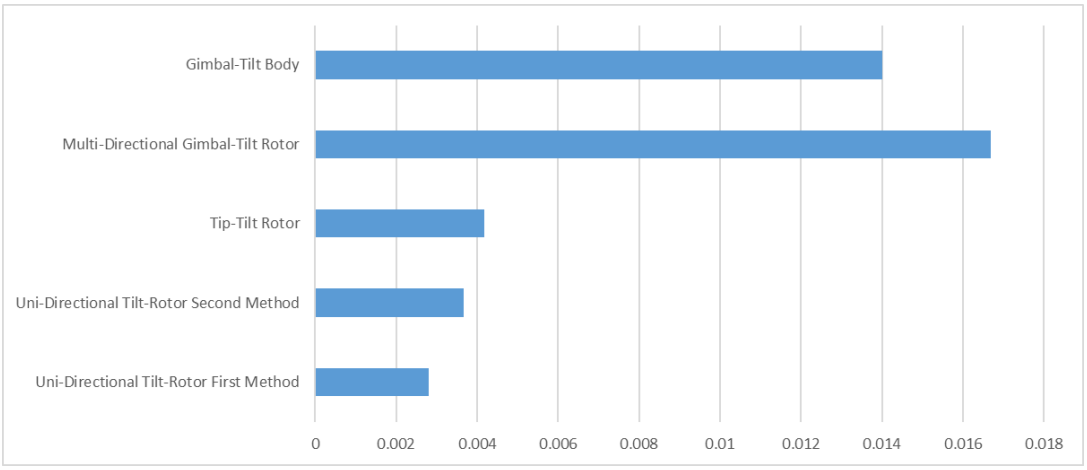

Figure 3.6: Comparative Friction Forces of the different Designs

3.1.2 Design for Further Development

On trying to determine a final design, multiple different aspects were taken into account, from ease of design, manufacturability, aesthetics, flight speed and of course the ability of the design to perform the dedicated task. In trying to make the decision, some of the designs were redesigned to take into account the placement of components and how they would fit size-wise (see below images).

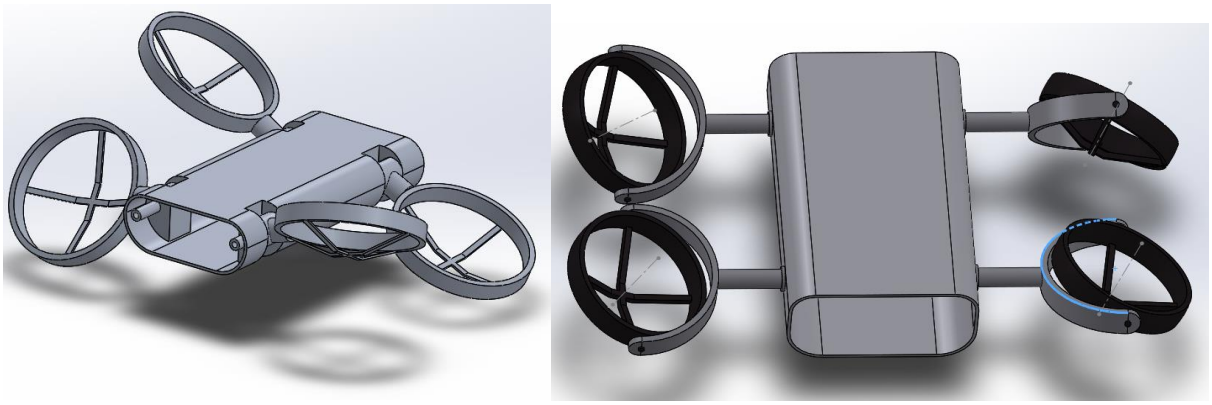

On reviewing the various designs, it was determined that the main focus of the project should be to develop the best functional design. Due to its ability for unlimited degrees of freedom with individual control of each rotor and hence its angles of attack, concept 3, the multi-directional gimbal tilt rotor design, was the optimal design to continue developing. This was due to it providing a stable platform, where the only changing factor would be the orientation of the rotors depending on the actuation of the gimbals. This means that the body of the drone could be streamlined and developed for efficient forward flight, but at the same

time, there would be minimal loss in flight through flying in other directions, as the drone propellers could easily change their angle of attack to fly in the given direction.

Concept 1 was determined to be a slower design in forward flight, due to not being as streamlined and designing for the two different flight patterns meant additional, undesired complexity. In addition, it was very similar in design to the New Atlas drone built by ETH in Switzerland, therefore to develop a more original design, the other concepts were preferred.

Concept 2, while providing an interesting solution appeared to be too much of an unstable platform, due to the tilting of the rotors in order for it to fly to the side. Because, the main goal of the project was to develop a stable platform, it was decided to go for a more reliable concept that would provide a constant stable platform. Additionally, this design appeared to be of a similar complexity to that of concept 3 in design, in having to develop the rotating rotors on top of the tilting arms.

Concept 4, while being simple in design with low weight requirements was seen to have too much of a surface area which would be affected by oncoming air resistance, as well as only being able to carry a size-limited payload due to its need to have an unhindered central gimbal.

Therefore, further development of the design was continued with concept 3 in mind. The best plan of action was to create a drone that when flying could adjust its gimbal settings automatically, without requiring any input from a pilot. To do this machine learning was the preferred solution. By connecting the orientation sensors and the motors that are controlling the gimbals and the thrust to a central micro controller, the drone should be capable of adjusting the output to the gimbal's motors and the thrust motors according to the readings provided by the sensors. In order to achieve this, a neural network would have to be developed that determined by itself what the optimal outputs should be.

3.2 COMPONENTS

The first step to developing a drone that would allow for stable-bodied flight was selecting the right components that support the function of the drone. This included determining how to run each component individually, whether it was developing the right code or downloading the right tools that allow it to work optimally. Following this, they had to be joined to work in harmony with each other. In order to control the drone and run machine learning on a drone, the first component that was required was a microcontroller.

3.2.1 Microcontroller

The micro controller acts as the brains of the operation, by performing the operations that are necessary for controlling the drone. The micro controller needed to be capable of performing high-level calculations, in order to perform machine learning, while sending and receiving information from the various components on board the drone in order to maintain stable and controlled flight. The three main microcontrollers that were looked at were a Teensy board, Arduino and a raspberry pi. The below information covers basic data of the standard microcontrollers.

3.2.1.1 Teensy 2.0 (NZD 22.94)

The Teensy board contains a 32-bit microprocessor, with up to 8 KB of RAM and no operating system (Murray, 2019). On-board the system has a USB-B power port, an SD slot and I/O pins. Teensy uses programs written in C++. This microprocessor uses ~20mA at idle. The Teensy is useful for cases where the program has just one purpose.

3.2.1.2 Arduino Uno (NZD 39.90)

The Arduino contains an 8-bit microcontroller, with 2KB of RAM and no operating system. On-board the system has a USB-B port, power input and I/O pins. Arduino uses programs written in C++. This microcontroller uses ~50 mA at idle. The Arduino is useful for cases where the program has just one purpose.

3.2.1.3 Raspberry Pi 4 Model B (NZD 107.66)

The Raspberry Pi contains a 64-bit microprocessor with 1GB of RAM, which is 500,000x more than that of the Arduino and runs an operating system, essentially being a microcomputer (Copes, 2019). On-board the Raspberry Pi, there are many more ports, including an SD, HDMI, DSI display, two USB 2.0, two USB 3.0, CSI camera, Wireless LAN ports, as well as a Gigabit Ethernet and an Audio Jack, Bluetooth 4.2 and I/O pins. Raspberry Pi typically uses a Linux operating system and runs programs using any programming language. This microprocessor uses 700+ mA at idle. The Raspberry Pi is useful where multiple programs need to run simultaneously and is more useful for more complex and intricate programs.

3.2.1.4 Selected Microcontroller

For the purpose of this design, the obvious selection was to use the Raspberry Pi for the reasons of it being much more capable than the other two microcontrollers are. Being a microcomputer, this device would be more than capable of handling any high-speed calculations that would need to be performed on-board the drone, alongside its I/O pins, which

allowed for easy connection with multiple other devices. The fast processing power is critical for ensuring that the drone remains stable under external factors, such as wind. In addition to this, the Raspberry Pi was capable of running Python Code, making it an easy processor to use for new programmers.

After selecting a microcontroller, the next step was to ensure the system was capable of recognizing its orientation, which requires the need for sensors that can provide such data, in the form of an Inertial Navigation System (INS).

3.2.2 INS

The INS is comprised of two systems, the Inertial Measurement Unit (IMU) and the Global Positioning System (GPS). The IMU is required for determining the orientation and motion of the drone. An IMU is a component that gives its pitch, yaw and role, by measuring orientation and motion with respect to an inertial reference frame (Arrow, 2018). It uses the centre of the Earth / Earth-Centred Inertial (ECI) Frame as the inertial reference frame (Smit009, 2015). There are two types of IMUs: one with 6 degrees of freedom, with a 3-axis accelerometer and a 3-axis gyroscope; and one with 9 degrees of freedom, which additionally has a 3-axis magnetometer. This unit has a high update frequency, with a high accuracy; however, the readings are subject to a lot of error from drift and interference, and therefore individual results cannot be used accurately.

3.2.2.1 Accelerometer

The accelerometer measures the changes in velocity of the system in the x, y and z directions and can be defined by (a_x, a_y and a_z). An accelerometer works through a 3-axis shifting mass to measure capacitance. As the accelerometer accelerates in a specific direction, the inertia on a spring held mass, causes the mass to approach fixed plates opposite to the direction of acceleration. With a current passed through this system, the change in capacitance can be recorded, therefore giving a readings equivalent to the acceleration of a unit (Omega, 2018). The accelerometers are measured relative to their absolute accelerations, which include North (A_N), East (A_E) and Down (A_D).

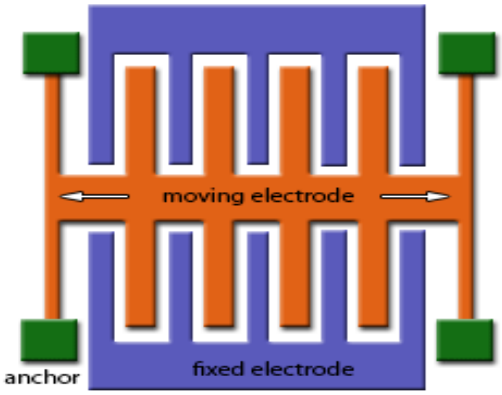

Figure 3.7: Accelerometer (Kirbas, 2021)

The measured accelerometer can be determined using a mathematical model, defined by:

$$\vec{a}_m = \vec{a} - (2\vec{\omega} \times \vec{v}) + (\vec{\omega} \times \vec{\omega} \times \vec{r})$$

$$Measured\ Accel = Linear\ \&\ Grav - Coriolis + Centripetal$$

In precise positioning, Coriolis and the Earth's rotation have to be taken into account, however for more applicable purposes, this can be ignored and as a result the accelerometer measurements can there be approximated to:

$$\vec{a}_m = \vec{a}$$

As well as measuring an objects acceleration, accelerometers can be used to measure tilt angles with respect to the constant acceleration of gravity. These tilt angles are determined by Roll (ϕ) and Pitch (θ) angles.

$$Roll = \emptyset = arc\tan\left(\frac{a_y}{a_z}\right) = atan2(a_y, a_z)$$

$$Pitch = \ \theta = arc\sin\left(\frac{a_x}{g}\right)$$

By integration and double integration, the velocity and position can be determined respectively. Direct integration is not recommended, as these are affected by drift. Therefore, to get results that are more accurate for orientation, velocity and position, the results of the accelerometer should be fused with those of the gyroscope, magnetometer and the GPS, using a filter, such as the Kalman Filter. In addition to drift, the accelerometer is subject to vibrations and noise, creating a very noisy output (Canal Geomatics, 2021). As a result, it is common to apply a low pass filter; however, this should not be applied to the Gyro measurements.

3.2.2.2 Gyroscope

The gyroscope is the most important aspect of determining the orientation of the system, as it measures the rate of angular rotation in the x, y and z directions and can be defined by (g_x, g_y and g_z). Similar to an accelerometer, the gyroscope measures change in orientation through change in capacitance. In this case, the moving mass is measured in relation to the Coriolis Effect, because of Earth's rotation (Brain, 2021). The mass within the gyroscope is constantly oscillating. This can either produce values in rad/s or deg/s, however the preferred use is rad/s.

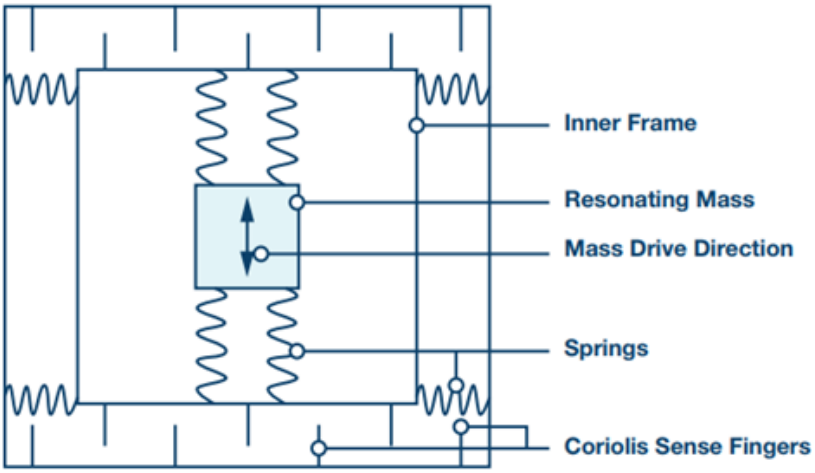

Figure 3.8: Gyroscope (Watson, 2021)

To get the actual orientation, the results could be integrated to provide the angle, however similar to the accelerometer, this is not recommended, as the results are subject to gyro bias, therefore leading to gyro drift. This bias can be corrected for by using an EKF and combining with other positional values.

3.2.2.3 Magnetometer

The magnetometer determines the orientation of the device relative to the Earth's magnetic field in the x, y and z directions and can be defined by (m_x, m_y and m_z) (Britannica, 2021). It works by one of two methods, the use of Hall Effect sensors or through magneto-resistive effect. The method of using Hall Effect sensors works by measuring the deflection of electrons in a metal plate, due to reacting with a magnetic field. By measuring the voltage on either side of the plate, the magnetic strength and direction could be determined. In contrast, the magneto-resistive effect causes a change in resistance in various materials because of being exposed to a magnetic field.

Often the magnetometer is not calibrated and therefore to calibrate, certain steps have to be taken to ensure it provides the appropriate readings. To calibrate the magnetometer, it is rotated to plot a sphere and then applying the offset can clean up the results of the magnetometer. In addition, magnets often point to magnetic north and not true north, such as in the case of San Francisco, the magnetic declination is 15° west of true north. This is because of Earth's shifting magnetic field away from the North Pole (McIntosh-Tolle, 2021). Therefore, the offset needs to be determined and then applied, so in this case 15° is added to the result to give true north. The magnetic declination in Auckland, NZ is approx. +20°, therefore to apply this 20° have to be subtracted from the reading, to show true north (GNS Science, 2021).

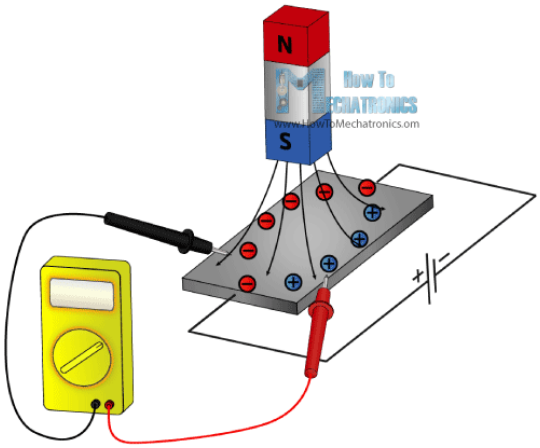

Figure 3.9: Hall Effect Sensor Magnetometer (Dejan, 2021)

3.2.2.4 GPS

The Global Positioning System (GPS) is generally separate to the IMU, but often works alongside it to give the position and heading of an object. The GPS gives the position of the device relative to position of the Earth (NASA, 2021). Depending on the strength of the GPS, it can give you its absolute position to within a couple of meters, however it usually takes time to update, due to having to contact at least four satellites.

As a result, by combining the GPS with the IMU, by means of Filter, the accuracy of the GPS can be improved.

3.2.2.5 Selected IMU

Two main IMU models were looked at, which were the Navio2 (NZD 240.85) and the MPU6050 (NZD 15.95). The MPU6050 is six DOF IMU system, which contains an accelerometer and a gyroscope and is often used as a general use IMU system. The Navio2 contains a two 9 DOF IMU systems, which include the accelerometer, gyroscope and magnetometer, as well as a GPS, barometer (for pressure) and a temperature gauge, and is

specifically dedicated as an Autopilot HAT (hardware attached on top) for use with Raspberry Pi powered robotic vehicles, such as drones. Motors are connected directly to the Navio2, instead of the Raspberry Pi when in use.

Due to the Navio2 being a specifically dedicated HAT, which included two IMUs as well as the GPS, to allow for sensor fusion, and could be easily integrated with the Raspberry Pi, this solution was selected. The Navio2 normally runs using AutoPilot, which is an in-built system; however, this is for standard drones and did not work with what was required for the drone to be running multiple different motor setups at the same time. To obtain the IMU readings from the Navio2, the following code was used (See 7.1 in Appendix for full code):

```
import argparse
import sys
import navio.mpu9250
import navio.util
import time

imu = navio.mpu9250.MPU9250()
IMU = navio.lsm9ds1.LSM9DS1()

navio.util.check_apm()
```

This section of the code imported the required libraries and assigned the IMU outputs to a variable, followed by the initialization of the selected IMU.

```
imu.initialize()
```

```
imu.read_all()
imu.read_gyro()
imu.read_acc()
imu.read_temp()
imu.read_mag()
```

To get the actual readings provided by the IMU, the above code runs the programs that provide the data, which could then be displayed using the code below. The below code is commented out in order to allow it to be used within a function.

```
#print("Accelerometer: ", imu.accelerometer_data)
#print("Gyroscope:     ", imu.gyroscope_data)
#print("Temperature:   ", imu.temperature)
#print("Magnetometer:  ", imu.magnetometer_data)

Accelerometer = imu.accelerometer_data
Gyroscope = imu.gyroscope_data

m9a, m9g, m9m = imu.getMotion9()

#print("Acc:", "{:+7.3f}".format(m9a[0]), "{:+7.3f}".format(m9a[1]), "{:+7.3f}".format(m9a[2]),)
#print("Gyr:", "y:{:+8.4f}".format(m9g[0]), "x:{:+8.4f}".format(m9g[1]), "z:{:+8.4f}".format(m9g[2]),)
#print(" Mag:", "{:+7.3f}".format(m9m[0]), "{:+7.3f}".format(m9m[1]), "{:+7.3f}".format(m9m[2]))
```

This code allowed the IMU to provide the raw data; however, this data still experienced some drift, with the values not staying constant, even though the Navio2 remained stationary on a flat surface.

At this stage is where data fusion was required.

3.2.2.6 Fusing

Two types of fusion could be used to remove the drift. The first solution was to fuse the outputs of the two separate IMU systems, in order to average out the effects of drift that the system was experiencing. The second method of fusion required was to fuse the gyroscope readings with that of the accelerometer and the magnetometer using a Kalman Filter, which is a Filter where the filter uses a combination of the trend and real time results to make an estimated guess of the actual values.

Error is present in all of the readings, whether it be from drift or interference. Therefore, once all the data has been collected, you can pass these values along with GPS data into an Attitude Heading Reference System (AHRS) to fuse those using filters, such as the Kalman Filters in order to cancel out the error between readings and therefore provide more accurate positioning system.

The next stage to developing a flying prototype was to determine the correct motors and propellers to allow the drone to fly efficiently.

3.2.3 Lift Propulsion System

The lift propulsion system composed of the propellers, the thrust motors and their ESCs. To achieve lift, the combination of motor and propeller had to be capable of providing enough lift, so that the upwards force was greater than the weight of the entire drone and all of components.

Table 3.6: Calculation of Estimated Drone Weight

Component	No. Required	Weight (g)	Sum of Weight (g)
Thrust Motors	4	65	260
Raspberry Pi	1	103	103
Radio Receiver	1	30	30
Battery Pack	2	892	1784
Rotors	4	17	68
ESCs	16	21	336
GB54-2 Motor	4	156	624
GB36-1 Motor	8	88	704
Slip Rings	8	12	96
Navio2	1	23	23
Drone Frame	1	250	250
Total Weight:			4278

The overall estimated weight is approximately 4.3 kg, therefore to provide enough lift; the lift propulsion system would have to produce more than 43 N of thrust split up over four motors. This is extremely heavy for a drone, for comparison, the Mavic Air 2 weighs 570 g (DJI, 2021).

3.2.3.1 Thrust Motors

The thrust motors are required to apply the angular velocity to the propellers in order to generate lift. Direct Current (DC) motors are the most popular motors found amongst drones and consist of a rotating commutator or armature and a stationary outer stator. DC motors can be found as two main variations, which include the Brushed DC motors and the Brushless DC motors. Brushed motors (*Figure 3.10*) tend to have a carbon brush that remains in contact with the commutator, which conducts the current to the coils on the commutator to induce a magnetic field, to act against permanent magnets in the stator, hence creating rotation. These tend to require high maintenance and have a low life span, however come at a low cost and are simple to control, due to just having a positive and negative terminal (Rippel, 2007).

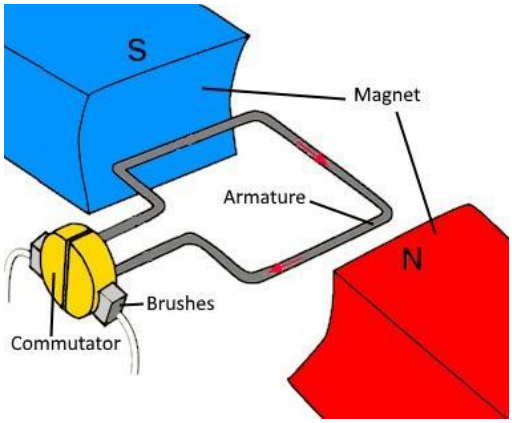

Figure 3.10: Brushed DC Motor (Sapiga, 2016)

In contrast, the brushless motors (*Figure 3.11*) have permanent magnets within the armature and electromagnets on the stator and work by using three different phases inducing magnetic fields in turn within the motors to cause both attraction and repulsion to determine the direction and speed of rotation. Brushed motors tend to be high speed and efficiency, with a long life span, and relatively low noise and maintenance, but this comes at an increased cost and complexity to control.

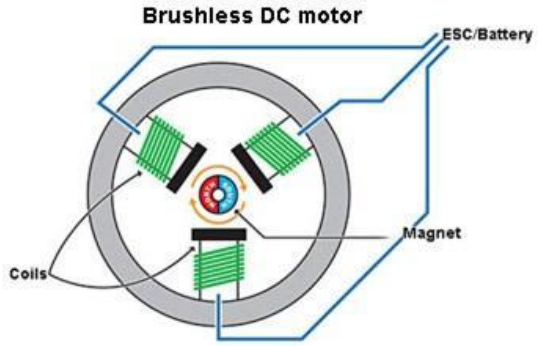

Figure 3.11: Brushless Motor (Sapiga, 2016)

For use in drones, the brushless DC motors are much more optimal compared to the brushed motors, due to their high speed and long life span with high intensity use. This is due to the motor needing to produce a high revolution speed with high efficiency to produce the lift required for flying the drone.

Due to brushless motors being 3 phase, they require a Pulse Width Modulation (PWM) signal, which is provided using an Electronic Speed Controller (ESC). The ESC is used to transform signal waves as a square wave from the microcontroller into sine waves, which allow the magnetic fields to be induced within the motor.

3.2.3.2 ESCs

An Electronic Speed Control (ESC) is used to control and regulate the electric motors speed. It can also be used for reversing a motor and dynamic breaking (Model Flight, 2019). The ESC can also act as a voltage regulator. There are two types of ESCs, which include a Battery Elimination Circuit (BEC) ESC and a No BEC ESC. A BEC ESC can send current back to the microcontroller in order to power servomotors, whereas a No BEC ESC does not provide this extra function, instead using the current from the power supply to just power the motor to which it is connected.

3.2.3.3 Propeller

The propeller is required to convert the rotational motion of the motors into the actual lift force on the drone. The length of the propeller, the number of blades, angle of attack and blade shape, can determine its characteristics. Typically, the longer the propellers and the greater the number of blades, the greater the lift is that is provided. Additionally, the optimal propeller for the design would be made of a lightweight material. Polymers such as carbon fibre is a common material used for propellers as it has the optimal properties; however tends to be very expensive. Cheaper options include nylon or PVC. Carbon Fibre propellers tend to be stiffer, therefore less prone to vibration, however are also more brittle and prone to breaking in crashes. The plastic propellers tend to be more durable, but are subject to vibration.

3.2.3.4 Motor/Propeller Selection

The selected lift propulsion system was the Air Gear 450 Set (*Figure 3.12*) from T-motor (T-motor, 2021), which provided a complete set of four brushless motors with their respective propellers and ESCs (NZD 186.45).

Figure 3.12: Air Gear 450 Set

This set was the optimum set cost wise, containing all of the necessary components for the lift propulsion system, while at the same time, still providing the necessary lift values. The

thrust values for the Air Gear 450 at 100% throttle were 5172 g, according to the data sheet (See *Table 3.7*), which is ~800 g more than the weight of the drone and all of its components. While not a high enough clearance for efficient flight, this amount of lift would be sufficient in order to be used for this project and an initial prototype.

Table 3.7: Air Gear 450 Data Sheet

Test Report-AIR2216										
Item No.	Propeller	Throttle	Voltage (V)	Torque (N*m)	Thrust (g)	Current (A)	RPM	Input power (W)	Efficiency (g/W)	Operating Temperature
AIR2216 KV880	T-motor T1045	50%	16	0.07	435	3.5	6015	56	7.77	53.5℃
		55%	16	0.08	527	4.6	6620	73.6	7.16	
		60%	16	0.09	608	5.6	7113	89.6	6.79	
		65%	16	0.11	702	6.8	7563	108.8	6.45	
		75%	16	0.13	888	9.5	8545	152	5.84	
		85%	16	0.15	1076	12.3	9442	196.8	5.47	
		100%	16	0.18	1293	16.2	10464	259.2	4.99	
Notes:Motor temperature is motor surface tenperature @100% throttle running 10 mins. (Data above based on benchtest of 2018 are for reference only. Comparison with that of other motor types is not recommended.)										

The thrust motors and ESCs could easily be connected to the Raspberry Pi and Navio2 using the I/O pins of the Navio2 in order to control the signal sent to the motors (*Figure 3.13*). For powering the motor, a battery pack or power supply could easily be used.

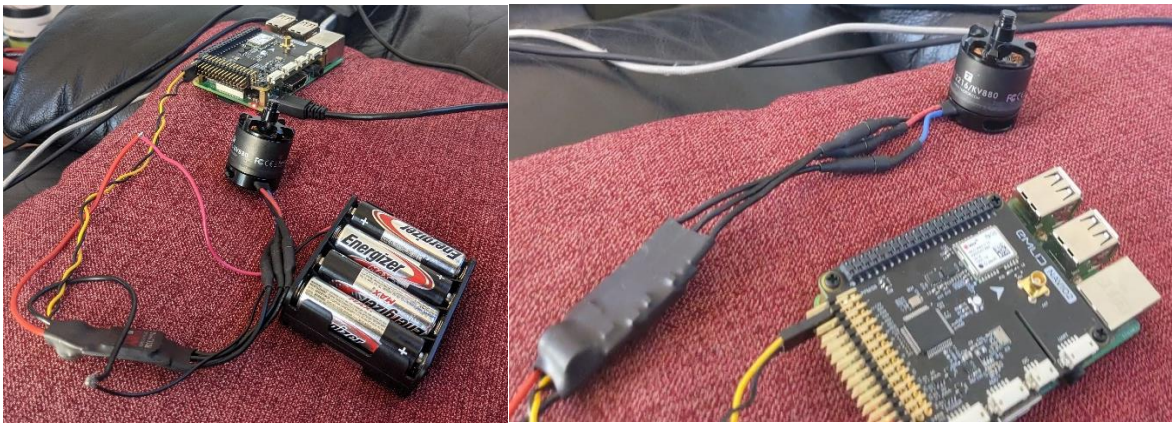

Figure 3.13: Setup for running Thrust Motor of Raspberry Pi

Although, to ensure that the lift values were accurate, separate experiments were performed, using the motors and propeller to test for the accuracy of the results. The motors were attached to the below seen testing rig (*Figure 3.14*) and then powered using different voltages and currents to view how this affected the thrust output of the motors (See 7.3 in Appendix).

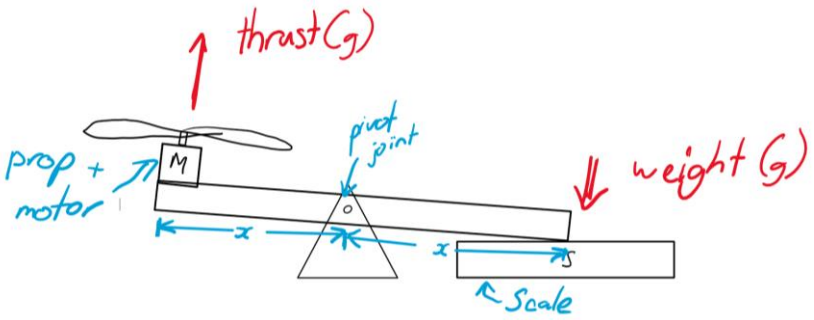

Figure 3.14: Motor Thrust Test Rig (Due to being a quick rig, no photos of actual setup were taken)

The pivot was placed at the centre beam, so that the effects of a lever arm were negligible. To test the motor thrust the lower limit of the PWM signal was found when running the motors off a raspberry pi and then the PWM signals were gradually increased, while the current and weights were recorded to plot the currents against the weights. The weights were not plotted against PWM signals, as these are different depending on the device used, such as was the case with the Navio2. The motors themselves were powered using a wall connected power supply, which had a max voltage at 33 V.

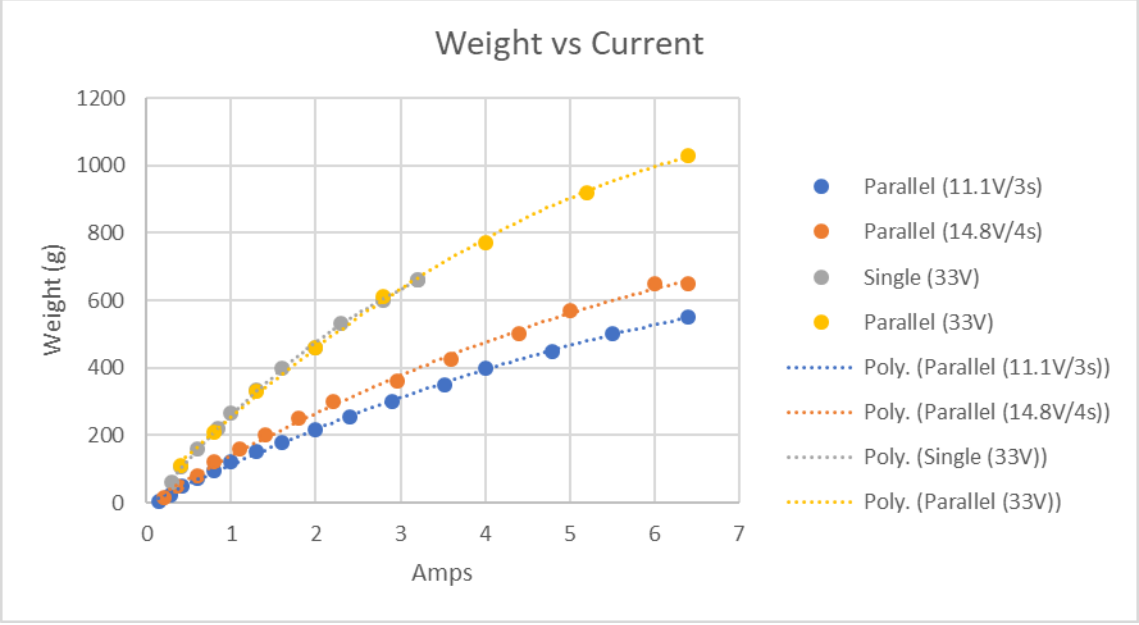

Figure 3.15: Graph of the Thrust Weights against current for different voltages

As can be seen in *Figure 3.15*, there is a clear correlation between the voltages and the output thrust of the motors, with the higher the voltage, the greater the amount of thrust. There is also a clear positively sloped relationship between the amperage and the amount of thrust; hence, with an increase in PWM signal, there will also be an increase in thrust force. However,

in testing, the data also showed that the max PWM value was ~6.8 when using just the Raspberry Pi for signal production, therefore the max thrust that was achieved was 1030 g.

This thrust was below the thrust specified in the data sheet, therefore in order to develop a successful design, either a means of increasing the supply voltage and current would have to be found, or the weight of the drone would have to be decreased in order to use the selected lift propulsion system.

3.2.3.5 Motor Code

To run the motors using the Navio2, the code (See 7.4 in Appendix) to apply the correct PWM signals had to be determined, as the motor ESCs connected directly to the Navio2, rather than to the Raspberry Pi.

```
import sys
import time

import navio.pwm
import navio.util

navio.util.check_apm()
```

As previously seen with retrieving the IMU data from the Navio2, running the motor required importing the dependent libraries and accessing the stored data in the Navio2.

```
PWM_OUTPUT = 0
SERVO_MIN = 1.250 #ms
SERVO_MAX = 1.750 #ms
x = 1.8
n = 0

with navio.pwm.PWM(PWM_OUTPUT) as pwm:
    pwm.set_period(50)
    pwm.enable()
    pwm.set_duty_cycle(0)

    while n < 1000:
        pwm.set_duty_cycle(1)
        n += 1

    print ("Motor Ready")

    while (True):
        pwm.set_duty_cycle(x)
```

To start the motors using the Navio2, the code needs to first enable the motor when it has a PWM output of 0 and then while running them, the motor needs to initially be set to its minimum point at 1 before running at the desired PWM signal.

A problem arose when disconnecting the ESC from the power source, in which the code had to be run twice in order to get the motor running.

The next stage was to be capable of varying the motor speeds in response to an input.

3.2.4 Gimbal Actuation

The gimbal is a 3-axis pivoting support that allows an object to rotate in every orientation. The gimbal setup allows the inner most object to move independently of the objects outside of the gimbal. The gimbal system can be used in this design to either create independent movement for the propellers. In this way, the body will be able to move separately to the propellers.

To achieve the control required for the gimbal movement, motors capable of position control and change in direction are required. Position control can be achieved in motors using Hall Effect sensors, where the sensor picks up on the angle of the motor depending on the magnetic field that was created by the motor.

In addition to positional control, the motors require the need to be able to change direction. This can be achieved by using servomotors, stepper motors, task specific motors, such as gimbal motors, or even brushless dc motors with the right setup. The amount of torque that the duct motors combined needed to provide was 310 Nm, whereas the gimbal arm motor needed to provide 430 Nm (See 7.5 in Appendix).

3.2.4.1 Actuation Method

Actuation can be achieved either through direct actuation, where a system is connected directly to a motor, or through indirect actuation, where other systems, such as gears, cables, lever arms, etc. These indirect actuation methods can be used to increase/decrease the force and speed or even to allow actuation from a distance, however, they come at a loss in overall efficiency, due to the greater number of joints.

One form of indirect actuation that is commonly used in robotics is with cables (Grosu, Rodriguez–Guerrero, Grosu, Vanderborght, & Lefeber, 2018). This means that the motor does not need to be connected directly to the joint; instead, it can be located in a more central position and transfer the force through the cables to the joint. However, cables are prone to slipping, which would result in a loss of the ability to function effectively.

Due to this, it was decided that direct actuation would be more efficient, by connecting the motors directly to the gimbal joints.

3.2.4.2 Servo Motor

A servomotor is part of a closed loop system containing a motor and a feedback device and a servo controller. Servo motors can range in the different motor types and feedback devices used, as long as there is a closed feedback loop to verify that the motor is working allowing for error correction (Gastreich, 2018). The type of servomotor depends on the aspect that needs to be controlled; hence, some servomotors are designed for speed control, whereas others are designed for positional control. The position control can be applied through a subset of loops, where the torque, which is proportional to the current, is used to accelerate/decelerate to a given angular rotation, which is proportional to the voltage (Kollmorgen Experts, 2020). Servomotors are capable of providing high levels of torque at high speed and work at a high efficiency. Servomotors can be quite expensive and can be very complex to use. Servomotors can be found used in robotics of all sorts where high precision and speed is required.

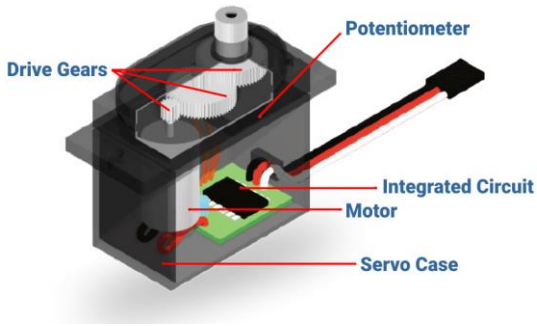

Figure 3.16: Servo Motor (robu.in, 2020)

3.2.4.3 Stepper Motor

Stepper motors have a high number of poles and control the angle of the motor by aligning a permanent magnet with one of these poles, therefore allowing the motor to rotate a fraction at a time, completing the rotation in steps, rather than having a continuous rotation. The ability to align with specific poles means that the stepper motor has a good holding torque, as well as being capable of high repeatability in return to a starting position, however is susceptible to resonance and vibration. In addition, they are capable of high torque at low speed, allowing very high precision, however this drops rapidly with an increase in speed. It is not a very efficient motor, and if exposed to too high a load, it will skip steps, giving it a low accuracy,

unless a feedback loop is used (robu.in, 2020). This motor can be found in 3D printing machines, CNC milling machines and other precision devices.

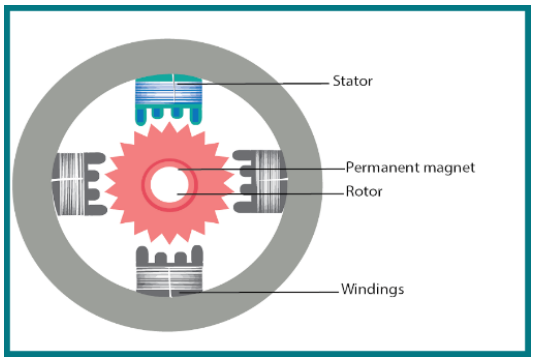

Figure 3.17: Stepper Motor (robu.in, 2020)

3.2.4.4 Brushless DC Motor

Brushless DC motors can be effectively paired with positional sensors to create a closed feedback loop and therefore becoming its own version of a servo motor. The problem with this however, is that depending on the ESC that is used; a brushless motor will just be capable of running in one direction. However, with brushless motors being 3 phase, it means that three separate signals are sent to the motor over three different connections with a delay between to allow for rotation. By switching any two of the connecting wires and hence changing the direction of current flow in those wires, the direction of the motor can be reversed. This can be achieved digitally, which are electronic switches. In connecting the relays in parallel, the relays form an H-bridge, which allows for the current flow in a circuit to be reversed.

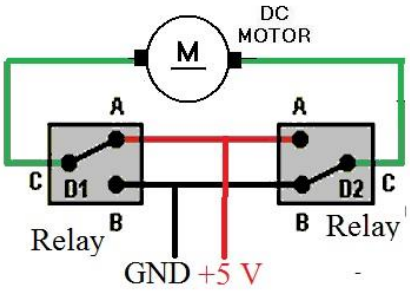

Figure 3.18: H-Bridge using Relays (Amirante, 2021)

The disadvantage in using relays for switching the motor's direction in cases such as this is that the relay has a limited lifespan and therefore would not be able to be run with constant fast switching for precision motor control. In addition to this, the coil in the relay introduces a high loss of efficiency. The relays could be replaced with transistors, however due to the motor

being inductive; the circuit would need a means of releasing the energy as the motor slows down (Alterach, 2021). To properly use this method, extra relays would be required in order to allow for braking; however overall, this method is not optimal for use in systems with constant rapid changes in motor direction.

3.2.4.5 Gimbal Motor

The gimbal motor is also a 3-phase brushless DC motor and a servo motor, however, unlike the motors used for thrust, the gimbal motors usually have more coil turns on the stator. This gives it a higher resistance and inductance, therefore allowing it to have a high torque while running off a lower current; however, it comes at a loss in speed. The gimbal motor works alongside an IMU, using an encoder, which allows it to determine its position and provide, therefore allowing it adjust to changes in the IMU orientation.

3.2.4.6 Selected Gimbal Actuation

The obvious choice for this design is to use a servomotor in the form of a gimbal motor. Using basic brushless motors with the relays is too slow to keep up with constant changes in direction that are required by the gimbal system in order to maintain a stable platform. Use of this system would quickly cause damage to the motor itself, as it would not allow for braking, due to switching the current direction in the circuit. The stepper motors, while capable of giving precise control, are subject to skipping steps, which would cause a loss in accuracy and therefore a loss to the ability to provide a stable platform. In addition to this, the stepper motors lose their torque at high angular velocities; however, a high angular velocity is required for making quick adjustments to the gimbal angles. The gimbal motors are an optimal solution, as they are easily able to integrate with an IMU, as their purpose is to maintain stability.

The gimbal motors that were selected for this design were the GB54-2 (NZD 106.76) for turning the gimbal arms and the GB36-1 (NZD 71.13) for turning the ducts (See 7.6 in Appendix).

a **b**

Figure 3.19: (a) GB54-2; (b) GB36-1 (T-motor, 2020)

Running the gimbal motors using the Navio2 proved to be a challenge, however, as the speed controllers designed for the thrust motors were not compatible with these motors, therefore a different method of running the motors themselves had to be determined. The solution to this may be to connect the gimbal motors directly to the Navio2, as they can run off a lower voltage compared to the thrust motors. To ensure the gimbal motors run properly, the appropriate PWM signals would need to be determined in order to control them, with a gimbal specific ESC.

3.2.5 Powering the Drone

To ensure that all of the components on-board the drone work efficiently, both power and data need to be transferred around the drone, whether it be from the microcontroller to the individual components or whether it was supplying power to the components themselves in order for them to run properly.

3.2.5.1 Power Supply

Within the drone itself, the different components themselves need a power source to be able to be run and be controlled in the first place, with different components requiring different voltages. The obvious solution is to use batteries to power the drone, which can also be used in this case. However, when testing components and determining how to run them and then test them, it can become a nuisance if the batteries run out already after 30 minutes of use. To compensate for this a power supply that can run off mains comes in as useful. Being able to vary the voltage and current that run to the different components means that they can be tested under varying conditions. This allowed for the tests on the motor to be completed, where the motors were tested at different currents and voltages. In addition to this, simple wall plugs could be used to power the Raspberry Pi and Navio2 in the coding phase.

Using the power supply is useful for testing the motors and running the components under test conditions, but to actually allow the drone to fly as an independent system, so too an independent power source is required. As previously covered in Section 2.2.5 on Power Supply, the power source for a drone can be provided by batteries or from a fossil fuel source. For both safety reasons and ease of use, it is easiest to use batteries.

The main types of batteries that can potentially be used for drones can be broken down to Li Ion Batteries and Li-Po. Lithium Ion Batteries are a rechargeable battery that are commonly found in portable electronics, such as phones and on electric vehicles. These batteries have a high energy density of between 250-670 Wh/L and tend to be quite cheap. In

addition, they do not have a memory effect, therefore do not lose their ability to be charged after a period, however can be unstable and can combust if damaged.

Li-Po batteries are very lightweight and robust, therefore can be found present in a lot of small drones and RC vehicles. They have a lower power density of 185-220 Wh/L compared to Li-ion batteries; therefore tend to be bigger and more expensive. These batteries do not tend to last as long; also, they suffer from memory effect, where they start as a gel-like substance and begin to harden, hence losing their life span (Reliance Digital, 2021).

Due to the reliability, robustness and lightweight properties of the Li-Po batteries, this is the more optimal solution for use on the drone. Typically, the batteries rating measures its voltage in terms of the standard S = 3.7 V, where a 4S battery is a 14.8 V battery and the milliamp hours (mAh) determines the charge on the battery, hence, the higher the charge, the longer the battery life, although at an increase in weight. Most motors run at a rating of 3-4S, however the testing earlier on proved that to be able to fly a higher voltage was required, therefore, the highest voltage battery should be used, with optimally the highest mAh as well.

The Tattu 6S Plus 15C 16000 battery meets the highest voltage at 22.2 V, but comes at a cost of NZD 328.24, whereas a shorter battery life with the Tattu 6S 10000, would be much cheaper at NZD 168.11.

Figure 3.20: Tatty 6S Plus 15C 16000 battery (AliExpress, 2021)

3.2.5.2 Signal/Power Transfer

Due to the rotation of the gimbals at the joints, an issue arises with transferring power to the thrust motors and the gimbal motors, which connect the gimbal arms to the ducts. With the constant rotating and moving at the joints, any wires that are used to transfer power to these subsystems would be subject to the same forces. Constant twisting and movement on the wires can result in the wires becoming damaged due to repetitive or excessive stress.

Two possibilities were viewed as solutions to this issue, with the first option being, to look into slip rings. Slip rings are a set of conductive rings that allow current to flow between a stationary surface and components that are on a rotating platform, without the fear of causing damage to the electronics. They are often used on robots or machines that have such a rotating platform and require data or power to be transferred. The slip rings come at the advantage of a decreased possibility of causing damage to wires, however with an increase in weight and mass of the drone.

The second option was to take the risk of allowing the wires to rotate freely. This second option was acceptable in terms of the design, due to the gimbals never needing to rotate more than 90° from the normal, at the extreme. In order for the drone to produce lift, the propellers would always require an upwards component to the force that they apply; therefore, having propellers facing downwards would be counterproductive to the goal of providing lift. Due to this, it can be concluded that the gimbal and hence the wires would not encounter any rotations greater than 90°, which in reality would be closer to 45° at maximum, as a drone while flying rarely has a gradient greater than this (Ingenieurbüro, 2021). In addition to this, the twisting that would result on the wire would be spread over a length of the wire, rather than at just one point, therefore would not cause any damage to it.

Following these discoveries, it was decided to forgo on the use of slip rings, in order to save on weight and space.

3.2.6 System Control

3.2.6.1 Ground Station & Remote Control

In order to control the drone remotely, a ground station and a remote controller are required. For the purpose of this section, radio controllers (RC) and remote controllers will be looked at as two different definitions, by which remote controllers are any means of controlling an isolated system remotely, whereas radio controllers are a type of remote control that works on radio frequencies specifically.

The common solution for hobbyists and commercial drones is to use a radio controller (RC), as this allows the controller to communicate with the drone up to a range of approximately 30 km with low interference. An RC device consists of a radio frequency (RF) transmitter, in the form of a PlayStation controller and a receiver, on-board the drone, to transmit signals to the microcontroller. The radio controller generally has eight channels and allows the pilot to control the throttle, blade angle, rotor pitch and tail rotor speed on single

motor rotor rotary-wing drones, in order to fly it. In multi-rotor drones, it is too complicated to control more than one rotor, therefore the pilot only controls the pitch, yaw, roll and thrust of the overall system, however the individual motor speeds are controlled by an on-board microcontroller.

This project requires being able to control what occurs with the on-board microcontroller; therefore, the use of a RC controller is not as necessary. Instead, a direct connection to the microcontroller needed to be established. Connecting to the Raspberry Pi and Navio2, could be achieved by plugging in an HDMI cable to connect to a monitor and attaching a mouse and keyboard to edit the code, which was initially used for setup. However, this does not work long term, as this would require the keyboard, mouse and monitor to be connected to a flying drone. Therefore, in order to create a wireless method of communication, the SSH and VNC modes were activated on the Raspberry Pi.

These allow access to the Raspberry Pi over the network, meaning it could be accessed off an isolated computer, such as a laptop and does not require a physical connection, as long as they are on the same network. This has a shorter compared with the RC controller, however allows more information to be transferred. The SSH shell establishes a connection with the Raspberry Pi's control shell, allowing information to be accessed and sent through command line. In contrast, the VNC viewer gives access to the Raspberry Pi's Graphical User Interface (GUI), effectively allowing the laptop to display the same thing that could be seen on a connected monitor.

3.2.6.2 Filters and Fusing

Filters are used to fuse data from different readings. This allows for more consistent, accurate and dependable results. In many cases, this is within reference to time. Sensor fusion has four main advantages, which include increasing data quality, increasing reliability, estimating unmeasured states and increasing coverage area (Jaiswal, 2018).

Fusion can increase the data quality by removing noise, such as in the case of accelerometers. By using more than one accelerometer, the output of the sensors can be averaged, causing noise reduction and the more sensors there are, the less the effects of noise. However, the same sort of interference can affect two sensors of the same type; therefore fusing two different sensors with a Kalman Filter, such as a gyroscope and an accelerometer can ensure that the noise is not correlated.

Increasing reliability can be achieved by having backup sources, so that if one sensor fails, there is still data being received from another, even if this results in a loss of accuracy. However, sensor failure can also be momentary failures and does not necessarily require permanent sensor loss. Reliability can also be introduced by eliminating outliers, through voting the more likely option.

Estimating unmeasured states can be used to determine factors that cannot directly be measured, such as using a second camera in computer vision to create depth perception. Increasing coverage area can be used in examples such as fusing sensors to create one coherent system map, such as in the case of self-parking vehicles.

A complementary filter, works by placing inputs of 100% trust on two ends of a scale and applying the amount of trust given to either of the variables depending on where the users input. As a result, the user defines the weighting of inputs on a ratio. An example of this is in fusing accelerometers with gyroscopes, by using 2% of the accelerometer output and adding it to 98% of the gyroscope data.

The Kalman Filter works in two steps: predict and update, which it achieves on an automatic basis by determining the optimal weightings.

The Kalman Filter is used to give an accurate estimation of position. Alone the accelerometer readings are not very accurate, as it gives no indication of initial position or velocity, however by combining this with the absolute positioning of the GPS, accurate results can be provided. The prediction phase uses the fast update rate of the IMU to determine the initial state and uses its average speed and time to create a predicted uncertainty. While the correction phase measures the state directly from the GPS, but due to the relatively slow update rate of the GPS, it creates a GPS uncertainty. By combining the predicted uncertainty with the GPS uncertainty in the correction phase, the filter is capable of creating a more accurate positioning and tracking system.

The Kalman Filter is also applied in determining the orientation of the drone. By combining the output of the accelerometer with that of the gyroscope, the accuracy of the roll and the pitch can be improved, however not the yaw. However, combining these results with the readings from the magnetometer, further improve the accuracy of the results.

A low pass filter is used to filter out unwanted values. It only allows values below a set cut-off frequency/value to pass. Anything above this value is eliminated and seen as a source of error.

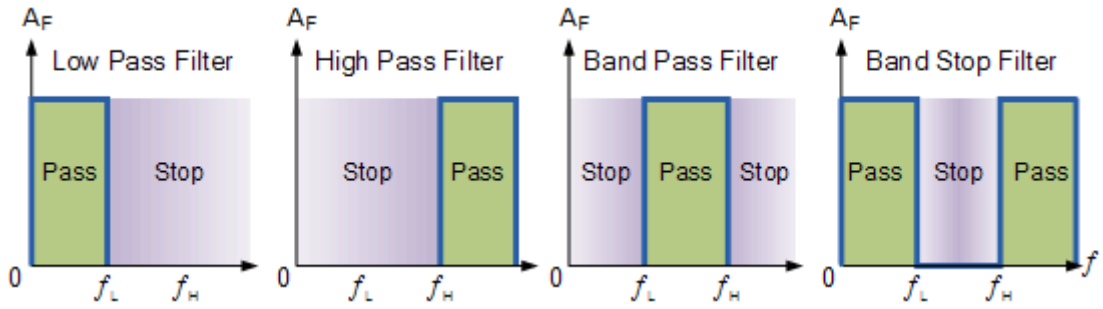

Figure 3.21: Ideal Filter Response Curves (Electronics Tutorials, 2020)

3.2.6.3 Stability Control

A major part in allowing the drone to maintain its stability is in controlling all of the various motors and determining which combination of gimbal angle and thrust output would ensure that the body of the drone remained stable. This means that there are three independent variables to control for each gimbal arm system, which are the arms roll, pitch and thrust. These combined with the other three arm systems, provide 12 variables which need to work in unison to control the drones overall yaw, pitch and roll.

This could be determined by figuring out the relationship between the three, however this would provide infinite results and selecting the optimal setup would effectively take forever. Therefore, it is much simpler to use machine learning and allow the drone computer to figure out what the optimal setup would be in order to provide a stable platform. The system would have to act as a closed feedback loop by which the microcontroller sends the 12 variables as commands to the motors and then measure the feedback from the INS to determine if the body is staying stable. If not, then the Raspberry Pi would have to update the commands sent to the motors to make sure that the body returned to being stable. This would need to be enacted in three different scenarios, which are while hovering, while flying in a certain direction and while under the influence of external factors, such as wind.

3.2.6.4 Machine Learning

There are a few different types of different machine learning, which include supervised learning, unsupervised learning and reinforcement learning (upGrad, 2019).

Supervised learning is mainly a form of classification learning, by giving the machine training data; the machine can determine a trend and from there apply the trend to test data (Petersson, 2021). Supervised learning is very task specific and is a common type of machine learning, because to improve it all you have to do is add more training data and is a very simple

form of machine learning. Examples for supervised learning include face recognition and spam filters; however, this cannot be applied to the drone design, as there is no training data in order for the drone to learn.

In unsupervised learning, no training data is provided and the machine has to come to its conclusions on given data, however this is very complicated to implement (IBM Cloud Education, 2020). Unsupervised learning is often used for finding outliers and data clustering or finding the difference between data. Examples for unsupervised learning include data categorization, recommendation systems and class segmentation, but this also is not applicable to the drone due to it once again only finding trends and not being an adaptive system.

Reinforcement learning is a form of learning by which the machine learns by making mistakes (Osiński & Budek, 2018). The ability of the machine to complete that task is rewarded or penalised using a weighting system, where the weightings vary depending on the results of the previous test. This can be a difficult form of machine learning to implement, however finds use throughout many different fields, including robotics and video games. This is the optimal machine learning system to use to find the best gimbal/thrust setup to allow the drone to maintain its stability, as it works using a trial & error method to narrow down to the best results.

In order to write the program, multiple open-source libraries can be used, such as Tensor Flow, which offers easily available tools for developing machine-learning code (Exastax, 2017). Tensor Flow programs are especially made with neural networks and training data in mind, where the code can be tested on a software interface such as Keras (keras, 2021) or Google Colab (Google, 2021).

To implement the reinforcement-learning program an effective weighting system needs to administered. While the 12 variables previously mentioned control the overall orientation of the drone. Different aspects of the orientation are only controlled by some of the variables; therefore, these can be split up in terms of their respective variables.

Pitch = Pitch motors and thrust motors

Roll = Roll motors and thrust motors

Yaw = Pitch motors, roll motors and thrust motors (However a change in yaw is not affecting its stability)

These three subsystems can then be combined to control the overall orientation of the drone, determined by the IMU readings.

Following this, the punishment/reward values need to be set in order show the system what outcomes are good and what outcomes are bad. This should be in terms of the variation of the IMU, where the greater the variation from zero, the worse the punishment. After testing, it requires a reset, in order for the drone to return to stationary, use the results from the previous test, and learn from it.

In order to test the output of the machine learning code and the drone's ability to react to them, a test rig would have to be set up in order to allow it to achieve, these results, without causing damage to the drone itself. To allow for this, two options were considered. The first option was to hang the drone from the ceiling, allowing it to have free-swinging motion underneath, therefore allowing it to adjust not only its AOAs, but also ensure that it would remain in the same place. The second idea was to attach it to the top of a post on a free moving ball joint, this way the drone could adjust its gimbals to optimize for the right settings for hovering; however, this case would not allow the system to learn the ability to maintain its position as well.

Once the best-case responses have been found the experiment can be repeated with the different conditions, to further improve the results and then implemented into the drone as part of its flight system.

3.2.7 Drone Body

3.2.7.1 Materials

The drone body needed to be capable of containing and carrying all of the components while at the same time not adding unnecessary weight. This meant that the material had to be both strong enough to be capable of working as support structures, while at the same time being of a low density. Several different options were considered throughout the development process. The material depended greatly on the manufacturing method and cost, which therefore in turn influenced the design of the frame.

The first method of determining what material to use was to look at current drones on the market and use materials similar to what they use. With looking at other drones also arose the question whether it was a good idea to retrofit a current drone design to fit to the project outline. However, this idea would not prove suitable for the design, due to the very specific nature of the project specifications. In order to create a stable-body drone, there would have to be a lot of moving parts on the drone, which most drones are not capable of fitting on-board or

providing enough thrust to carry. Hence, due to not being able to retrofit a drone, the second question was as to whether a similar material to commercial drones could be used.

The material most commonly used in commercial drones such as the Mavic 2 is a magnesium alloy (Hall, 2019), which is extremely lightweight, with a density of 1.81 g/cm^3 , strong, with a tensile strength of 230 MPa and easy to cast in comparison to other metals. Mostly these metal frames are made using a die cast or a sand permanent mould. Both of these processes are too arduous to use for this design, due to having to get the correct mould shape and working with molten metal alloy.

Another option that could be considered was high impact polystyrene (HIPS). This too is a very lightweight material with a low density of 1.08 g/cm^3 and depending on the thickness can be used structurally, due to its tensile strength of ~55MPa (Curbell Plastics, 2021). HIPS can be thermoformed, however to obtain the thicker results it has to be injection moulded, which requires an expensive mould to be formed. It can also be 3D printed, but is mainly used as a soluble support structure.

For 3D printed solutions, there are two main options ABS and PLA. ABS has a density of 1.07 g/cm^3 and a tensile strength of ~43 MPa, whereas PLA has a density of 1.25 and a tensile strength of 33 MPa (Giang, 2021). Of the two materials, PLA is much easier to 3D print and is better for detailed prints, however, is not as strong or as light as ABS. Another option for 3D printing was ONYX, which is extremely strong and lightweight, due to being a carbon fibre composite, however this makes it very expensive.

Another option for use are fibre-reinforced polymers such as carbon fibre and fibreglass. Carbon fibre has a density of 1.6 g/cm^3 with a tensile strength up to 5500 MPa, depending on the composites and treatment, while fibreglass has a density of 2.11g/cm^3 depending on the glass used, and tensile strength of 2415 g/cm^3 (nine11design, 2019). Carbon fibre tends to be stronger and more lightweight compared to fibreglass, however also tends to be more brittle and more expensive. Manufacturing the polymers, generally involves the use of a mould, such as with open moulding or vacuum moulding.

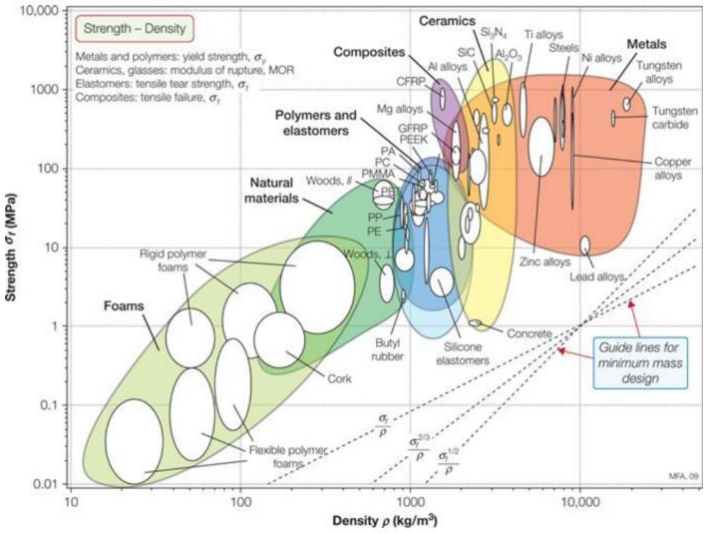

Figure 3.22: Material Selection Graph (Ashby, 2011)

3.2.7.2 Selected Materials

Originally, the material that was selected for use in the drone was carbon fibre, due to its high properties. Nevertheless, while preparing for the use of carbon fibre, fibreglass was used as a practice run, to determine how to best produce the structural components. The fibreglass components proved to be lightweight enough with a high enough stiffness to be used as the structural components; therefore, the main material for the drone body was switched to fibreglass.

Chapter 4: Product Development

The development process as with many cases in engineering was not a linear process. It was a constant iterative trial and error process, by which a design or aspects of a design would be conceived, tested and then confirmed or discarded, depending on how it fit in with the overall product. There were often cases by which a design would be pursued and then a better option would be discovered, without certain components, or the design was no longer seen as feasible and then it would be back to the drawing board. The following sections will outline this process and the steps that were taken in developing a good solution. All of the flight simulations were performed with the Drone flying at 20 m/s.

4.1.1 Design Process

4.1.1.1 Size Determining Design

The original design for the drone took one-step further from a sketch to hollow out the body in order to determine the overall sizing of the drone body and figure out what components would be capable of fitting inside the drone body. At this point, the decision had not yet been made whether to use cables for gimbal actuation or whether to use directly connected motors. This design also does not take into account appropriate propeller size for thrust motors.

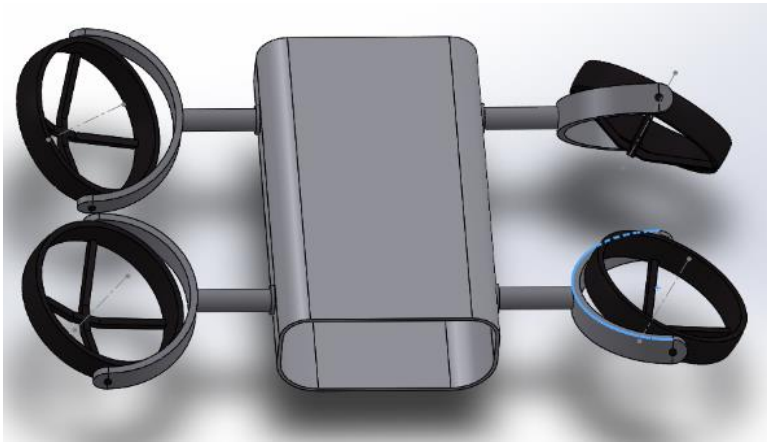

4.1.1.2 Duct Design

Once the appropriate lift calculations had been performed to determine the propeller size, the duct could be designed in order to fit to the propeller. This required a scaling up in the size of the ducts, while at the same time having to take into account how the duct would be mounted to the drone and how the motor would be mounted on the duct. An additional design change

was to optimize the airflow through the duct, based of existing fans and duct designs, with sloping edges for directing the flow of air.

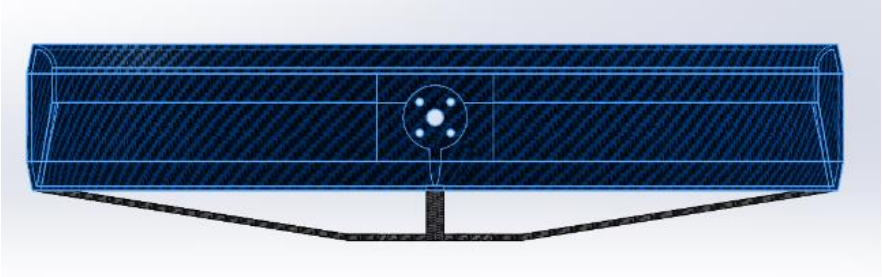

4.1.1.3 Aerodynamic Full Scale Design

After determining what were all the major components that were required for the drone to function properly, a redesign of the drone frame was made for a more aerodynamic design, which was capable of containing all of the components. This design was heavily influenced from an aesthetic standpoint in order to look fascinating. At this point the slip ring was still seen as a necessary component, that would assist the function of the drone, hence a slip ring was attached to the opposite side of the duct as the motor, as well as in front of the motors on-board the drone. This detail, alongside ensuring that the drone was balanced by having the motors equally spread apart led to the size of the drone. This model contained all connecting points, as well as a battery slot.

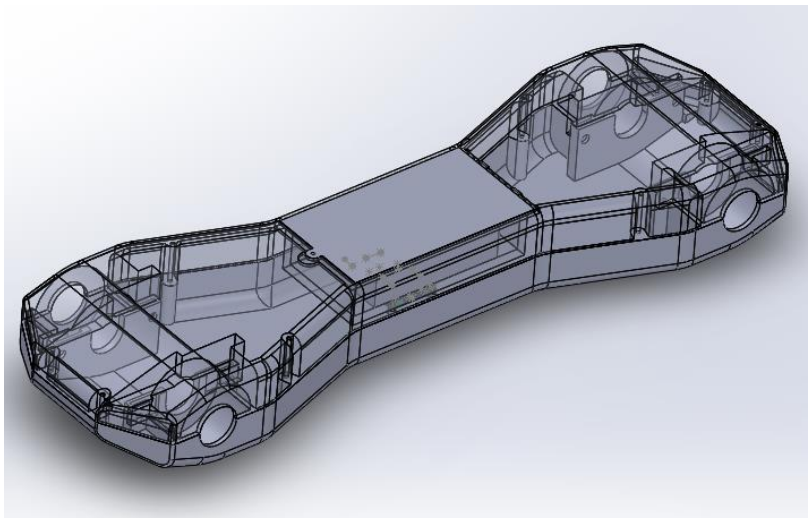

Due to the complexity of the joints connecting the two halves of the design, this version was designed with the use of HIPS plastic through injection moulding in mind. However, after discovering the price for making the mould of such a large drone design, injection moulding was no longer seen as an option. In addition to this, this design proved to be much too heavy for the motors, and any increase in the thrust motor size had follow on effects on the torque

required to rotate the gimbal arms and the motor required to turn it, making this model infeasible, due to weight and cost.

To solve this issue, the slip rings were deemed unnecessary, by which the model could be scaled down by a large degree and the frame could be made more minimalistic.

4.1.1.4 Minimalistic Design without Slip Rings

The removal of the slip rings left the gimbal arm unbalanced, therefore to balance the system and to increase the torque on the duct, a second gimbal motor was placed on the other side of the duct.

By removing the slip rings, the gimbal arms no longer had a support structure and would just be hanging off of the motor, hence to reduce the strain on the motor, it was decided to add an extra structural layer in the form of a ball bearing, which allowed for rotation, inside of a casing. In addition to this, a minimalistic sandwich frame was designed to support the arms, while not adding excessive weight.

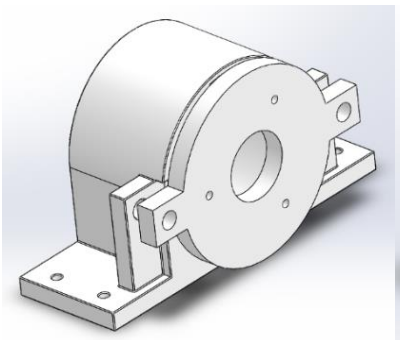

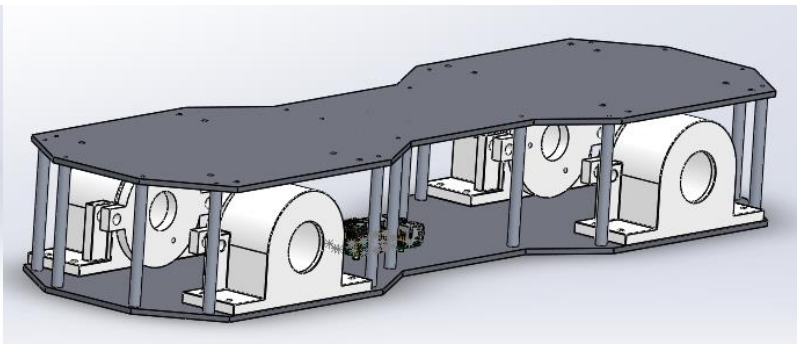

4.1.1.5 Simplified Gimbal Arm

It was realised that by reducing the distance of gimbal arm and hence the duct from the motor, would reduce the overall torque that the gimbal arm exerts on the motor, therefore eliminating the need for any support structure and therefore allowing for a more compact drone design. This allowed for the gimbal arm to be redesigned and any unnecessary parts to be removed.

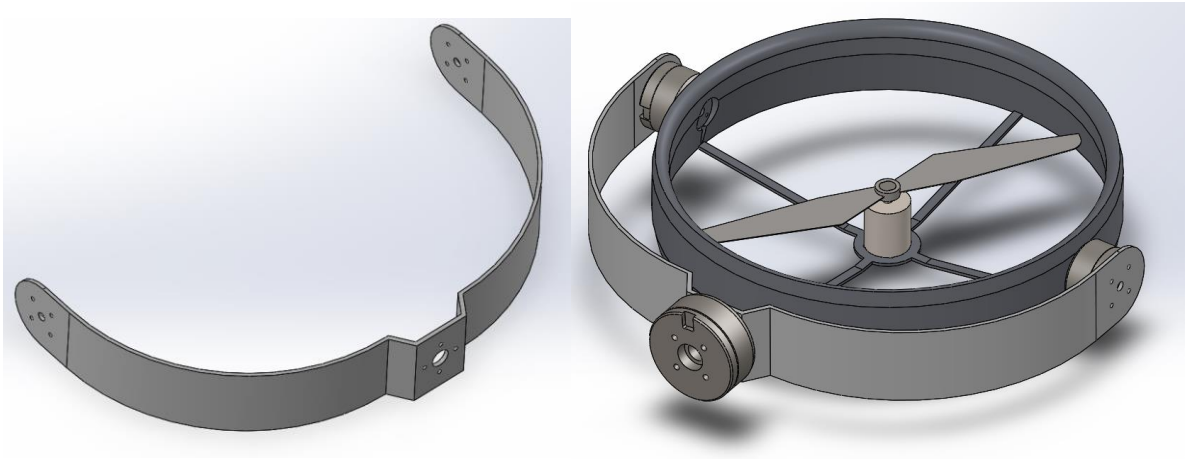

4.1.1.6 Prototype 1

Bringing the ducts closer in meant that there was no longer a need for such a wide frame, however, the gimbal motors holding the drone arms still required a structural support. From this, it was decided to make the frame structural, creating a much thinner design, which removed the need for the many fastening points required by the sandwich design. This design could be easily manufactured using composites and therefore became the design used for the first prototype.

Finally, having a prototype to work off, the aerodynamics of the design could be tested in Solidworks, to determine the effects of air resistance on it. This design, similar to the initial concept design produces a fair bit of airflow deflection behind it, with a loss of air speed reaching a maximum of 17 m/s, due to the size of the propeller ducts (*Figure 4.1*). The air speed

of the rear ducts is still less compared to that of the lead ducts, meaning that the rear propellers have to exert more thrust to provide the same amount of lift compared to the front propellers. The maximum friction force experienced by this design is ~0.28 N, which is more than the concept design, which was ~ 0.0167 N, however this is most likely because of the scaled up size of the drone, compared to the concept design (See *Table 4.1*). In forward flight, the prototype has a positive force of 7.55 N in the y-axis, showing that there is a fair amount of lift advantage due to the design.

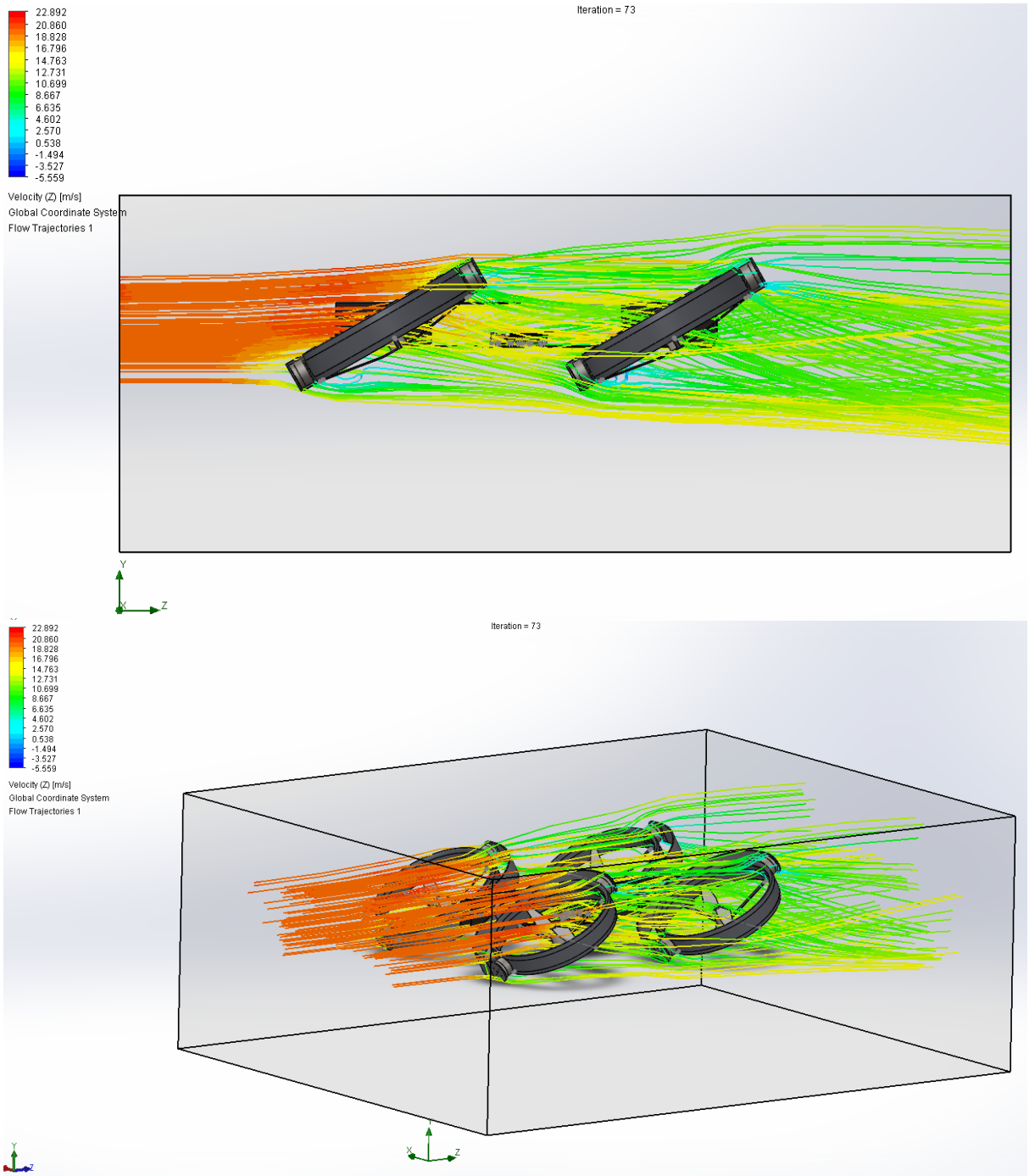

Figure 4.1: Aerodynamics of Prototype 1 in Forward Flight

Table 4.1: Aerodynamics Data of Prototype 1 in Forward Flight

Goal Name	Unit	Value	Averaged Value	Minimum Value	Maximum Value
GG Maximum Total Pressure 1	[Pa]	101955.1944	101953.3151	101943.727	101963.0676
GG Maximum Total Temperature 1	[K]	293.4056337	293.4026447	293.3995876	293.405727
GG Maximum Velocity 1	[m/s]	23.08173561	23.45836035	23.07996467	25.68414692
GG Maximum Velocity (X) 1	[m/s]	18.80468473	19.13993878	18.64874922	19.60718028
GG Maximum Velocity (Y) 1	[m/s]	13.72916256	13.64210564	13.14998162	14.09527668
GG Maximum Velocity (Z) 1	[m/s]	23.04724051	22.89298501	22.8201032	23.10791254
GG Force (Y) 1	[N]	7.520605547	7.528052615	7.510086897	7.549495993
GG Friction Force (Z) 1	[N]	0.270115519	0.271863104	0.265632628	0.279731961

Iterations [ ]: 73

Analysis interval: 23

In addition to forward flight, the angled flight of the drone was also analysed to observe the streamline and drag. This allows for a representation of when it is necessary for the drone to fly in a non-optimal direction, instead of just straight ahead. In angled flight, the drag profile of prototype 1 is significantly greater, due to the drone not flying in the direction of its streamlined body. This flight method creates some turbulence behind it and reaches a maximum loss in air speed of ~20 m/s (*Figure 4.2*). In angled flight, the rear ducts still experience some of the effects of following in the airflow of the leading duct, therefore still have a loss in their lift output. The maximum of the friction force for angled flight can be calculated to ~0.283 N, which is only slightly higher when compared to forward flight (See *Table 4.2*). In addition, in angled flight it has a positive force of 7.33 N in the y-axis, showing that even in angled flight, the design has induced lift.

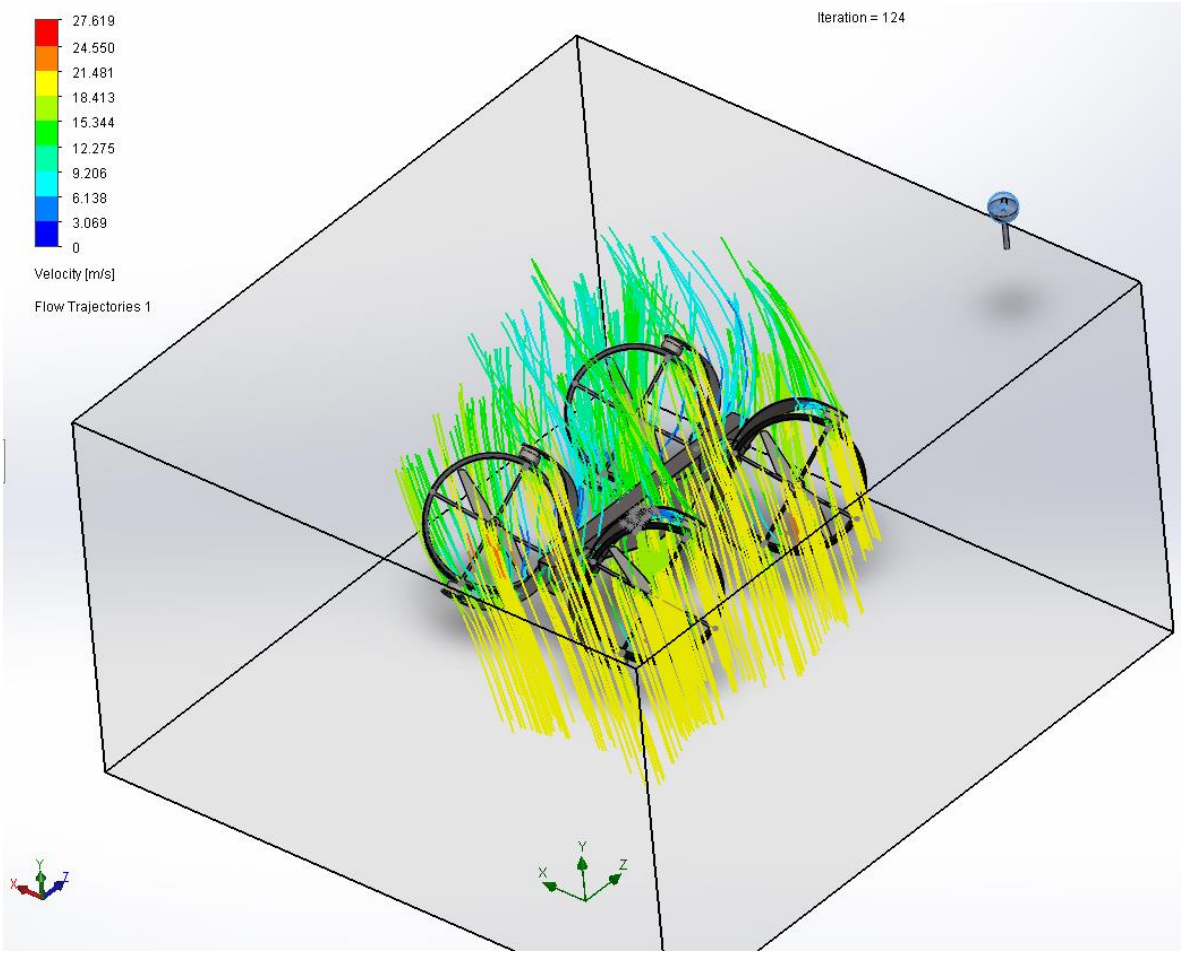

Figure 4.2: Aerodynamics of Prototype 1 in Angled Flight

Table 4.2: Aerodynamics Data of Prototype 1 in Angled Flight

Goal Name	Unit	Value	Averaged Value	Minimum Value	Maximum Value
GG Maximum Total Pressure 1	[Pa]	102293.9388	102294.5453	102293.9388	102295.1178
GG Maximum Total Temperature 1	[K]	293.4168511	293.4168092	293.4167586	293.4168714
GG Maximum Velocity 1	[m/s]	26.60572224	26.68160151	26.60572224	27.09638408
GG Maximum Velocity (X) 1	[m/s]	25.42892006	25.44480684	25.42892006	25.4586241
GG Maximum Velocity (Y) 1	[m/s]	19.05163904	19.13483024	19.05163904	19.21660132
GG Maximum Velocity (Z) 1	[m/s]	19.85303355	19.8115232	19.73818885	20.46125252
GG Force (Y) 1	[N]	7.317395069	7.303734394	7.287999996	7.325541858
GG Friction Force (X) 1	[N]	0.205143756	0.204114166	0.202921916	0.208003515
GG Friction Force (Z) 1	[N]	0.207735123	0.205753337	0.203152756	0.207735123

Iterations [ ]: 124

Analysis interval: 25

The overall weight of this design comes out to approx. 4400 g, which is greater than the output thrust of the motors, which is an issue that would have to be covered in the manufacture process, in order to develop a more lightweight solution, so that the thrust motors could be used on this model. The overall cost of this design would come out to ~NZD 2340.

Table 4.3: Prototype 1 Components List

Component	No. Required	Weight(g)	Sum Mass	Cost (NZD)	Sum Cost
Body	1	300	300	81.97	81.97
Gimbal Arm	4	55	220		
Gimbal Arm Motor	4	137	548	106.76	427.04
Duct	4	140	560		
Duct Motor	8	88	704	71.13	569.04
Thrust Motor	4	67	268	186.45	745.8
Propeller	4	17	68		
ESC	4	21	84		
Raspberry Pi	1	103	103	107.66	107.66
Navio2	1	23	23	240.85	240.85
Battery Pack	1	1517	1517	168.11	168.11
Overall		**4395**	**g**	**NZD**	**2340.47**

4.1.2 Manufacturing Process

Fabrication of the drone required creating a drone frame, based off the chosen design, that was capable of carrying all of the drone components, being both strong enough to not break from the weight of the components, while at the same time not adding too much excessive weight to the drone.

4.1.2.1 Drone Ducts

To produce prototype ducts 3D printed ducts were created using PLA. These prototype ducts were used to give an idea of the actual size of the product and to see how the propellers and motors would fit to the duct. This 3D printed duct also gave an estimate of the overall weight of the design if the whole thing were to be made of PLA. It could then be used for proving what changes could be made to the duct thickness and size in order to make it lighter, without breaking. The duct had to be 3D printed in three separate parts as the duct halves and the base and then be joined using a slot and key method.

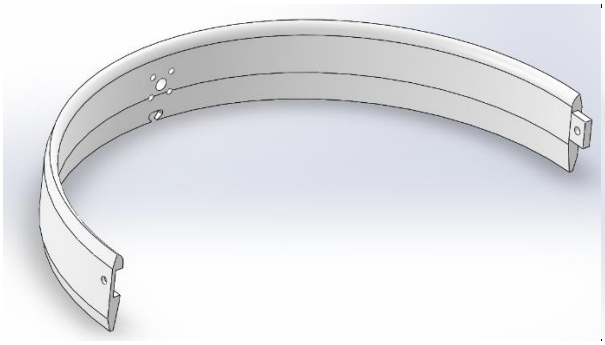

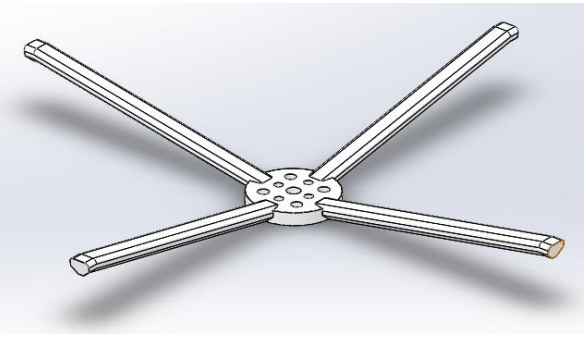

It was quickly determined that these PLA filament ducts were much too heavy for the drone, as they were only a small portion of the drone itself, but weighed approximately 400 g each, together weighed almost half of the take-off weight.

4.1.2.2 Polymer Manufacturing

After deciding to use the polymer carbon fibre in order to reduce the weight, the next stage was to determine how to best proceed in applying the polymer and shaping into the required design. Carbon fibre can be a difficult material to work with and requires a mould to which the material can be fit and then the application of epoxy allow the material to take on the properties that are so seeked after. To manufacture using carbon fibre, the options that were entertained were vacuum forming, laying carbon fibre strips and hand pressing them into shape or 3D printing using the carbon fibre composite of ONYX. 3D printing could make the most complicated designs, vacuum forming left a good finish and allowed for some complicated designs and hand pressing did not allow for complex designs, but was the simplest method of manufacture.

3D printing the carbon fibre proved to be much too expensive, and the 3D printer for ONYX was much too small to produce any large parts on it. Due to simplicity in producing, hand pressing the carbon fibre material onto cut-to-shape Styrofoam moulds was determined to be the best option. However, in order to hand-press the polymer onto the ducts, the design of the ducts had to be simplified down to a basic hoop design and the base could be laser cut from MDF and attached to the bottom of the duct, using brackets and screws. This meant that the duct would not have the same flow qualities as the previous design, but would be much more lightweight.

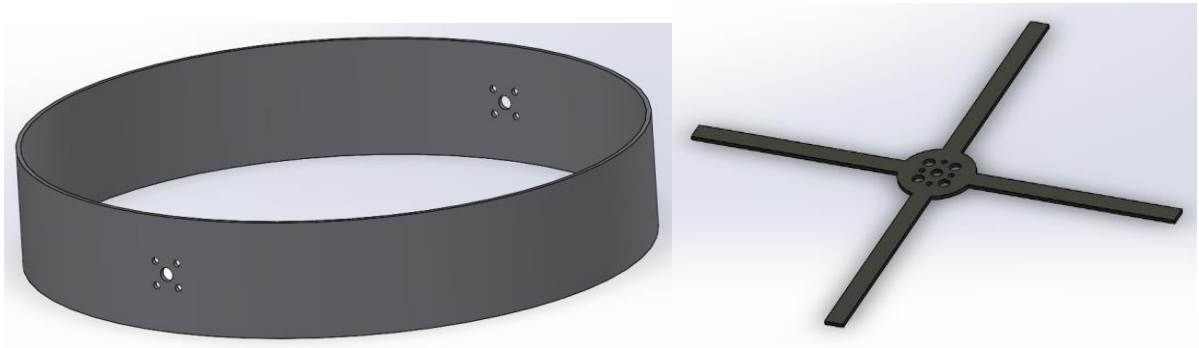

In order to create the mould out of Styrofoam, a hot wire cutter was used to cut the material into the correct shape, using MDF boards as an outline and then the different sections could be glued together to complete a mould (*Figure 4.3*). The foams surface proved much too rough to lay a polymer directly onto it, therefore the solution to this was to cover the mould with three layers of epoxy resin and sand them down each time. Covering this with a release agent allowed for a non-stick surface to be created that would ensure that the resin from the

polymer would not stick to the resin of the moulds. After the release agent had dried, the polymer could be applied in layers wrapped around the duct.

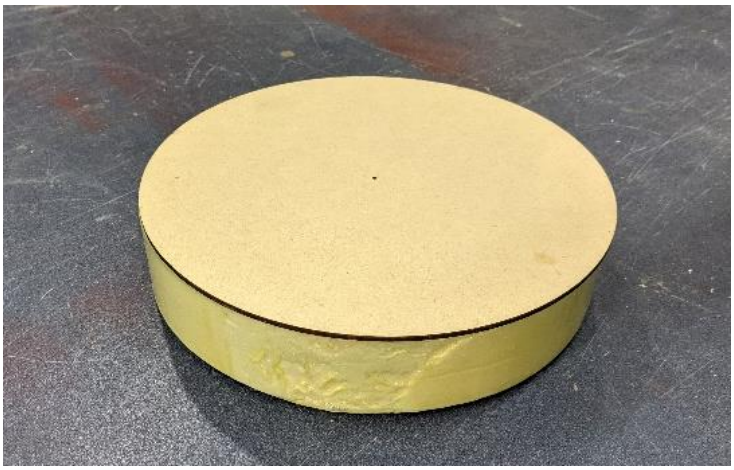

Figure 4.3: Duct mould with MDF outline board

In preparation for using carbon fibre, fibreglass was used as a practice run in order to determine the best method of applying the polymer material. The entire process of preparing the mould, laying the fibreglass and letting it dry took approximately 2 days. After drying, the fibreglass duct could be removed from the mould by soaking it in water, allowing the release agent to dissolve and then pushing out the mould. This fibreglass test mould proved to be very lightweight and just a little flimsy, which could be solved by adding more layers to it.

On receiving the carbon fibre, the same process was applied to it, however, the carbon fibre cloth proved much more difficult to work with, fraying at the edges, leaving the ducts with a bad finish and very sharp edges (*Figure 4.4*). To remove the sharp edges and give the carbon fibre a good finish, would require the edges to be sanded down, however due to the brittle nature of the carbon fibre, it was prone to cracking. Therefore, it was decided to continue using fibreglass and make the remaining body parts from it.

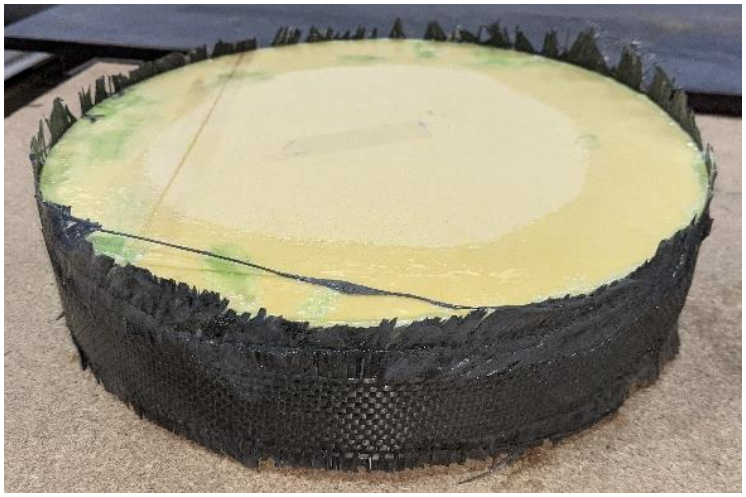

Figure 4.4: Hand-Formed Carbon Fibre Duct Outcome

4.1.2.3 Fibreglass Manufacturing

In order to effectively use the fibreglass structurally, the thickness of the walls had to be increased by laying more layers. The Test Duct was made up of three layers, whereas the structural ducts were made by applying five layers. The process of developing the mould could be repeated for three more ducts, as well as the gimbal arms (*Figure 4.5*) and the drone body.

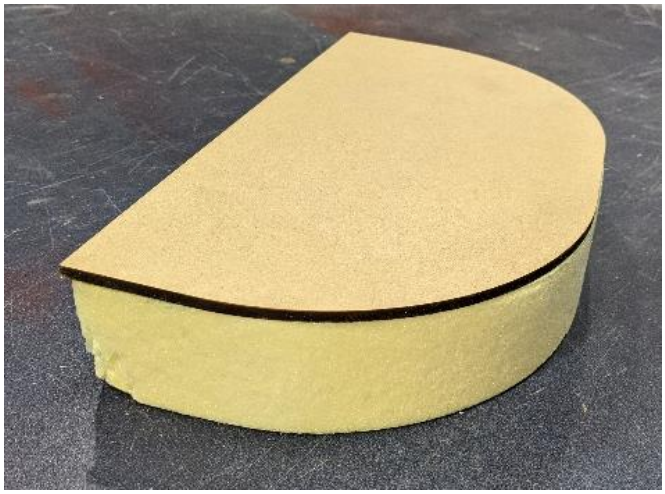

Figure 4.5: Gimbal Arm Mould

The moulds for the ducts and the gimbal arms were easy enough to remove, leaving a finished product that could be sanded down in order to provide a better finish, however in the case of the drone body, removing the mould was not as simple as pushing it out, due to the more complicated shape of the design. The solution to this was to melt out the Styrofoam, using acetone, which could then be scooped out, leaving behind just the frame.

After creating the moulds from the fibreglass, the next step was to create the connection points through drilling accurate holes and mounting holes. In order to assure that the holes were evenly placed, simple laser printed MDF jigs were created to consistently place the holes in the same place on each of the parts and then the holes could be drilled using a hand drill (see following images).

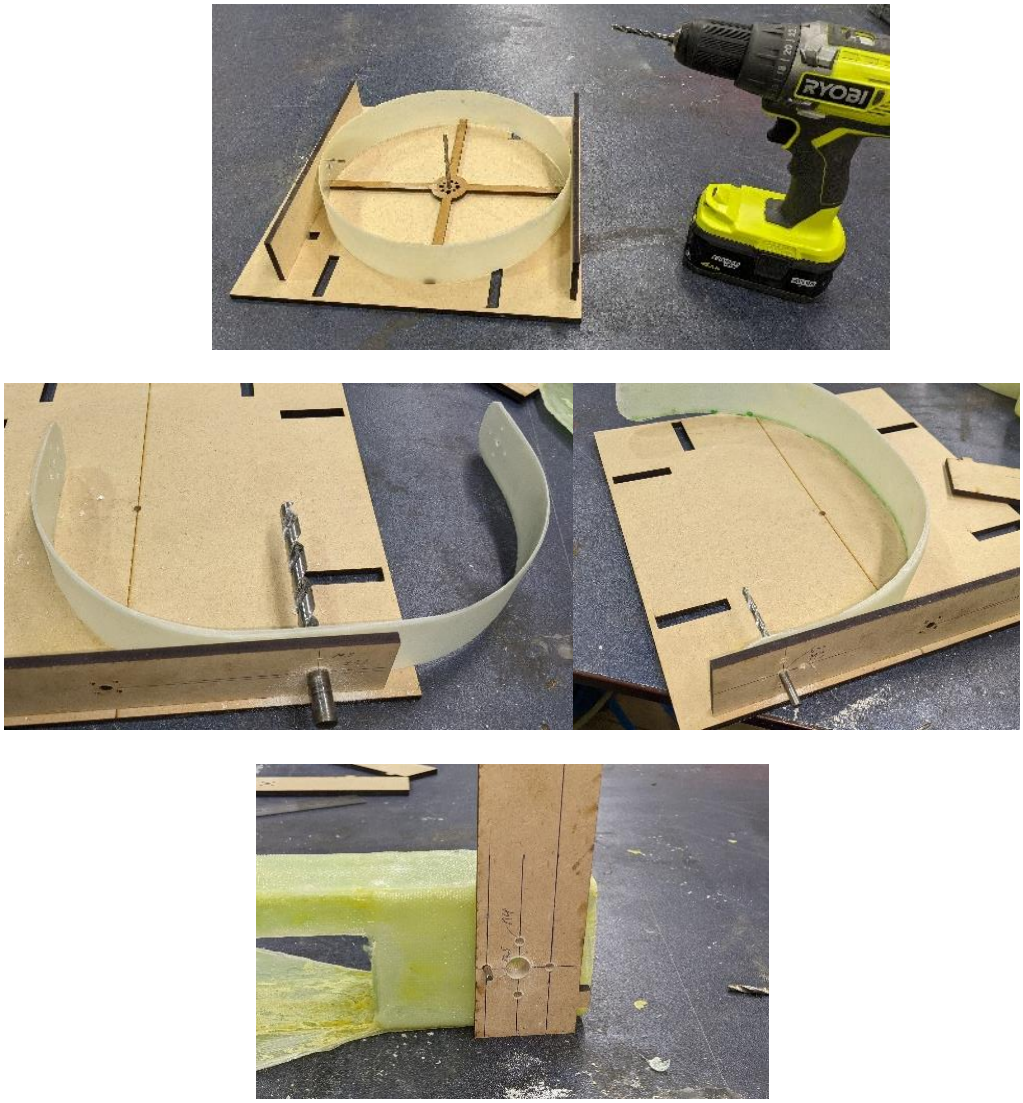

Figure 4.6: Hole Drilling Jigs

Finally, all of the body parts were completed and just required the mounting of all of the control and actuation components.

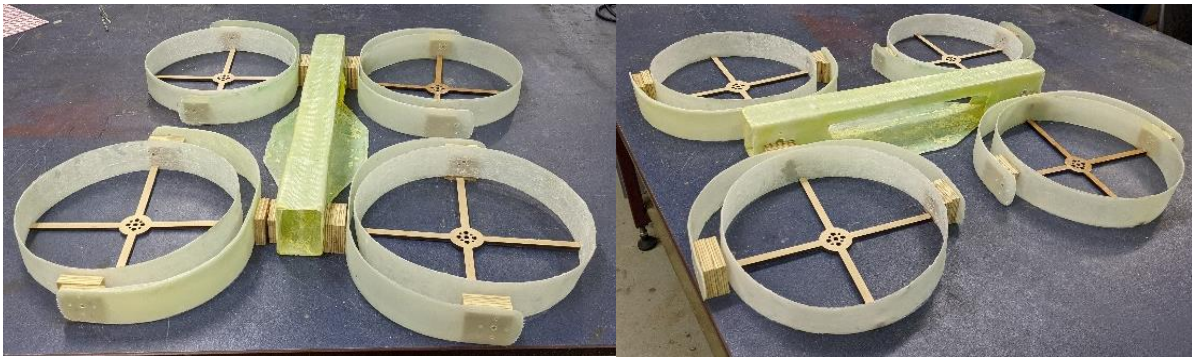

Figure 4.7: Completed Prototype 1 Body

4.1.3 Last Minute Design Changes

It was late on in the project by the time the body parts had been fully manufactured and the overall design still proved to be very heavy, reaching the upper limit of the motors lift capabilities, due to the weight of the overall drone being more than previously predicted, with all of the extra material and required components. Determining how to use carbon fibre more effectively and leaving a better finish would prove to take too much time, not leaving enough time to perfect the system control and program needed to maintain the drone stability.

Therefore, on reviewing the previous concepts, it was decided that another design would be more practical for pursuing as a final design, without needing to train the data through machine learning in order to maintain stability. By reducing the surface area on the Gimbal Tilt-Body Design, the overall effects of drag could be reduced to make a more streamlined design. In addition to this, the carrying capacity of this design proved to not be as limiting as previously believed, due to the same reason that the slip rings were no longer required.

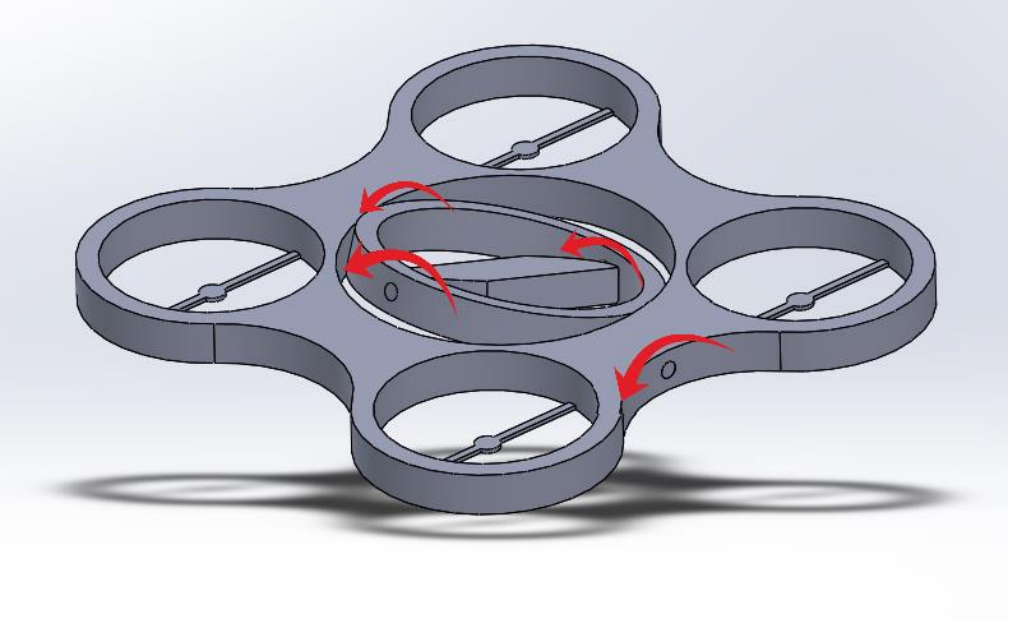

4.1.3.1 Streamlined Gimbal Body Redesign

Originally, it was believed that the carry capacity of this drone design was limited to the size of the centre of the gimbal, as the gimbal had to be capable of moving freely and unhindered, without affecting its ability to rotate. However, after concluding that each of the gimbal rings would never really pass and angle much greater than 45° from the angle of incidence, as this would no longer be conducive to flight, as the propellers would therefore no longer be providing a sufficient amount of upwards thrust. This means that the load capacity of this drone could be greatly increased by adding the loads underneath or above the drone body, as long as they did not interfere with the rings ability to rotate at least to a 45° angles.

Preferably, any added load would be placed underneath the drones centre body, as this would also assist in the stability of the centre section. An initial worry was that this design would result in undesired swinging of the centre section, but by using ball bearings as connecting joints, friction would be reduced. In addition to this, the added increased inertia of any added mass would just add to the overall stability of the central section, as inertia is directly related to mass, as seen in the below equation.

Equation for Inertia of hoop about diameter:

$$I = \frac{1}{2}MR^2$$

Finally, another major issue that needed to be taken into account was that the proposed concept design was not very aerodynamic, and therefore would be greatly affected by air resistance as it flies. To reduce the air resistance, the overall surface was decreased, in order to

develop a drone that would be designed purely for function, with thin gimbal rings, that would not produce a large amount of air resistance as it flies in the given direction.

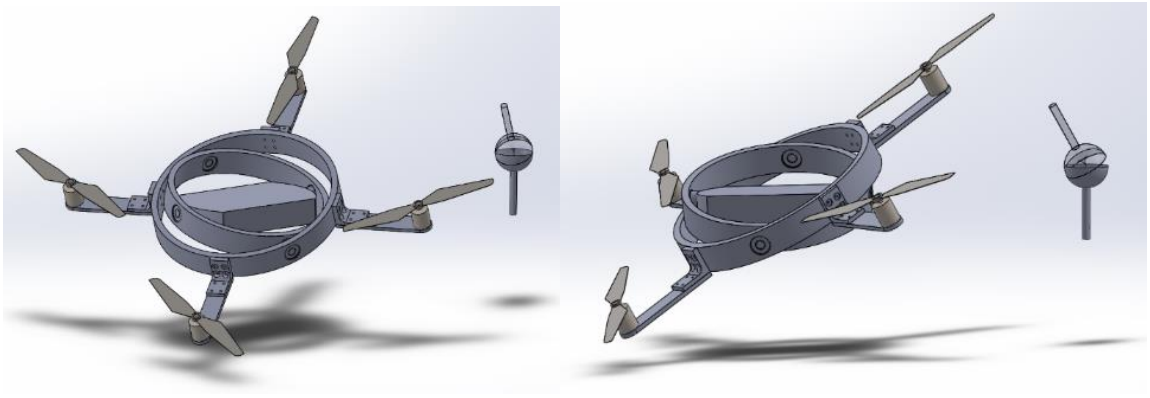

In order to compare the aerodynamics of this design with the previous design, it was also run under flow modelling in SolidWorks, to determine the effects of turbulence and drag on it. This was also repeated at angled flight, in order to determine the effects of having all of the gimbal rings out of alignment.

The gimbal body drone produced very little flow deflection with a small profile drag, where the maximum loss of air speed was 14 m/s, which is significantly less compared to prototype 1 (*Figure 4.8*). In addition to this, unlike with the concept model, no turbulence is formed at the centre of the gimbal; instead, the air just flows around the gimbal. In contrast with prototype 1, none of the effects of the leading edge propeller were experienced by the trailing propeller, meaning that there is no loss in lift; however, this may vary depending on the speed and angle of attack of the drone. The maximum friction force of this design is ~0.097 N, which is significantly less compared with prototype 1's friction force of ~0.28 N, showing that it is indeed more streamlined (See *Table 4.4*). Prototype 1 does have a greater positive force in the y-axis, where the design has a greater lift advantage, however this is offset by the increased overall weight of the design. The lift gain of the gimbal body drone is at max 0.97 N.

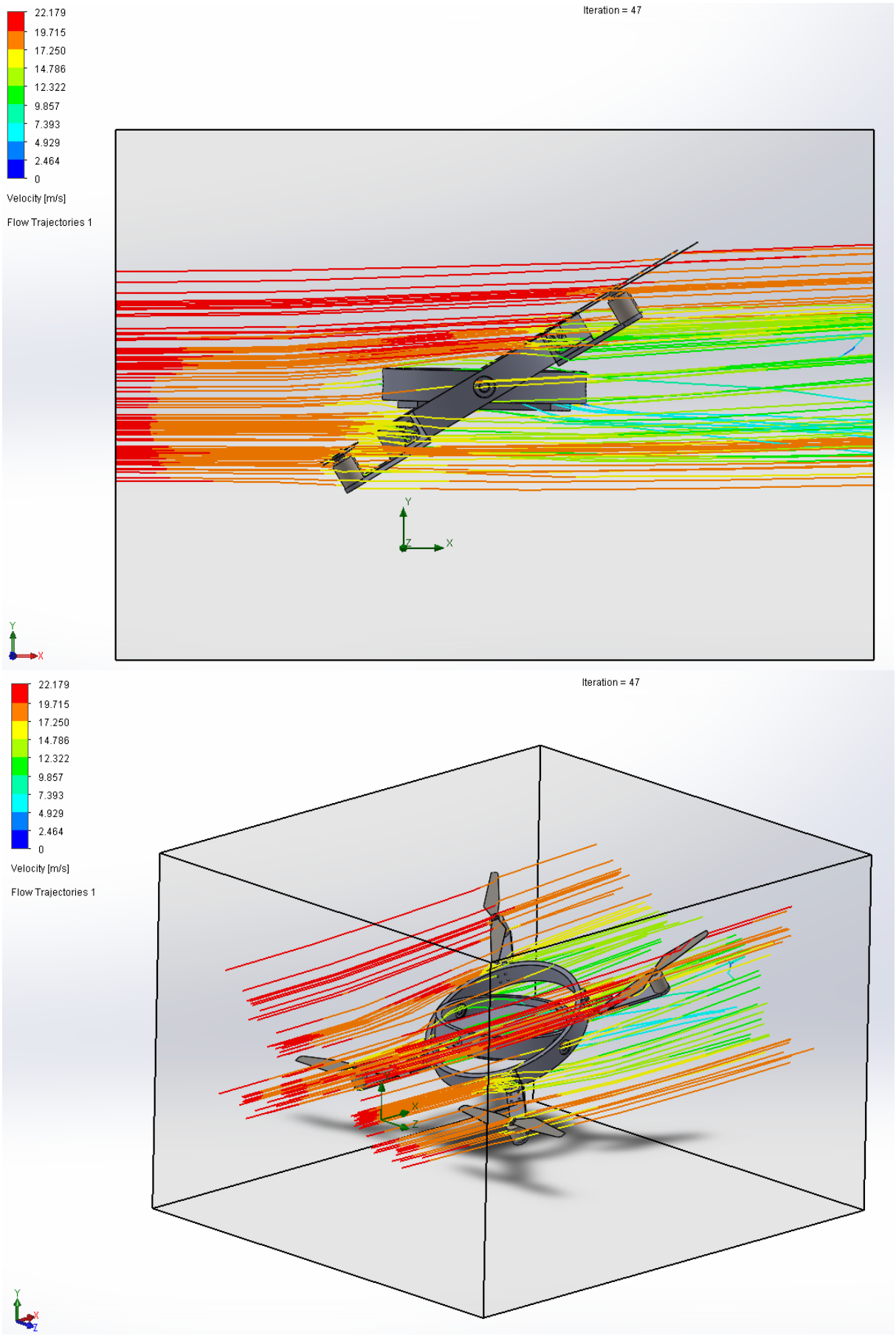

Figure 4.8: Aerodynamics of Gimbal Body Drone in Forward Flight

Table 4.4: Aerodynamics Data of Streamlined Gimbal Body Drone in Forward Flight

Goal Name	Unit	Value	Averaged Value	Minimum Value	Maximum Value
GG Maximum Total Pressure 1	[Pa]	101885.5859	101868.494	101831.8412	101899.6242
GG Maximum Total Temperature 1	[K]	293.3991069	293.3991144	293.3989689	293.4004617
GG Maximum Velocity 1	[m/s]	23.83056176	23.36253922	22.85361155	23.94269854
GG Maximum Velocity (X) 1	[m/s]	22.75171543	22.50390856	21.83954413	22.7600941
GG Maximum Velocity (Y) 1	[m/s]	6.333948402	6.266114615	6.131939614	6.362658694
GG Maximum Velocity (Z) 1	[m/s]	9.483042482	9.512327577	8.953961818	9.806585213
GG Force (Y) 1	[N]	0.219381702	0.155296192	0.111571947	0.219381702
GG Friction Force (X) 1	[N]	0.093778994	0.094049454	0.092370893	0.097008526

Iterations [ ]: 47
Analysis interval: 21

For the gimbal body drone in angled flight, there is not much of an increase in profile drag, with the deflection of air from the body remaining minimal. The maximum loss in air speed at angled flight is also ~14 m/s (*Figure 4.9*). Similar to when in forward flight, in angled flight, none of the drone's propellers affect the airstreams of the other propellers; hence, there is not decreased lift generation from down wash. The friction force of the gimbal body drone in angled flight can be calculated to ~0.08 N, which is significantly less than that of prototype 1 and is even less than that of the gimbal body drone in forward flight, showing that is more streamlined in angular flight. However, it has a negative force of ~0.04 N in the y-axis meaning that the design provides a slight downwards force when in angled flight.

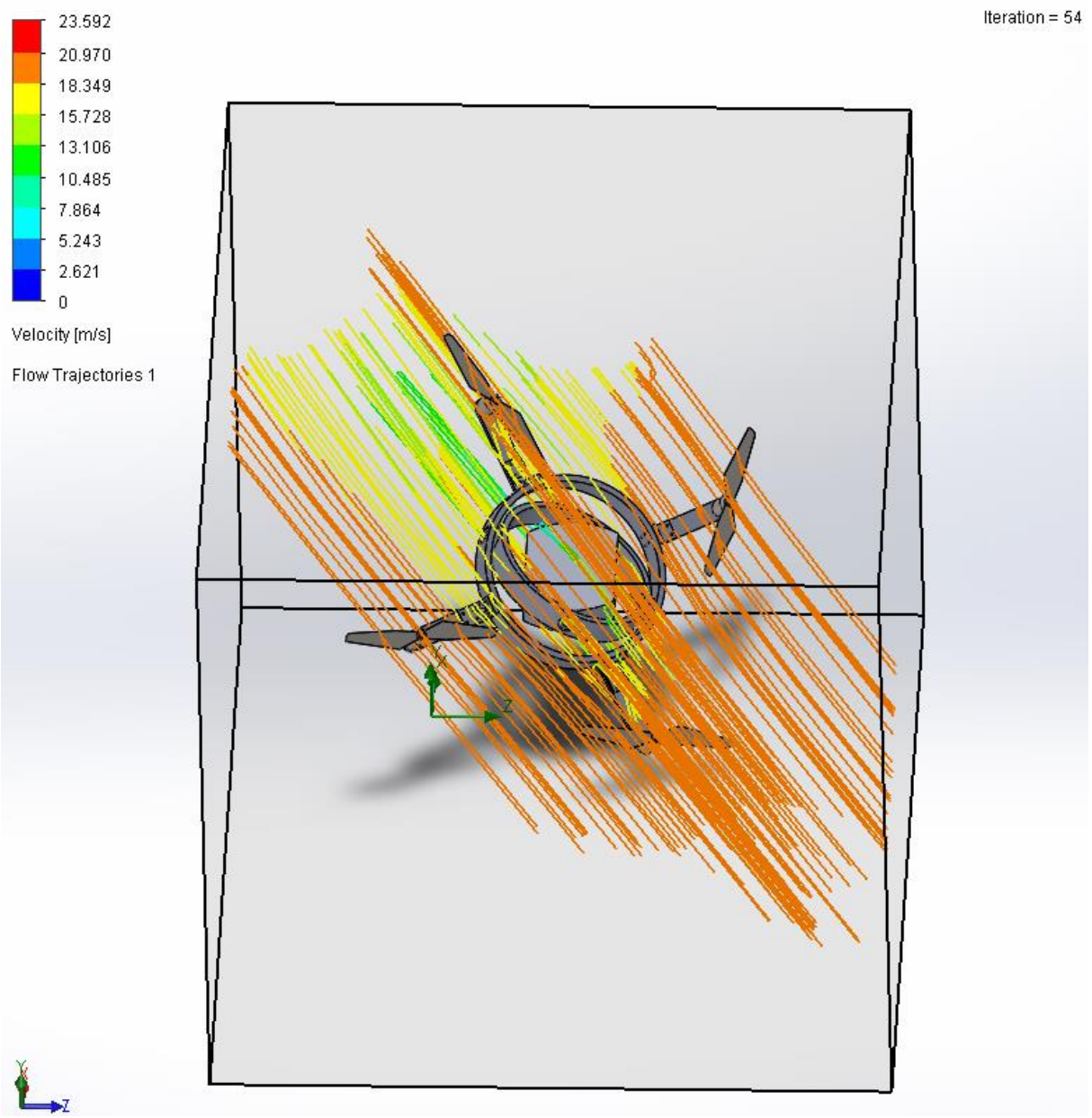

Figure 4.9: Aerodynamics of Gimbal Body Drone in Angled Flight

Table 4.5: Aerodynamics Data of Streamlined Gimbal Body Drone in Angled Flight

Goal Name	Unit	Value	Averaged Value	Minimum Value	Maximum Value
GG Maximum Total Pressure 1	[Pa]	102444.8018	102472.9165	102444.8018	102517.2046
GG Maximum Total Temperature 1	[K]	293.4107131	293.4107165	293.4107009	293.410732
GG Maximum Velocity 1	[m/s]	25.67668154	25.98351922	25.67668154	26.53985011
GG Maximum Velocity (X) 1	[m/s]	20.28610038	20.30509251	20.28610038	20.32608815
GG Maximum Velocity (Y) 1	[m/s]	3.724145841	3.73550053	3.723839061	3.762643117
GG Maximum Velocity (Z) 1	[m/s]	9.32085576	9.584135116	9.32085576	10.06287504
GG Force (Y) 1	[N]	-1.59796402	-1.584837445	-1.597964022	-1.567537992
GG Friction Force (X) 1	[N]	0.071382773	0.071418905	0.071349482	0.071526979
GG Friction Force (Z) 1	[N]	-0.03715593	-0.037209772	-0.037332578	-0.037148659

Iterations [ ]: 54

Analysis interval: 21

Further advantages of using this design are that there is a significant decrease in overall weight (See *Table 4.6*), as no consideration needs to be made to adding extra motors for controlling the gimbal rotation, as well as their required ESCs. In addition, this drone could fly off fewer batteries, or even store a larger battery pack to allow for a longer flight time, due to the reduced weight. To further reduce the weight of the drone, the gimbals can be made thinner. In addition to this, it is also a cheaper design at almost half the price with ~NZD 1350.

Table 4.6: Gimbal Body Drone Components

Component	No. Required	Weight(g)	Sum Mass	Cost (NZD)	Sum Cost
Gimbal Outer Ring	1	350	350	30	30
Gimbal Inner Ring	1	363	363	24	24
Gimbal Centre	1	246	246		
Connecting Rod	4	3.4	13.6	1	4
Ball Bearing	6	21	126	4.33	25.98
Arms	4	24	96		
Mounting Bracket	4	19	76	1.91	7.64
Thrust Motor	4	67	268	186.45	745.8
Propeller	4	17	68		
ESC	4	21	84		
Raspberry Pi	1	103	103	107.66	107.66
Navio2	1	23	23	240.85	240.85
Battery Pack	1	1517	1517	168.11	168.11
Overall		**3333.6**	**g**	**NZD**	**1354.04**

As previously mentioned, this design does not require the same amount of programming, making it much simpler to develop, without the need for machine learning or integrating several different systems to work in unison, just to make it able to fly. Instead, it is capable of flying like any other drone by varying its motor speed.

The disadvantages of this design are the same aspects that give it many of its advantages. Due to it being uncontrolled at its joints, it means that this design can be easily influenced by external factors, such as wind. Any amount of wind can lead the centre point of the design to start swinging and therefore lose its ability to maintain stable flight. However, this can be circumvented, by designing a central section that will take into account the effects of wind. By making the central section a naturally aerodynamic shape, such as an oval, hopefully, any effects of wind can be minimized and therefore make it more stable in these conditions.

Additionally, just because this model does not require any on-board motors to allow for stability, does not mean that they are out of question. By replacing, the ball bearing joints with gimbal motors, it would allow the centre of the drone to be more easily controlled, which would come at an increase of weight. Although the additional weight would still be less than in the earlier proposed design.

To further increase the aerodynamics of the drone, the arms of the drone could be redesigned to resemble a teardrop or circular shape. This means that as the drone flies in any direction, it does not create a large amount of exposed surface area to be affected by air resistance.

4.1.3.2 Gimbal Body Manufacturing

With limited time, the manufacturing of the gimbal body drone was performed using easily workable materials on-hand. The easiest material and most accessible material is wood. Due to this, the rings were made from gluing lightweight wooden disks together and cutting out the hole using a jigsaw to produce the gimbal hoops/rings. The through-holes for placement of the ball bearings could be achieved by drilling holes in the sides of the hoops with a Forstner Drill Bit. The central gimbal was one of the cutout centres of the gimbal hoops, which was slightly modified to move more easily within the gimbal.

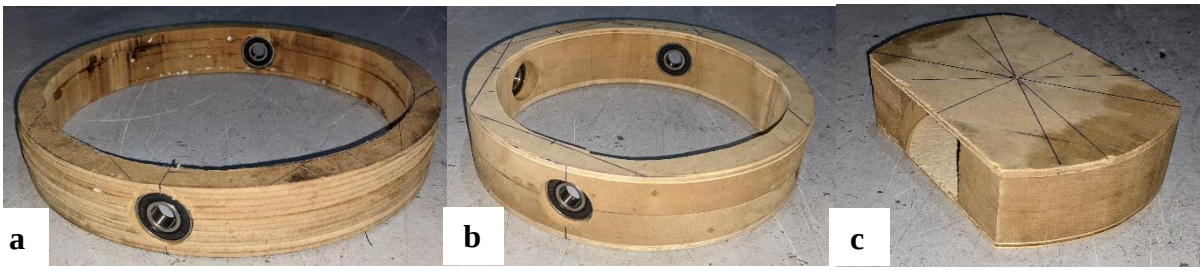

Figure 4.10: (a) Gimbal Outer Ring; (b) Gimbal Inner Ring; (c) Gimbal Centre

On completing the gimbal sections, the individual rings could be connected using wooden dowels that fit to the size of the ball bearings inner diameter. By slotting these together, the gimbal part of the drone was completed.

To create the drone arms, flat wood pieces were cut to size and holes for the motor were drilled at each end. The arms could then be mounted onto the outer gimbal ring, using a combination of brackets and glue. Overall, this design was much simpler to complete and therefore did not require too many steps.

Figure 4.11: Drone Arms

Figure 4.12: Gimbal Body Drone Completed Frame

Chapter 5: Conclusion and Limitations

This Research & Design Thesis shows that developing a means by which to have stable bodied flight can be useful in a range of different situations, including construction and transportation.

Stable-bodied flight can be implemented in drones through a range of different options, varying from concepts that require rotating arms to ideas that use gimbals to maintain stability within the body. However, the idea remains the same in that the drone needs to be able to change the angle of attack of its propellers, without affecting the angle of attack (AOA) of the body.

Two main drone types were looked at for development, both with the use of gimbals to allow for infinite degrees of freedom, while isolating the AOA of the rotors from the body. One option was to place the rotors on the gimbals and controlling their AOA using gimbal motors, the other was to make the drone body a gimbal, allowing the inertia and weight of the body to maintain stability, while the propellers and outer gimbal ring fly like a typical drone. The gimbal rotor drone requires the use of machine learning to accurately determine the appropriate response to a change in the IMU readings, which gives it absolute control over the drone's motion, whereas the gimbal body drone, works on the concept of unhindered movement and inertia to maintain its stability and is less controlled.

The gimbal body drone proved to be an overall more streamlined design, and a much simpler design, allowing it to be more easily manufactured, while the gimbal rotor design was a much more complex design with a lot more moving parts and components, which resulted in it being more likely to have weight issues. Due to these reasons, it was decided that the gimbal body drone should be the final design and this was pursued for developing into a final product.

The very same factor that makes the gimbal body drone so simple, are what give it its limitations in maintaining stable bodied flight. The bodies rotation is not controlled, instead it uses gravity and inertia to maintain its stability, however if this were to be exposed to extreme forces, such as very rapid acceleration and high gusts of wind, it could lead to the body starting to swing from the resulting effects. In order to counteract the effects of rapid acceleration, ball bearings with less friction would be required in order to not feel the effects of the rapid acceleration. To reduce the effects of the extreme conditions such as wind, the body shape can

be aerodynamically optimized, such as developing a more spherical body, with a higher bottom weight in order to not react as much to the effects of the wind. In addition to this, the use of gimbal motors can be added to the design to allow for controlled rotation, but this would come at a loss in simplicity.

Recommendations for further development would be to pursue an even more aerodynamic design, such as round-arm stalks in order to further reduce the effects of drag on the drone design, or any one of the previously mentioned limitations, such as the more aerodynamic body. Additionally, the model can be scaled up to create a bigger model capable of carrying a larger payload.

In conclusion, it is possible to develop a drone with stable-bodied flight in order to provide a non-tilting platform for carrying payloads in the future and there are a range of possibilities for further developing this design and making it more efficient.

Chapter 6: References

Acharya, R. (2014). *Understanding Satellite Navigation.* Cambridge, Massachusetts: Academic Press.

Adamski, M. (2017). Analysis of propulsion systems of unmanned aerial vehicles. *Journal of Marine Engineering & Technology, Volume 16*, 291-297.

Aerospace Engineering. (2012, July 12). *Composites Manufacturing*. Retrieved from Aerospace Engineering Blog: https://aerospaceengineeringblog.com/composite-manufacturing/

AerospaceEngineeringBlog. (2016, September 18). *On Boundary Layers: Laminar, Turbulent and Skin Friction*. Retrieved from AerospaceEngineeringblog: https://aerospaceengineeringblog.com/boundary-layers/

Airforce Technology. (2021, August 8). *Harfang MALE Unmanned Aerial Vehicle (UAV)*. Retrieved from Airforce Technology: https://www.airforce-technology.com/projects/harfang-drone/

Airforce Technology. (2021, August 8). *Phantom Eye HALE Unmanned Aerial Vehicle (UAV)*. Retrieved from Airforce Technology: https://www.airforce-technology.com/projects/phantomeyeunmannedae/

Airforce Technology. (2021, August 15). *V-22 Osprey Tilt-Rotor Aircraft*. Retrieved from Airforce Technology: https://www.airforce-technology.com/projects/osprey/

Albert A. Espinoza, M. K. (2020). The Effects of UAV Quadcopter Propeller Tilt Angle. *18th LACCEI International Multi-Conference for Engineering, Education, and Technology* (pp. 1-4). Buenos Aires: Universidad Ana G. Méndez – Recinto de Gurabo, Puerto Rico.

AliExpress. (2021, August 4). *ACE TATTU LiPo Battery 4S-6S 35C 25C 6600mAh 10000mAh 12000mah 16000mAh Plus 15C 25C 22.2V Lithium RC Battery for UAV Plane*. Retrieved from AliExpress: https://he.aliexpress.com/item/4001077327398.html

Alterach, G. Á. (2021, August 3). *DC motor control with H bridge*. Retrieved from gzalo: https://gzalo.com/en/articles/hbridge/

Amazon. (2021, July 29). *Amazon Prime Air*. Retrieved from Amazon: https://www.amazon.com/Amazon-Prime-Air/b?ie=UTF8&node=8037720011

Amirante, F. (2021, August 3). *Relay H-bridge (Relay Motor controller)*. Retrieved from nvhs.wordpress.com: https://nvhs.wordpress.com/project/catspberry/motor-controller/

Arrow. (2018, December 12). *What is IMU? Inertial Measurement Unit Working & Applications*. Retrieved from Arrow.com: https://www.arrow.com/en/research-and-events/articles/imu-principles-and-applications

Ashby, M. F. (2011). *Material Selection in Mechanical Design, Fourth Edition.* Oxford, UK: Butterworth-Heinemann.

Ather, S. H. (2020, December 28). *How to Calculate Lifting Force*. Retrieved from Sciencing: https://sciencing.com/calculate-lifting-force-6402937.html

Austin, R. (2010). *Unmanned Aircraft Systems: UAVS Design, Development and Deployment.* West Sussex, United Kingdom: John Wiley & Sons Ltd.

Baichtal, J. (2015). Choosing an Airframe for Your Quadcopter Drone. In J. Baichtal, *Building Your Own Drones: A Beginners' Guide to Drones, UAVs, and ROVs* (p. 15). Indianopolis: Que.

Blain, L. (2020, April 06). *Coaxial tilt-rotor drone hovers smoothly in any orientation*. Retrieved from New Atlas: https://newatlas.com/drones/omnidirectional-tilt-rotor-drone/

Blue Skies Drones. (2021, August 8). *FINDING MISSING PEOPLE, KIDS AND PETS FROM THE AIR*. Retrieved from Blue Skies Drones: https://www.blueskiesdronerental.com/industries/search-and-rescue/

Brain, M. (2021, August 15). *https://science.howstuffworks.com/gyroscope.htm*. Retrieved from HowStuffWorks: https://science.howstuffworks.com/gyroscope.htm

Britannica, T. E. (2021, August 15). *Magnetometer*. Retrieved from Britannica: https://www.britannica.com/technology/magnetometer

Buzz Flyer. (2021, August 14). *Why Choose a 2.4G RC Helicopter or Drone?* Retrieved from Buzz Flyer: https://www.buzzflyer.co.uk/t-24G-RC-Guide.aspx

Cai, H., & Ang, H. (2011, December 4). *683. Design and analysis of a ducted fan UAV* . Retrieved from core: https://core.ac.uk/download/pdf/323313093.pdf

Canal Geomatics. (2021, August 15). *IMU Accuracy Error Definitions*. Retrieved from Canal Geomatics: http://www.canalgeomatics.com/knowledgebase/imu-accuracy-error-definitions/

Carpenter, P. (2021, August 14). *Radio Control Gear Explained*. Retrieved from RC Airplane World: https://www.rc-airplane-world.com/radio-control-gear.html#:~:text=The%20basic%20components%20of%20a,to%20power%20all%20the%20components.

Cebeci, T., & Smith, A. M. (1968). Calculation of profile drag of airfoils at low Mach numbers. *Journal of Aircraft*, 535.

Chana, W. F., & Sullivan, T. M. (1992). The Tilt Wing Advantage - For High Speed VSTOL Aircraft. *SECTION 1: JOURNAL OF AEROSPACE*, 1535-1543.

Chopra, D. I., & al., e. (2011, June). *Excalibur.* Maryland: University of Maryland.

Composites Lab. (2021, August 14). *Processes*. Retrieved from Composites Lab: http://compositeslab.com/composites-manufacturing-processes/

Copes, F. (2019, February 27). *Arduino vs Raspberry Pi*. Retrieved from Flavio Copes: https://flaviocopes.com/arduino-vs-raspberry-pi/

Copters. (2021, August 14). *Dissymmetry of Lift*. Retrieved from Copters: http://www.copters.com/aero/lift_dissymetry.html

Curbell Plastics. (2021, August 15). *High Impact Polystyrene*. Retrieved from Curbell Plastics: https://www.curbellplastics.com/Research-Solutions/Materials/High-Impact-Polystyrene

Dejan. (2021, August 2). *MEMS Accelerometer Gyroscope Magnetometer & Arduino*. Retrieved from How To Mechatronics: https://howtomechatronics.com/how-it-works/electrical-engineering/mems-accelerometer-gyrocope-magnetometer-arduino/

Deng, S., Wang, S., & Zhang, Z. (2020). Aerodynamic performance assessment of a ducted fan UAV for VTOL applications. *Aerospace Science and Technology, Vol: 103*, 105895.

DJI. (2021, August 5). *Mavic Air 2 Specs*. Retrieved from DJI: dji.com/nz/mavic-air-2/specs

Electronics Tutorials. (2020, August 8). *Passive Low Pass Filter*. Retrieved from Electronics Tutorials: https://www.electronics-tutorials.ws/filter/filter_2.html

Engineered Foam Products. (2021, August 14). *UAV's and Drones*. Retrieved from Engineered Foam Products: https://www.engineeredfoamproducts.com/products/uavs-and-drones/

Engineers Australia. (2021, August 15). *The buzz about drones: how it could benefit transport in the future*. Retrieved from Engineers Australia:

https://www.engineersaustralia.org.au/News/buzz-about-drones-how-it-could-benefit-transport-future
English, T. (2020, February 2). *The Perfect Helicopter: Understanding Coaxial Rotor Design*. Retrieved from Interesting Engineering: https://interestingengineering.com/the-perfect-helicopter-understanding-coaxial-rotor-design
EP Films. (2019, January 13). *Meet the Voliro hexacopter: a drone capable of performing acrobatic maneuvers*. Retrieved from EP Films: https://epfilms.tv/meet-voliro-hexacopter-drone-capable-performing-acrobatic-maneuvers/
Exastax. (2017, February 3). *TOP FIVE USE CASES OF TENSORFLOW*. Retrieved from Exastax: https://www.exastax.com/deep-learning/top-five-use-cases-of-tensorflow/
FAA. (2017). Chapter 5: Aerodynamics of Flight. In F. A. Administration, *Pilot's Handbook of Aeronautical Knowledge* (pp. 5-1 - 5-53). New York City, NY, USA: Skyhorse.
FAASafety. (2021, July 30). *General Aerodynamics - Part 2*. Retrieved from Learning Center Courses Content: https://www.faasafety.gov/gslac/alc/course_content_popup.aspx?cID=104&sID=448
Flight Mechanic. (2021, August 15). *Automatic Flight Control System (AFCS) and Flight Director Systems*. Retrieved from Flight Mechanic: https://www.flight-mechanic.com/automatic-flight-control-system-afcs-and-flight-director-systems/
Fly Dragon. (2021, July 29). *FLY-380 VTOL*. Retrieved from Fly Dragon: http://www.dronefromchina.com/product/FLY-380-VTOL.html
Flynt, J. (2017, July 9). *Differences Between Hexacopters, Quadcopters and Octocopters*. Retrieved from 3D Insider: https://3dinsider.com/hexacopters-quadcopters-octocopters/
Fradenburgh, E. A. (1991). The High Speed Challenge for Rotary Wing Aircraft. *Vol. 100, Section 1: JOURNAL OF AEROSPACE, Part 2*, 1969-1987.
Gastreich, W. (2018, October 1). *Servo Motors Advantages and Disadvantages*. Retrieved from Realpars.com: https://realpars.com/servo-motors-advantages/
Geo-matching. (2021, July 29). *Delair UX11*. Retrieved from Geo-matching: https://geo-matching.com/uas-for-mapping-and-3d-modelling/ux11
Gessow, A., & Myers, G. C. (1952). *Aerodynamics of the Helicopter.* New York: The Macmillan Co.
Get FPV. (2021, August 14). *All about Multirotor Drone FPV Propellers*. Retrieved from getfpv.com: https://www.getfpv.com/learn/new-to-fpv/all-about-multirotor-fpv-drone-propellers/
Giang, K. (2021, August 15). *PLA vs. ABS: What's the difference?* Retrieved from Hubs: https://www.hubs.com/knowledge-base/pla-vs-abs-whats-difference/
Glenn Research Center. (2021, July 29). *The Lift Equation*. Retrieved from National Aeronautics and Space Administration: https://www.grc.nasa.gov/www/k-12/airplane/lifteq.html
GNS Science. (2021, August 2). *Declination around New Zealand*. Retrieved from GNS Science: https://www.gns.cri.nz/Home/Our-Science/Land-and-Marine-Geoscience/Earth-s-Magnetic-Field/Declination-around-New-Zealand
Google. (2021, August 15). *Frequently Asked Questions*. Retrieved from Colaboratory: https://research.google.com/colaboratory/faq.html
GPS World Staff. (2018, December 3). *New multi-rotor UAV can lift 200 pounds*. Retrieved from GPS World: https://www.gpsworld.com/new-multi-rotor-uav-can-lift-200-pounds/
GreigRS. (2021, April 8). *What you need to know about battery-powered vs fossil fuels*. Retrieved from Design Spark: https://www.rs-online.com/designspark/what-you-need-to-know-about-battery-powered-vs-fossil-fuels

Grosu, S., Rodriguez–Guerrero, C., Grosu, V., Vanderborght, B., & Lefeber, D. (2018). Evaluation and Analysis of Push-Pull Cable Actuation System Used for Powered Orthoses. *Advances in Mechatronics and Biomechanics towards Efficient Robot Actuation*, 105.

Groupidea. (2015, January 26). *Interference Drag in a Transport Airplane Illustration*. Retrieved from Groupidea.com: https://groupidea.com/image/interference-drag-in-a-transport-airplane-illustration-2507c43f

Hall, T. (2019, September 14). *What Are Consumer Drones Made Of?* Retrieved from Let Us Drone: https://www.letusdrone.com/what-are-consumer-drones-made-of/

Hassananlian, M., & Abdelkefi, A. (2017). Classifications, applications, and design challenges of drones: A review. *Progress in Aerospace Sciences*, 99-131.

Hoerner, D. I. (1965). *Fluid-Dynamic Drag.* New York City, NY: Author.

Hoffman, G. M., Huang, H., Waslander, S. L., & Tomlin, C. J. (2011). Precision flight control for multi-vehicle quadrotor helicopter testbed. *Control Engineering Practice*, 1023-1036.

Hollister, S., & Pavic, V. (2019, December 11). *SKYDIO 2 REVIEW: A DRONE THAT FLIES ITSELF*. Retrieved from The Verge: https://www.theverge.com/2019/12/11/21009994/skydio-2-review-self-flying-autonomous-drone-camera-crash-proof-price

Houghton, E., Carpenter, P., Collicott, S. H., & Valentine, D. T. (2013). Chapter 1 - Basic Concepts and Definitions. In e. a. Alina Alexeenko, *Aerodynamics for Engineering Students (Sixth Edition)* (pp. 1-68). Oxford, United Kingdom: Butterworth-Heinemann.

IBM Cloud Education. (2020, September 21). *Unsupervised Learning*. Retrieved from IBM: https://www.ibm.com/cloud/learn/unsupervised-learning

Ingenieurbüro, T. B. (2021, August 14). *Stable flying and hovering drone*. Retrieved from Technische Beratung & Ingenieurbüro: https://www.technik-consulting.eu/en/analysis/stable_drone.html

Intertek. (2021, August 15). *Ultrasonic thickness measurement (UTM)*. Retrieved from Intertek: https://www.intertek.com/non-destructive-testing/materials-testing/ultrasonic-thickness-measurement-utm/

Jackson, B. (2021, February 24). *Fixed Wing vs Multirotor Drones for Surveying*. Retrieved from coptrz.com: https://coptrz.com/fixed-wing-vs-multirotor-drones-for-surveying/

Jaiswal, P. (2018, August 12). *Sensor Fusion — Part 1: Kalman Filter basics*. Retrieved from Towards Data Science: https://towardsdatascience.com/sensor-fusion-part-1-kalman-filter-basics-4692a653a74c

Jia, Y., Guo, L., & Wang, X. (2018). Real-time control systems. *Transportation Cyber-Physical Systems*, 81-113.

Junaid, A. B., Sanchez, A. D., Bosch, J. B., Vitzilaios, N., & Zweiri, Y. (2018). Design and Implementation of a Dual-Axis Tilting Quadcopter. *Kinematics and Robot Design I, KaRD2018*.

Kardasz, P., Doskocz, J., Hejduk, M., Wiejkut, P., & Zarzycki, H. (2016). Drones and Possibilities of Their Using. *Journal of Civil & Environmental*, 6:3.

keras. (2021, August 15). *keras*. Retrieved from keras: https://keras.io/

Kim, H. W., & Brown, R. E. (2010). A Comparison of Coaxial and Conventional Rotor Performance. *JOURNAL OF THE AMERICAN HELICOPTER SOCIETY 55*, 012004.

Kim, S. (2021, July 29). *LQ Tracker-based Hovering Control of Ring-wing-type UAV*. Retrieved from ResearchGate: https://www.researchgate.net/publication/273135121_LQ_Tracker-based_Hovering_Control_of_Ring-wing-type_UAV

Kim, Y., & Bang, H. (2018). *Introduction to Kalman Filter and Its Applications.* Fraunhofer: Felix Govaers.

Kirbas, I. (2021, August 2). *Simplified-internal-structure-of-the-accelerometer_fig1_336116117*. Retrieved from ResearchGate: https://www.researchgate.net/figure/Simplified-internal-structure-of-the-accelerometer_fig1_336116117

Knight, M., & Curliss, D. (2003). Composite Materials. In E. e. Aboufadel, *Encyclopedia of Physical Science and Technology, Third Edition* (pp. 455-468). Amsterdam: Robert A. Meyers. Retrieved from https://www.twi-global.com/technical-knowledge/faqs/what-is-a-composite-material

Kollmorgen Experts. (2020, September 29). *How Servo Motors Work.* Retrieved from kollmorgen.com: https://www.kollmorgen.com/en-us/blogs/_blog-in-motion/articles/how-servo-motors-work/

Krossblade Aerospace. (2021, August 15). *HOW TO BUILD A FAST AND EFFICIENT AIRPLANE*. Retrieved from Krossblade Aerospace: https://www.krossblade.com/efficiency-and-speed-of-airplanes

LaFay, M. (2021, August 15). *Battery Considerations for Your Drone*. Retrieved from dummies.com: https://www.dummies.com/consumer-electronics/drones/battery-considerations-for-your-drone/

Lanner, Ø. (2017, October 18). *Review: Aimdroix XRay Tilt-Rotor FPV Quadcopter*. Retrieved from https://oscarliang.com/aimdroix-xray-tilt-rotor-fpv-quad/

Lanning, W. (2020, April 3). *What Are Drones Made Of?* Retrieved from Matmatch: https://matmatch.com/blog/what-are-drones-made-of/

Lu, K., Liu, C., Li, C., & Chen, R. (2019). Flight Dynamics Modeling and Dynamic Stability Analysis of Tilt-Rotor Aircraft. *International Journal of Aerospace Engineering* , 15.

McIntosh-Tolle, L. (2021, August 2). *How to Adjust the Declination on a Compass*. Retrieved from rei.com: https://www.rei.com/learn/expert-advice/compass-declination.html

McNab, H. (2020, January 10). *Uber and Hyundai Have Established a Drone Taxi System That Just Might Work*. Retrieved from Drone Life: https://dronelife.com/2020/01/10/uber-and-hyundai-have-established-a-drone-taxi-system-that-just-might-work/

Microtell Informatics. (2021, July 31). *HARIFALI IQBAL ELALMIŞ TOY MODEL CAR MODEL HELICOPTER EDUCATIONAL TOY CONTROLLED TOYS*. Retrieved from serifalibilgisayartamiri.com: http://serifalibilgisayartamiri.com/oyuncak-model-araba-model-helikopter-egitici-oyuncak-kumandali-oyuncaklar/

Military.com. (2021, August 14). *RQ-4 Global Hawk*. Retrieved from Military.com: https://www.military.com/equipment/rq-4-global-hawk

Model Flight. (2019, February 6). *What is an Electronic Speed Controller and how does it differ from brushed to brushless motors?* Retrieved from Model Flight: https://www.modelflight.com.au/blog/electronic-speed-controllers

Morris, D. Z. (2015, November 18). *Tesla Veteran Explains How Electric Motors Crush Gas Engines*. Retrieved from Fortune.com: https://fortune.com/2015/11/17/electric-motors-crush-gas-engines/

Murray, M. (2019, December 15). *TEENSY VS. ARDUINO: WHAT'S THE DIFFERENCE?* Retrieved from The Geek Pub: https://www.thegeekpub.com/237273/teensy-vs-arduino-whats-the-difference/

NASA. (2021, August 15). *How Does GPS Work?* Retrieved from Space Place: https://spaceplace.nasa.gov/gps/en/

NASA. (2021, July 30). *What is Drag?* Retrieved from National Aeronautics and Space Administration: https://www.grc.nasa.gov/www/k-12/airplane/drag1.html

Nemati, A., Soni, N., Sarim, M., & Kumar, M. (2016). Design, Fabrication and Control of a Tilt Rotor Quadcopter. *ASME 2016 Dynamic Systems and Control Conference* (p. 7). Minneapolis, Minnesota, USA: The American Society of Mechanical Engineers.

Newman, S. (1994). *Foundations of Helicopter Flight.* Oxford, United Kingdom: Butterworth-Heineman Ltd.

nine11design. (2019, August 14). *CARBON FIBER VS. FIBERGLASS: TEXTURE, STRENGTH, AND COST*. Retrieved from nine11design: https://www.nine11design.com/blog/carbon-fiber-vs-fiberglass-texture-strength-and-cost/#:~:text=As%20the%20names%20imply%2C%20fiberglass,fit%20any%20shape%20or%20mold.

O'Meara, M. M., & Mueller, T. J. (1987). Laminar separation bubble characteristics on an airfoil at low Reynolds numbers. *AIAAJ*, 1033.

Omega. (2018, August 18). *How to Measure Acceleration?* Retrieved from Omega.com: https://www.omega.com/en-us/resources/accelerometers

OpenEI. (2021, August 14). *Power density*. Retrieved from OpenEI: https://openei.org/wiki/Definition:Power_density

Orms-Direct. (2021, July 29). *DJI Mavic 2 Pro Drone*. Retrieved from Orms-Direct: https://www.ormsdirect.co.za/dji-mavic-2-pro-drone-refurbished

Osiński, B., & Budek, K. (2018, July 15). *What is reinforcement learning? The complete guide*. Retrieved from Deepsense.ai: https://deepsense.ai/what-is-reinforcement-learning-the-complete-guide/

Page, R. (1965). Aircraft with Variable-Sweep Wings: A Discussion Outlining the Advantages and Disadvantages of Variable-Sweep Aircraft and the Principal Features of Three Possible Types: a Trainer, a Strike Fighter and a Supersonic Transport. *Aircraft Engineering and Aerospace Technology*, 295-299.

Patrik, A., Utama, G., Gunawan, A. A., Chowanda, A., Suroso, J. S., Shofiyanti, R., & Budiharto, W. (2019). GNSS-based navigation systems of autonomous drone for delivering items. *Journal of Big Data*, s40537-019-0214-3.

Petersson, D. (2021, August 15). *supervised learning*. Retrieved from searchenterpriseai: https://searchenterpriseai.techtarget.com/definition/supervised-learning

Position Partners. (2020, October 15). *Different Types of Survey Drones and How they Take Off, Fly and Land*. Retrieved from Position Partners: https://www.positionpartners.com.au/nz/news/survey-drones/

Rapp, B. E. (2017). Fluids. *Microfluidics: Modelling, Mechanics and Mathematics*, 243-263.

Rayonier. (2021, August 15). *HIGH POWER DRONES ARE A SAFETY GAME-CHANGER IN TOWER LOGGING*. Retrieved from Rayonier: https://www.rayonier.com/stories/high-power-drones-are-a-safety-game-changer-in-tower-logging/

Reliance Digital. (2021, August 3). *Better Understanding Of Batteries – Li-Ion Vs. Li-Po*. Retrieved from Reliance Digital: https://www.reliancedigital.in/solutionbox/better-understanding-of-batteries-li-ion-vs-li-po/

Renesas. (2021, August 14). *What are Brushless DC Motors*. Retrieved from Renesas: https://www.renesas.com/us/en/support/engineer-school/brushless-dc-motor-01-overview

Rippel, W. (2007, January 9). *Induction Versus DC Brushless Motors*. Retrieved from Tesla: https://www.tesla.com/en_NZ/blog/induction-versus-dc-brushless-motors

robu.in. (2020, April 20). *What is Servo Motor – Advantages, Disadvantages Applications*. Retrieved from robu.in: https://robu.in/what-is-servo-motor/

robu.in. (2020, April 28). *What Is Stepper Motor?* Retrieved from robu.in: https://robu.in/what-are-the-advantages-disadvantageous-of-the-stepper-motor/

Rock West. (2017, December 7). *Carbon Fiber VS. Fiberglass Tubing: Which Is Better?* Retrieved from Rock West Composites: https://www.rockwestcomposites.com/blog/carbon-fiber-vs-fiberglass-tubing-which-is-better/

Rotaru, C., & Todorov, M. (2017). Helicopter Flight Physics. In e. a. Ali Al-Abadi, *Flight Physics* (p. DOI: 10.5772/intechopen.71516). London: Konstantin Volkov.

Rotorworks Inc. (2019, October 18). *Helicopter Ground School – Drag*. Retrieved from Rotorworks Blog: https://www.rotorworks.com/2019/10/helicopter-ground-school-drag/

Sapiga, A. (2016, July 29). *Brushed vs Brushless Dc Motor: An Overview*. Retrieved from Progressive Automations: https://www.progressiveautomations.com/blogs/how-to/brushed-vs-brushless-dc-motor-an-overview

Science Learning Hub. (2021, August 14). *Wing loading*. Retrieved from Science Learning Hub: https://www.sciencelearn.org.nz/resources/301-wing-loading

Skybrary. (2019, April 8). *Angle of Attack (AOA)*. Retrieved from Skybrary.aero: https://www.skybrary.aero/index.php/Angle_of_Attack_(AOA)

SKYbrary. (2021, August 14). *Induced Drag*. Retrieved from SKYbrary: https://www.skybrary.aero/index.php/Induced_Drag

Smit009. (2015, July 12). *2. The Different Frames and the Keplerian Elements*. Retrieved from ADCS For Beginners: https://adcsforbeginners.wordpress.com/tag/earth-centred-inertial-frame/

Technology, U. S. (2021, August 8). *Hybrid VTOL Fixed-Wing UAV Manufacturers*. Retrieved from Unmanned Systems Technology: https://www.unmannedsystemstechnology.com/category/supplier-directory/platforms/hybrid-vtol-uav-manufacturers/

T-motor. (2020, August 3). *Gimbal Type*. Retrieved from T-motor: https://store.tmotor.com/category.php?id=45

T-motor. (2021, August 2). *Air Gear 450*. Retrieved from T-motor: https://store.tmotor.com/goods.php?id=726

Triggs, R. (2021, May 8). *Lithium-ion vs lithium-polymer: What's the difference?* Retrieved from Android Authority: https://www.androidauthority.com/lithium-ion-vs-lithium-polymer-whats-the-difference-27608/

UAV Coach. (31, July 2021). *How to Fly a Drone*. Retrieved from UAV Coach: https://uavcoach.com/how-to-fly-a-quadcopter-guide/

University of Minnesota. (2013, June 05). *University of Minnesota researchers control flying robot with only the mind*. Retrieved from University of Minnesota: https://cse.umn.edu/college/news/university-minnesota-researchers-control-flying-robot-only-mind

upGrad. (2019, November 14). *Types of Machine Learning: 3 Machine Learning Types You Must Know*. Retrieved from upGrad blog: https://www.upgrad.com/blog/types-of-machine-learning/

Vertical Flight Society. (2021, July 29). *A³ Vahana eVTOL Tiltwing*. Retrieved from Electric VTOL News: https://evtol.news/news/a-vahana-evtol-tiltwing

Ward, R. (2018, April 6). *The Long Road to the Tiltrotor*. Retrieved from AIN Online: https://www.ainonline.com/aviation-news/business-aviation/2018-04-06/long-road-tiltrotor

Watson, J. (2021, August 2). *MEMS Gyroscope Provides Precision Inertial Sensing in Harsh, High Temperature Environments*. Retrieved from Analog Devices: https://www.analog.com/en/technical-articles/mems-gyroscope-provides-precision-inertial-sensing.html

Wikipedia. (2021, July 30). *Lift (force)*. Retrieved from Wikipedia: https://en.wikipedia.org/wiki/Lift_(force)

Williams, L. (2020, March 20). *Bio-inspired drones: the natural evolution of UAVs*. Retrieved from Engineering and Technology: https://eandt.theiet.org/content/articles/2020/03/bio-inspired-drones-the-natural-evolution-of-uavs/

Windsor, S. (2014). Real world drag coefficient – is it wind averaged drag? *The International Vehicle Aerodynamics Conference*.

Wingtra. (2021, August 8). *Vertical take-off and landing (VTOL)*. Retrieved from Wingtra: https://wingtra.com/mapping-drone-wingtraone/vtol-drone/

Yoma, Y. (2017, April 12). *History Hour: YH-21 tandem-rotor helicopter takes first flight*. Retrieved from Aerotime Hub: https://www.aerotime.aero/18249-history-hour-yh-21-tandem-rotor-helicopter-takes-first-flight

Yonhap News. (2021, July 29). *South Korea Unveils Tilt Rotor UAS*. Retrieved from UAS Vision: https://www.uasvision.com/2011/12/01/south-korea-tilt-rotor-uas/

Young, L. A. (2018). What is a Tiltrotor? A Fundamental Reexamination of the Tiltrotor Aircraft Design Space. *AHS International Technical Meeting of Aeromechanics Design for Transformative Vertical Flight* (p. 1). San Francisco, CA: NASA Ames Research Center.

Zhu, H., Nie, H., Zhang, L., Wei, X., & Zhang, M. (2020). Design and assessment of octocopter drones with improved aerodynamic efficiency and performance. *Aerospace Science and Technology Volume 106*, 106206.

Zipline. (2021, July 29). *Delivery at the speed of life*. Retrieved from Zipline: https://flyzipline.com/

Chapter 7: Appendix

7.1 IMU CODE

```
import argparse
import sys
import navio.mpu9250
import navio.util
import time

imu = navio.mpu9250.MPU9250()
IMU = navio.lsm9ds1.LSM9DS1()

navio.util.check_apm()

if imu.testConnection():
        print("Connection established: True")
else:
        sys.exit("Connection established: False")

imu.initialize()

time.sleep(1)

#y = pitch (left-right)
#x = roll (front-back)
#z = yaw (up-down)
```

```
def IMU(Acc = False,Gy=False,Cal=False):

        imu.read_all()
        imu.read_gyro()
        imu.read_acc()
        imu.read_temp()
        imu.read_mag()

        #print("Accelerometer: ", imu.accelerometer_data)
        #print("Gyroscope:     ", imu.gyroscope_data)
        #print("Temperature:   ", imu.temperature)
        #print("Magnetometer:  ", imu.magnetometer_data)

        Accelerometer = imu.accelerometer_data
        Gyroscope = imu.gyroscope_data

        m9a, m9g, m9m = imu.getMotion9()

        #print("Acc:", "{:+7.3f}".format(m9a[0]), "{:+7.3f}".format(m9a[1]), "{:+7.3f}".format(m9a[2]),)
        #print("Gyr:", "y:{:+8.4f}".format(m9g[0]), "x:{:+8.4f}".format(m9g[1]), "z:{:+8.4f}".format(m9g[2]),)
        #print(" Mag:", "{:+7.3f}".format(m9m[0]), "{:+7.3f}".format(m9m[1]), "{:+7.3f}".format(m9m[2]))

        if Gy:
                return imu.gyroscope_data[0], imu.gyroscope_data[1], imu.gyroscope_data[2]
        if Acc:
                print(Accelerometer)
        if Cal:
                return imu.gyroscope_data[0], imu.gyroscope_data[1], imu.gyroscope_data[2]
```

7.2 INS FUSION CODE

```
import sys
import time
import numpy as np

from IMUReading import *
from servoMotor import *

import navio.pwm
import navio.util

def Calibrate(calNum):
        y = 0
        x = 0
        z = 0

        print("CALIBRATING.....................................")
        print("DO NOT MOVE!!!")

        for a in range(calNum):
                y1,x1,z1 = IMU(Cal=True)
                y += y1
                x += x1
                z += z1

        y = y/calNum
        x = x/calNum
        z = z/calNum

        return y,x,z


def Motor(calNum=1000):
        pSum = 0
        rSum = 0
        yaSum = 0
        SERVOMAX = 2.6
        SERVOMIN = 0.5
        AngMax = 45
        AngMin = -45
        i = 0
        pos = 0

        p1,r1,ya1 = Calibrate(calNum)
        PWMset()
```

```
        y = y/calNum
        x = x/calNum
        z = z/calNum

        return y,x,z


def Motor(calNum=1000):
        pSum = 0
        rSum = 0
        yaSum = 0
        SERVOMAX = 2.6
        SERVOMIN = 0.5
        AngMax = 45
        AngMin = -45
        i = 0
        pos = 0

        p1,r1,ya1 = Calibrate(calNum)
        PWMset()

        while True:
                p,r,ya = IMU(Gy=True)

                #time.sleep(0.5)
                p = p-p1
                r = r-r1
                ya = ya-ya1
                #print("{:+8.3f}".format(p),"{:+8.3f}".format(r),"{:+8.3f}".format(ya))

                pSum += p
                rSum += r
                yaSum += ya
                #print("{:+8.3f}".format(pSum),"{:+8.3f}".format(rSum),"{:+8.3f}".format(yaSum))

                #if i % 100 == 0:
                        #print("{:+8.3f}".format(pSum))
                #       pos = np.interp(pSum, [-35,50], [0.5,2.6])
                #       print(pos)

                servoMotor(position=pos)
                i += 1


Motor(calNum=100)
```

7.3 MOTOR LIFT DATA

Single (33V)		
PWM Readings	**Amp**	**Weight (g)**
5.2	0	0
5.3	0.3	60
5.4	0.4	107
5.5	0.6	160
5.6	0.84	220
5.7	1	266
5.8	1.3	335
5.9	1.6	400
6	2	460
6.1	2.3	530
6.2	2.8	600
6.3	3.2	660
6.4	3.2	660

Parallel (33V)		
PWM Readings	**Amp**	**Weight (g)**
5.2	0	0
5.4	0.4	110
5.6	0.8	210
5.8	1.3	330
6	2	460
6.2	2.8	610
6.4	4	770
6.6	5.2	920
6.8	6.4	1030

Parallel (11.1V/3s)			
PWM Readings	**Amp**	**Amps (*2)**	**Weight (g)**
5.2	0	0	0
5.4	0.07	0.14	5
5.6	0.14	0.28	23
5.8	0.21	0.42	48
6	0.3	0.6	72
6.2	0.4	0.8	97
6.4	0.5	1	120
6.6	0.65	1.3	152
6.8	0.8	1.6	180
7	1	2	215
7.2	1.2	2.4	254
7.4	1.45	2.9	300
7.6	1.76	3.52	350
7.8	2	4	400
8	2.4	4.8	450

8.2	2.75	5.5	500
8.4	3.2	6.4	550

Parallel (14.8V/4s)			
PWM Readings	**Amp**	**Amps(*2)**	**Weight (g)**
5.2	0	0	0
5.4	0.1	0.2	17
5.6	0.18	0.36	50
5.8	0.3	0.6	80
6	0.4	0.8	120
6.2	0.55	1.1	160
6.4	0.7	1.4	200
6.6	0.9	1.8	250
6.8	1.1	2.2	300
7	1.48	2.96	360
7.2	1.8	3.6	425
7.4	2.2	4.4	500
7.6	2.5	5	570
7.8	3	6	650
8	3.2	6.4	650

Parallel (14.8V/4s)		
PWM Readings	**Amps**	**Weight (g)**
Max	6.4	650

7.4 MOTOR CODE

```
import sys
import time

import navio.pwm
import navio.util

navio.util.check_apm()

PWM_OUTPUT = 0
SERVO_MIN = 1.250 #ms
SERVO_MAX = 1.750 #ms
x = 1.8
n = 0

with navio.pwm.PWM(PWM_OUTPUT) as pwm:
    pwm.set_period(50)
    pwm.enable()
    pwm.set_duty_cycle(0)

    while n < 1000:
        pwm.set_duty_cycle(1)
        n += 1

    print ("Motor Ready")

    while (True):
        pwm.set_duty_cycle(x)
```

7.5 TORQUE CALCULATIONS

Table 7.1: Torque Calculations for Duct

Estimated values for Torque Calculations								
Mass of Air Duct	400	g	**Mass of Motor**	100	g	**Rotational Angle, Θ**	3.141593	
Radius of Air Duct, R	140	mm	**Radius of Motor**	15	mm	**Period of rotation, t**	0.2	s
			Length of Motor	30	mm	**Safety Factor, sf**	1.5	
Rotational Inertia of Air Duct, IAD	0.00392	kgm2		**Angular Velocity, ω**		15.70796	rads-1	
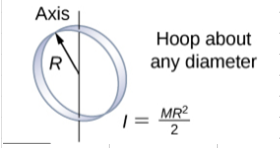	$I = \frac{MR^2}{2}$			$\omega = \frac{\theta}{t}$				
Rotational Inertia of Lift Motors, IM	1.31E-05	kgm2		**Angular Acceleration, α**		78.53982	rads-2	
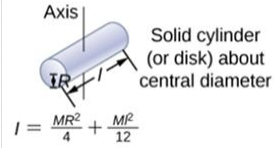	$I = \frac{MR^2}{4} + \frac{Ml^2}{12}$			$\alpha = \frac{\omega}{t}$				
Torque for Duct Motors, τ	308.906915	Nm						
$\tau = I\alpha$								
Torque with Safety Factor	**463.360373**	**mNm**						
Power, P	**0.06178138**	**Watts**						
$P = I\alpha$								
Torsion, T	**0.31308133**	**kg/4S**						
$T = \frac{\tau}{14.8} \times \frac{100}{10}$								

Table 7.2: Torque Calculations for Gimbal Arm

Mass of Air Duct	400	g	Mass of Thrust Motor	100	g	Mass of Arm			
Radius of Air Duct, R	140	mm	Radius of Thrust Motor	15	mm	Radius of Arm			
			Length of Thrust Motor	30	mm				
Rotational Inertia of Air Duct, IAD		0.00392	kgm2	**Rotational Inertia of Arm, IA**			0.000000405	kgm2	
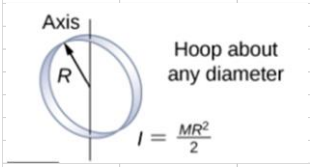		$I = \frac{MR^2}{2}$		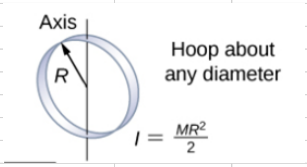					
Rotational Inertia of Lift Motors, IM		1.31E-05	kgm2	**Rotational Inertia of Gyro Motors, IGM**			0.0000784	kgm2	
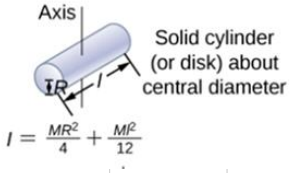		$I = \frac{MR^2}{4} + \frac{Ml^2}{12}$		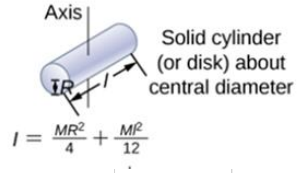					
Torque for Gyro Motors, τ		429.9607	Nm						
$\tau = I\alpha$									
Torque with Safety Factor		**644.9411**	**mNm**						
Power, P		**0.429961**	**Watts**						
$P = I\alpha$									
Torsion, T		**0.435771**	**kg/4S**						
$T = \frac{\tau}{14.8} \times \frac{100}{10}$									

10	g	Mass of Gyro Motors	100	g	Mass of Rolling Seat	130	g	Rotational Angle, Θ	3.141593
9	mm	Radius of Gyro Motors	56	mm	Radius of Rolling Seat	150	g	Period of rotation, t	0.2 s
		Length of Motors	40	mm				Safety Factor, sf	1.5
Rotational Inertia of Rolling Seat, IRS		0.001463	kgm2						
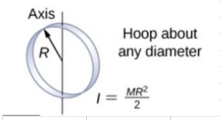		$I = \frac{MR^2}{2}$							
Angular Velocity, ω		15.70796	rads-1						
$\omega = \frac{\theta}{t}$									
Angular Acceleration, α		78.53982	rads-2						
$\alpha = \frac{\omega}{t}$									

7.6 GIMBAL MOTOR SPECS

Table 7.3: GB54-2 Motor Specifications (T-motor, 2020)

Specifications			
Test Item	GB54-1	KV	33
Motor Dimensions	ø60.7*23mm	Motor Weight(Incl. Cable)	137g
Cable Length	35cm	Hole Size	12.7mm
Configuration	12N14P	Internal Resistance	15.6Ω
Motor's Torsion ((KG.CM)/V)	1.8kg/4S	Rated Voltage (Lipo)	3-6S

Table 7.4: GB36-1 Specifications (T-motor, 2020)

Specifications			
Test Item	GB36-1	KV	50
Motor Dimensions	ø41.8*24.3mm	Motor Weight(Incl. Cable)	88g
Cable Length	35cm	Hole Size	5.6mm
Configuration	12N14P	Internal Resistance	15.6Ω
Motor's Torsion ((KG.CM)/V)	1.5kg/4S	Rated Voltage (Lipo)	3-6S